universität wien

MASTERARBEIT / MASTER'S THESIS

Titel der Masterarbeit / Title of the Master's Thesis

„Effects of TAT-MeCP2 treatment on cells of the neurovascular unit“

verfasst von / submitted by

Fabian Huber, BSc

angestrebter akademischer Grad / in partial fulfilment of the requirements for the degree of

Magister pharmaciae (Mag.pharm.)

Wien, 2023 / Vienna 2023

Studienkennzahl lt. Studienblatt / degree programme code as it appears on the student record sheet:	UA 066 605
Studienrichtung lt. Studienblatt / degree programme as it appears on the student record sheet:	Masterstudium Pharmazie
Betreut von / Supervisor:	Prof. Dipl.-Ing. Dr. Winfried Neuhaus

Acknowledgement

First, I would like to thank Prof. Dr. Winfried Neuhaus for his guidance, encouraging support and his patience during my work on my master´s thesis. Thank you for always taking time for me and setting up meetings whenever I needed advice for my work.

Furthermore, I want to thank Prof. Dr. Franco Laccone for giving me the chance to do my master's thesis in his research group.

My sincere thanks also go to Dr. Hannes Steinkellner and Mag.ª Anna Huber for introducing me to all the laboratory work and of course their helpful input in all our "Friday meetings".

Finally, I would like to express my gratitude to my father for always believing in me and giving me the opportunity to finish my pharmacy studies with his emotional and financial support.

Content

Abstract

Rett syndrome (RTT) is a severe progressive neurodevelopmental disorder, causing mental retardation in affected patients. RTT affects almost exclusively females with an incidence of 1:10,000-15,000. The main reason for RTT is a loss of function mutation in the gene for the methyl-CpG binding protein 2 (MeCP2). The blood-brain barrier (BBB) separates the central nervous system (CNS) from the blood circulation by forming a selective barrier layer at the endothelium of brain capillaries. In many neurological disorders like epilepsy or Alzheimer's disease, as well as recently proposed in RTT, blood-brain barrier properties are functionally altered.

One aim of this work was to develop quantification methods for new possible MeCP2 dependent genes and for well-known targets. A second aim was to investigate if the addition of TAT-MeCP2 fusion protein could reverse aberrant protein marker expression in immortalized mouse brain capillary endothelial MeCP2 knock-out cells (cerebENDs).

Literature research and primer design were used to receive reliable primers for quantification of predetermined targets. Experiments with various concentrations of TAT-MeCP2 were performed with three cerebEND cell lines (wildtype, HDR control and knock-out). Western blot and qPCR were performed to display differences in the protein and mRNA expression levels of predetermined targets.

Data analysis of qPCR revealed abnormal expression of the BBB markers Bcrp and Pgp, as well as the DNA-methyltransferase DNMT1 in MeCP2 KO cerebENDs. Furthermore, TAT-MeCP2 addition was able to reverse pathological increase in Pgp protein expression in cerebEND knock-out cells. This finding may contribute to potential protein replacement therapy for RTT patients.

List of Abbreviations

ABC	ATP-binding cassette
ABCG2	ATP-binding cassette super-family G member 2
AMT	adsorptive mediated transcytosis
APS	Ammonium persulfate
BBB	Blood-brain barrier
BCA	Bicinchoninic acid
BCRP	Breast cancer resistance protein
BDNF	Brain Derived Neurotrophic Factor
bp	base pairs
BSA	Bovine serum albumin
CDKL5	Cyclin-dependent kinase-like 5
cDNA	Complementary Deoxyribonucleic acid
cerebEND	Immortalized mouse cerebellar capillary endothelial cells
CNS	central nervous system
CO_2	Carbon dioxine
CTRL	HDR control cell line
Da	Dalton
ddH_2O	Double destilled Water
DNA	Deoxyribonucleic acid
DNMT3A	DNA (cytosine-5)-methyltransferase 3A
FOXG1	Forkhead box protein G1
GABA	γ-Aminobutyric acid (gamma-aminobutyric acid)
GAPDH	Glyceraldehyde-3-Phosphate Dehydrogenase
GAPDH	Glyceraldehyde-3-phosphate dehydrogenase

gDNA	Genomic Deoxyribonucleic acid
HCl	Hydrochloric acid
HRP	Horseradish peroxidase
IGF-1	Insulin like grwoth factor 1
KCl	Potassium chloride
KH_2PO_4	Potassium dihydrogen phosphate
Kir4.1 (KCNJ10)	ATP-sensitive inward rectifier potassium channel 10
KO	Knockout
M	Molar
MeCP2	Methyl CpG binding protein 2
MEF2C	Myocyte Enhancer Factor 2C
MW	Molecular weight
Na_2EDTA	Ethylenediaminetetraacetic acid disodium salt dihydrate
$Na_2HPO_4 \cdot 2\ H_2O$	di-Sodium hydrogen phosphate dihydrate
NaCl	Sodium chloride
NaN_3	Sodium azide
NMDA	N-methyl-D-aspartic acid
PBS	Phosphate-buffered saline
PBST	PBS + 0.1% Tween 20
P-gp	P-glycoprotein 1
PIC	Protease inhibitor cocktail
q.s.	latin: quantum satis [the amount which is enough]
RCF	Relative centrifugal force
RIPA	Radioimmunoprecipitation assay buffer
RMT	receptor mediated transcytosis
RNA	Ribonucleic acid

RT	Room temperature
RTT	Rett Syndrome
SDS	Sodium dodecyl sulfate
SLC	Solute carrier transporter
TEMED	N,N,N′,N′-Tetramethylethylendiamin
TRIS	Tris(hydroxymethyl)aminomethane
UV	Ultraviolet
VIS	Visable light
WT	Wildtype

List of Figures

List of Tables

1 Introduction

1.1 Rett Syndrome

Rett syndrome (RTT) is a severe progressive neurodevelopmental disorder, causing mental retardation in affected patients, starting at the age of 6 to 18 months. RTT is highly associated with mutations in variants of the gene encoding for the methyl-CpG-binding protein 2 (MeCP2). RTT affects almost exclusively females with an incidence of 1:10,000-15,000 (Amir et al., 1999), however rare cases of male patients with RTT have been reported (Moog et al., 2003).

1.1.1 History

RTT was first described by the Austrian pediatrician Dr. Andreas Rett in 1966 in Vienna. Dr. Andreas Rett observed a stereotype of hand use in two girls in his waiting room. After examination of these two girls, he described certain characteristics in the case history: autistic behavior, dementia, the loss of face expression and apraxia of gait (Rett, 1966). Dr. Rett continued his research and reported 21 more cases with the same syndrome in 1968 (Rett, 1968). Years later, in 1983, Swedish neurologist Dr. Bengt Hagberg identified 35 more cases of patients with the same symptoms, resulting in the first recognition of the Rett syndrome (Hagberg et al., 1983). The main cause of RTT was identified in 1999, when geneticist Huda Zoghbi and his research group located mutations in the gene for the methyl-CpG-binding protein 2 (MeCP2) (Amir et al., 1999). Since then, considerable progress in the understanding of the molecular mechanisms of Rett Syndrome has been made.

1.1.2 Causes of Rett Syndrome

1.1.2.1 MeCP2

The main reason for classical RTT in about approximately 90% of all cases is a loss of function mutation in the gene for the methyl-CpG binding protein 2 (MeCP2) (Bienvenu et al., 2000). MeCP2 is located on the long arm of the X-chromosome in band 28 (Xq28) (Sirianni et al., 1998) and is composed of four exons and three introns (Singh et al., 2008). The gene consists of two distinct translational start sites resulting in two different isoforms. MeCP2e1 is encoded by exon 1, 3 and 4 and is mainly found in the brain. The second isoform MeCP2e2 originates from exon 2, 3, and 4 and is more likely expressed in lung, liver, spleen and the prostate gland (Mnatzakanian et al., 2004). MeCP2 is assigned to the family of nuclear proteins, that are capable of binding to methylated DNA and contains two main functional domains: the methyl binding domain (MBD), that interacts with DNA and the transcriptional repressor domain (TRD), which leads to protein-protein interaction (Wakefield et al., 1999). The protein further includes a C-

terminal domain (CTD) and an isoform specific N-terminal sequence (Zachariah & Rastegar, 2012) (Figure 1).

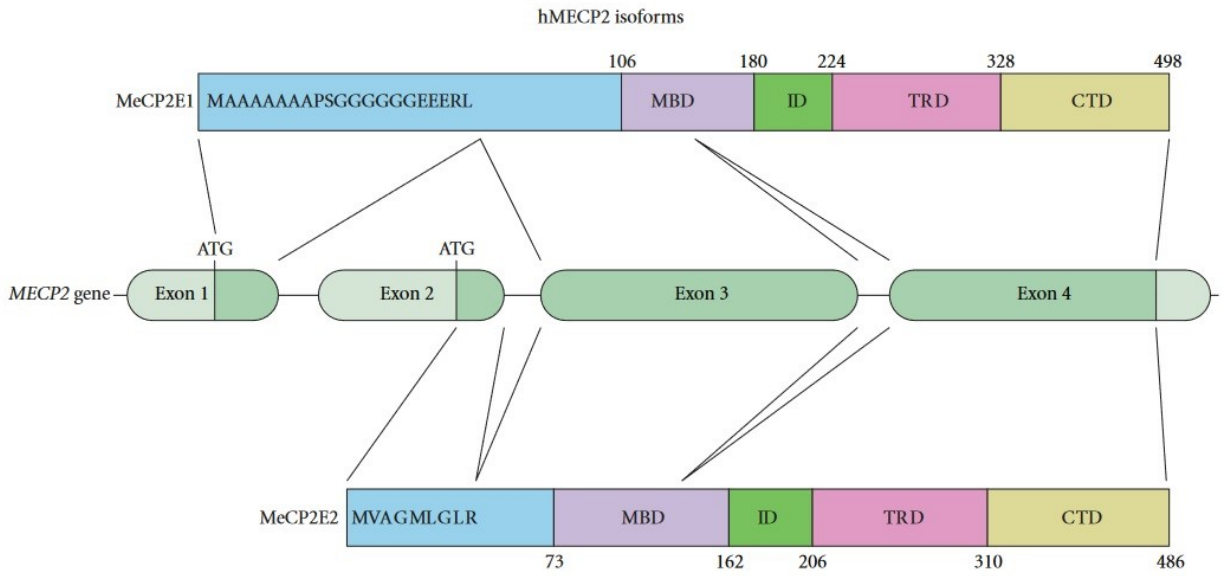

Figure 1: Illustration of the gene MeCP2 and its two protein isoforms MeCP2E1 (498 amino acids) and MeCP2E2 (486 amino acids). Exon 1 contains the translational start site for MeCP2E1, while MeCP2E2 has its start codon in Exon 2. The different N-termini are displayed in blue. Additionally, the methyl-binding domain (MBD), the intervening domain (ID), the transcriptional repressor domain (TRD) and the C-terminal domain (CTD) are shown. (Image taken from an open access article distributed under the Creative Commons Attribution License (Zachariah & Rastegar, 2012)).

The function of MeCP2 comprises various mechanisms of gene regulation, as the protein acts mainly as a transcriptional regulator (Chahrour et al., 2008). MeCP2 is involved in transcriptional repression (Nan et al., 1998), transcriptional activation (Chahrour et al., 2008), modulation of chromatin structures (Horike et al., 2005), regulation of RNA splicing (Young et al., 2005) and the expression of micro RNAs (Szulwach et al., 2010). Because of its role as an epigenetic regulator, MeCP2 can alter the expression of hundreds of downstream targets (Chahrour et al., 2008), which makes it challenging to understand the pathogenic mechanisms of Rett Syndrome.

Expression levels of MeCP2 are highest in brain, spleen and lung tissue compared to tissue with lower expression like in heart, kidney and intestine (Shahbazian et al., 2002). Within the brain the largest amount of MeCP2 can be found in neurons, followed by astrocytes, oligodendrocytes and microglia (Zachariah et al., 2012). MeCP2 plays a crucial role in the development of neuronal maturation as its level increases progressively postnatal (Shahbazian & Zoghbi, 2002).

Recent studies have shown that there are more than 900 identified mutations in the MeCP2 gene, of which more than a half are pathogenic or likely pathogenic. The majority of mutations leading to RTT phenotype are truncation or missense mutations in the methyl binding domain and the transcriptional repressor domain (Gold et al., 2018). Interestingly, the type and the location of the

mutation in the MeCP2 gene is strongly associated with disease severity of RTT patients (Cuddapah et al., 2014).

1.1.2.2 Other causes of RTT Syndrome

Although the main reason for RTT are mutations in the MeCP2 gene, a low percentage (5-25%) of patients with typical or atypical RTT exhibit a wildtype, non-mutated MeCP2 gene (Neul et al., 2014). Additionally, mutations in the genes for the cyclin-dependent kinase-like 5 (CDKL5) (Tao et al., 2004), the forkhead box protein G1 (FOXG1) (Ariani et al., 2008) and the myocyte enhancer factor 2C (MEF2C) (Zweier et al., 2010) can be responsible for RTT phenotype.

1.1.3 Onset and Progression

According to Hagberg, progression of Rett syndrome is characterized by four distinct stages: After a normal pre- and postnatal development, the first abnormalities occur at the age of approximately five to six months. The first stage of RTT, which usually covers the months 6 to 18 is characterized by an “early onset of stagnation”. In this stage patients with Rett syndrome show a delayed progress in their neurodevelopment, usually accompanied by a delayed ability to speak and growth arrest. Additionally, deceleration in head growth is observed, which is leading to microencephaly in the second year of life. Stage two occurs at the age of one to four and is mainly defined by the loss of acquired motoric and language skills. In addition to this, autistic features, seizures, respiratory problems, stereotypic hand wringing, and gait ataxia take shape in this stage. The following stage (stage three) is referred to as “pseudo-stationary” and marks an amelioration of autistic features. Patients in stage three are capable of regaining language and motoric skills, even though epileptic seizures, breathing abnormalities and scoliosis tend to deteriorate. This phase normally starts at the age of four and lasts until adolescence. In the last stage, the “late motor deterioration”, which lasts for years or decades, dystonia and parkinsonism occur and patients with RTT often become wheelchair dependent. However, a minority of RTT patients can reach ages from 60-70, though in a severely mentally and physically disabled condition (Chahrour & Zoghbi, 2007; Hagberg, 1993).

In addition, Rett syndrome is highly associated with several comorbidities, which affect life quality of patients noticeable:

- **Epilepsy**: About 80% of RTT patients suffer from epilepsy with an onset of seizures at the age of two years (Jian et al., 2006). The brain-derived neurotrophic factor BDNF, a MeCP2 dependent target, is suggested to play a significant role in the severity of epilepsy (Zeev et al., 2009). Form and expression of seizures can vary dramatically within RTT patients and about 30% of epilepsy are drug resistant (Pintaudi et al., 2010). Frequent

occurrence of generalized tonic-clonic seizures have a major impact on the quality of life of RTT patients and their families (Bahi-Buisson et al., 2008).

- **Cardiac abnormalities:** Incidence of QT-interval prolongation is significantly higher in RTT patients compared to general population (Sekul et al., 1994). Furthermore, parasympathetic-induced bradyarrhythmia and ventricular tachycardia as a result of prolonged QT intervals are commonly reported (Byard, 2006). Manifestation of cardiac abnormalities increase during progression of RTT and cardiac electrical instability is seen to be a prime suspect cause for sudden death in patients (Guideri et al., 1999).
- **Growth:** One of the main characteristics of RTT patients is the occurrence of microcephaly. Patients seem to develop normal head circumferences until the age of two to three months, but often exhibit reduced brain weight after that life span. The size of cerebral hemispheres in RTT patients is reduced, compared to healthy population (Armstrong, 2002). Although the mean body mass index (BMI) of RTT patients is comparable to normal population, there is a significant difference between classic and atypical RTT. Growth failure is more associated to classic than to atypical RTT, and studies suggest a link between certain MeCP2 mutations and reduced growth (Tarquinio et al., 2012).
- **Autonomic dysfunction:** Gastrointestinal dysmotility, low bone mineralization and biliary tract diseases are common side effects of patients, who suffer from RTT. Due to high prevalence of obstipation, nearly every second patient needs to be treated with laxatives. Additionally, feeding problems like swallowing difficulties, regurgitation and chewing problems often lead to malnutrition and growth abnormalities (Motil et al., 2012).

1.1.4 Diagnosis criteria

To date two main forms of RTT are described, classic or typical RTT and atypical RTT. Both forms require a history of regression followed by recovery or stabilization, but differ in clinical appearance. The requirements, main and supportive criteria for both variants of Rett Syndrome are given in the table below (Table 1). In some other neurological disorders (e.g., trisomy 21) all main criteria can be present, however these cases should not be considered as RTT, because onset and course are crucial for the diagnosis of RTT (Neul et al., 2010). Although about 95% of patients, who suffer from typical RTT, exhibit a MeCP2 mutation (Neul et al., 2008), solely the clinical features determine a RTT diagnosis. Additionally, only 50 to 70% of individuals with atypical RTT show mutations in the MeCP2 gene (Percy et al., 2007), making gene mutations not necessary for the diagnosis of RTT. Three distinct variants of atypical RTT are described: The preserved speech variant (Zappella, 1992), the early seizure variant (Hanefeld, 1985) and the congenital variant (Rolando, 1985). Each variant is characterized by specific clinical features and various genetic causes (Neul et al., 2010) (Table 2).

RTT diagnosis criteria 2010	Consider diagnosis when postnatal deceleration of head growth observed.
Required for typical or classic RTT	• A period of regression followed by recovery or stabilization • All main criteria and all exclusion criteria • Supportive criteria are not required, although often present in typical RTT
Required for atypical or variant RTT	• A period of regression followed by recovery or Stabilization • At least 2 of the 4 main criteria • 5 out of 11 supportive criteria
Main criteria	• Partial or complete loss of acquired purposeful hand skills • Partial or complete loss of acquired spoken language • Gait abnormalities: Impaired (dyspraxic) or absence of ability • Stereotypic hand movements such as hand wringing/squeezing, clapping/tapping, mouthing and washing/rubbing automatisms
Exclusion criteria for typical RTT	• Brain injury secondary to trauma (peri- or postnatally), neurometabolic disease, or severe infection that causes neurological problems • Grossly abnormal psychomotor development in first 6 months of life
Supportive criteria for atypical RTT	• Breathing disturbances when awake • Bruxism when awake • Impaired sleep pattern • Abnormal muscle tone • Peripheral vasomotor disturbances • Scoliosis/kyphosis • Growth retardation • Small cold hands and feet • Inappropriate laughing/screaming spells • Diminished response to pain • Intense eye communication - ‘‘eye pointing’’

Table 1: Revised RTT diagnosis criteria (Neul et al., 2010)

Variant forms of atypical RTT		
Preserved Speech Variant (Zappella Variant)	Early Seizure Variant (Hanefeld Variant)	Congenital Variant (Rolando Variant)

Clinical features:
• Regression at 1-3 years, prolonged plateau phase
• Milder reduction of hand skills
  ○ better retained hand use
• Recovery of language after regression
  ○ Mean age of recovery is 5 years
  ○ Single words or phrases
• Milder intellectual disability (IQ up to 50)
• Autistic behaviors common
• Decreased frequency of typical RTT features
  ○ Rare epilepsy
  ○ Rare autonomic dysfunction
  ○ Milder scoliosis and kyphosis
  ○ Normal head circumference
  ○ Normal height and weight in most
 	
Molecular Genetics:
Mutations in MeCP2 found in the majority of cases
	Clinical features:
	• Early onset of seizures
	  ○ Before 5 months of life
	  ○ Infantile spasms
	  ○ Refractory myoclonic epilepsy
	  ○ Seizure onset before regression
	• Decreased frequency of typical RTT features
	
	Molecular Genetics:
	Mutations in MeCP2 rarely found
	Analysis for mutations in CDKL5 should be performed
		Clinical features:
		• Grossly abnormal initial development
		  ○ Severe psychomotor delay
		  ○ Inability to walk
		• Severe postnatal microcephaly before 4 months
		• Regression in first 5 month
		• Lack of typical intense “RTT” eye gaze
		• Typical RTT autonomic abnormalities present
		  ○ Small cold hands and feet
		  ○ Peripheral vasomotor disturbances
		  ○ Breathing abnormalities while awake
		• Specific movement abnormalities
		  ○ Tongue stereotypes
		  ○ Jerky movements of the limbs
		
		Molecular Genetics:
		Mutations in MeCP2 rarely found
		Analysis for mutations in FOXG1 should be performed

Table 2: Specific variant forms of RTT (Neul et al., 2010)

1.1.5 Therapeutic approaches

To date there is no cure for Rett Syndrome, consequently current therapeutic approaches are restricted to alleviating the symptoms of the disease. However, considerable progress in understanding the pathophysiology of RTT in the last years has led to potential treatment options targeting downstream cellular processes. These downstream targets of MeCP2 include the neurotransmitter system, growth factors and proteins of the metabolic system. (Leonard et al., 2017)

Neurotransmitter system: It has been shown that MeCP2 deficiency results in decreased number and growth of dendrites, which consequently leads to dysfunction of the neurotransmitter system (Armstrong, 1992). Dysregulation in the signaling systems of dopamine (Wenk, 1995), serotonin (Paterson et al., 2005), norepinephrine (Viemari et al., 2005), GABA (Chao et al., 2010) and glutamate (Katz et al., 2016) have been described and were taken into consideration as potential therapeutic targets. For instance the benzodiazepine midazolam, which acts as an allosteric modulator in the GABAergic system could ameliorate breathing disturbances in MeCP2 deficient mice (Voituron & Hilaire, 2011). Additionally, desipramine, a norepinephrine reuptake inhibitor (Zanella et al., 2008) and sarizotan, a serotonin 1a agonist and dopamine D2-like receptor antagonist (Abdala et al., 2014) show therapeutic potential against breathing abnormalities. Another MeCP2 dependent downstream target, the NMDA receptor, which is irregularly expressed in RTT patients could be a therapeutic target. Low dose administration of the NMDA receptor antagonist ketamine showed the potential to rescue RTT phenotype by improving cortical processing and connectivity (Patrizi et al., 2016).

Growth factors: Since the expression of the brain derived neurotrophic factor BDNF is significantly reduced in RTT syndrome (Chang et al., 2006), it is seen as a potential target for pharmacological intervention. Due to the fact that exogenic BDNF is unable to cross the blood-brain barrier (BBB), BDNF itself is not suitable for therapeutic intervention. However, the sphingosine-1 phosphate receptor modulator fingolimod, which is capable of passing the BBB, could partially increase BDNF levels and improve CNS function (Deogracias et al., 2012). Another potential therapeutic target is Insulin-like growth factor-1 (IGF-1), which expression is regulated by MeCP2 (Itoh et al., 2007). IGF-1 treatment of MeCP2 deficient mice showed extension of life span, amelioration of breathing disturbances and improvement of locomotor function (Tropea et al., 2009).

Metabolic defects: Cholesterol synthesis is perturbed in brain and liver of MeCP2-null mice leading to abnormal serum cholesterol and triglycerides (Justice et al., 2013). Interestingly, cholesterol plays a main role in neuronal tissue in membrane traffic, signal transduction, neuropeptide formation and myelin formation (Pfrieger & Ungerer, 2011). Statin drugs like

Fluvastatin and Lovastatin, that inhibit HMG-CoA reductase, could ameliorate motor symptoms and extend life span of MeCP2-null mice by interfering in the lipid metabolism, showing promising therapeutic potential (Justice et al., 2013).

1.1.5.1 Innovative treatments targeting MeCP2

So far Rett Syndrome is an incurable disease and current therapy options focus on alleviating symptoms. However, over the last years various strategies have been established, focusing on the approach to restore physiological levels of MeCP2 (Panayotis et al., 2023). One of the main issues of these approaches is that overexpression of MeCP2 can lead to RTT like phenotype, making it crucial to restore physiological concentrations of MeCP2 in the cells (Van Esch et al., 2005).

A frequently used gene therapy method is to introduce non mutated genes via adeno-associated viruses (AAVs). The advantages of AAVs are long term expression profiles, cell specific tropisms and a low immunogenic potential (Panayotis et al., 2023). A study in 2013 showed that administration of a single strand AAV9-MeCP2 vector could reverse RTT phenotype features and extend lifespan of MeCP2 knock out mice. Although brain transduction was efficient, only about 4% of the neurons exhibited the inserted MeCP2 leading to an explanation for the limited improvement of RTT symptoms (Gadalla et al., 2013).

Another approach to restore MeCP2 function focuses on so called translational readthrough inducing drugs (TRIDs). These TRIDs are able to suppress nonsense codons in a mutated gene and lead to expression of a non-truncated, functional protein. However, TRIDs can only exchange stop codons for amino acids, which results in a missense mutated protein that has limited biological function and therefore show restricted improvement of RTT symptoms (Nagel-Wolfrum et al., 2016).

Reactivation of inactive X-chromosome is a promising therapeutical option for heterozygous females, who carry a healthy and a mutated version of MeCP2 (Balaton et al., 2018). X-chromosome inactivation (XCI) is carried out by non-coding RNA, which can be targeted by small molecules, allowing reactivation of the X-chromosome carrying the healthy allele of MeCP2. Females with RTT could then express a normal copy of MeCP2, which is under control of their own physiological regulatory mechanisms. A massive concern of this method is however that uncontrolled activation of Xi will lead to long term adverse effects due to disrupting epigenetic patterns throughout the genome (Vashi & Justice, 2019).

1.2 The Blood-Brain Barrier

The blood-brain barrier (BBB) separates the central nervous system (CNS) from the blood circulation (Abbott, 2005). The discovery of the BBB started in the early 1900s when Goldmann (1909) and Wislocki (1920) carried out experiments in which trypan blue was injected into organisms, staining every tissue blue except for the brain. These findings suggested a separation of the brain from the remaining body (Saunders et al., 2014). In 1967 Reese and Karnovsky finally confirmed a structural barrier in the brain endothelial cells through electron microscopy of brain tissue (Reese & Karnovsky, 1967).

1.2.1 Function, cellular composition and structure

The BBB is responsible for maintaining neuronal homeostasis by forming a selective barrier layer between the endothelium of brain capillaries and nerve tissue (Abbott et al., 2006). One of the main tasks of the BBB is regulating the exchange of nutrients, ions, metabolites and oxygen between the blood and the CNS (Abbott et al., 2010). The barrier properties are maintained by the specific anatomic structure of different cell types: endothelial cells, neurons, pericytes and nerve glial cells (e.g., astrocytes), which together with the extracellular matrix form the neurovascular unit (NVU) (Saili et al., 2017). (Figure 2)

Brain endothelial cells differ from endothelial cells in other vascular tissue by being highly polarized. They exhibit specific expression of transport proteins to limit the exchange of polar molecules and tightened cell-cell adhesion (Kadry et al., 2020). The tight connection between the endothelial cells, which allows a division in basolateral and luminal portions in the BBB is formed by tight junctions (TJs) and adherens junctions (AJs) (Begley, 2004). The TJs are formed by the protein family of Claudins, Occludin and junctional adhesion proteins (JAMs). These proteins link neighboring cell membranes and therefore restrict paracellular transport (Kadry et al., 2020). Furthermore, AJs which include the proteins cadherins and catenins are crucial for the integrity and organization of tight junctions due to their ability to connect with actin filaments of the cell scaffold (Wolburg & Lippoldt, 2002).

Another notable cell type of the NVU are CNS pericytes, located at the basal membrane adjacent to endothelial cells. They exhibit a wide range of functionality in the BBB including signal processing, angiogenesis, clearance of metabolites and microvascular stability (Sweeney et al., 2016). Additionally, pericytes are able to control BBB permeability by altering blood flow in capillaries through contraction and dilatation of the vessels (Hall et al., 2014). Disruption of pericyte functionality is associated with various diseases like Alzheimer's disease (Farkas & Luiten, 2001), dementia (Montagne et al., 2015) or amyotrophic lateral sclerosis (ALS) (Winkler et al., 2011).

Astrocytes are star-shaped glial cells with major biochemical tasks in the CNS. Their “end-feet” cover most of the surface of brain capillaries, providing an interface between the NVU and the CNS. The high density of ionic transporters in the contact areas between their end-feet and the basal lamina indicates the regulatory function on the BBB (Kadry et al., 2020). Primarily, potassium (K^+) buffering via the astrocytic ion channel Kir4.1 plays a key role in maintenance of excitability and neuronal function. Interestingly, secretion of brain derived neurotrophic factor (BDNF), a major factor in neurogenesis, is highly dependent of Kir4.1 expression (Kinboshi et al., 2020) Furthermore, astrocytes are indispensable for pH regulation, neurotransmitter uptake, nutrition of neurons and synapse formation (Clarke & Barres, 2013).

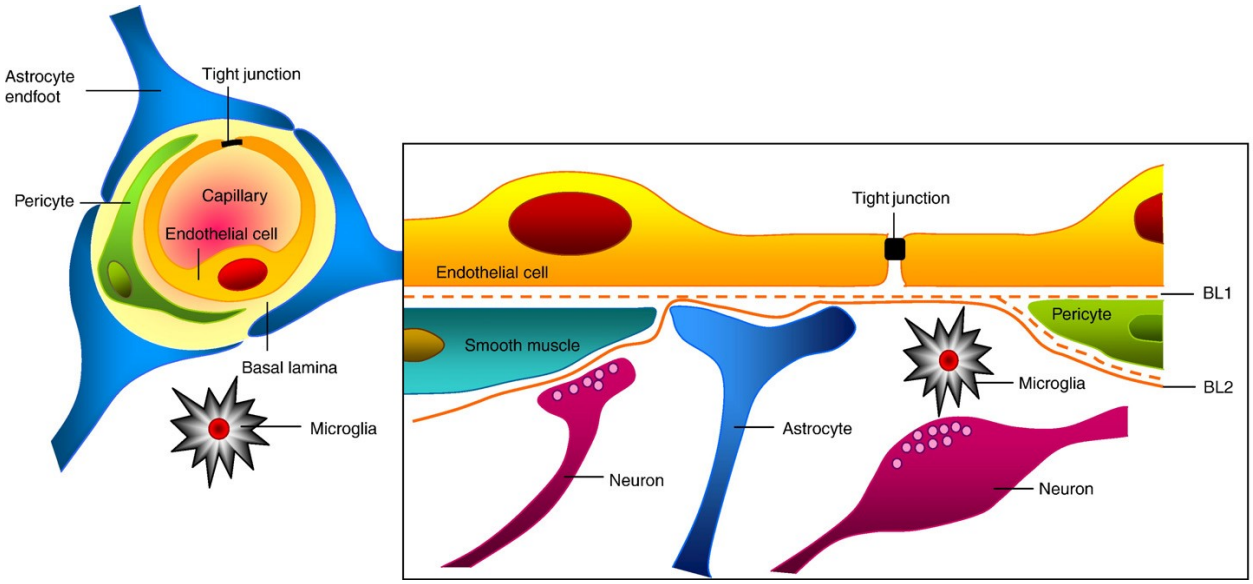

Figure 2: Composition of the blood-brain barrier and the neurovascular unit. Arrangement of the different cell types that form the BBB are shown. BL1=basal lamina 1; BL2=basal lamina 2 (Abbott et al., 2010), Copyright clarified with Elsevier under the license number 5567271121885

1.2.2 Transport across the Blood-Brain Barrier

Since paracellular transport is restricted by the formation of tight junctions between brain endothelial cells, molecules have to take further pathways to reach the CNS (Abbott et al., 2010).

Passive diffusion: In general, only lipid-soluble, small molecules can diffuse passively through brain endothelial cells to enter the brain (Liu et al., 2004). Blood gases like oxygen (O_2) and carbon dioxide (CO_2) passively move across the BBB by following their concentration gradient. Additionally, molecules that exhibit certain physico-chemical factors have an increased potential to migrate into the CNS passively. According Lipinski´s “Rule of Five” (Lipinski et al., 2001) these factors include a molecular weight <500 Da, maximum formation of 5 hydrogen bonds, log P_{oct}

(n-octanol/water partitioning coefficient) values under 5 and the absence of rotable bonds (Kadry et al., 2020).

Active Efflux: A large number of lipid-soluble molecules with a potential to penetrate into the CNS are actively transported against their concentration gradient out of the brain endothelium. The family of ABC transporters (ATP-binding cassette) mainly located on the luminal side of the endothelial cells are responsible for the efflux of substances back in the bloodstream. The ABC transporter family comprises 49 members, which are divided into 7 subgroups (ABCA to ABCG) (Vasiliou et al., 2009). Two of the best studied representatives are P-gp (P-gylcoprotein/ABCB1) and BCRP (breast cancer resistance protein/ABCG2) which are highly associated with drug resistance. Many drugs like immunosuppressants, opiates, antibiotics and antidepressants are substrates of these efflux pumps and are consequently transported out of the CNS as well as potential neurotoxins (Mahringer & Fricker, 2016).

Carrier mediated transport: Another route for small molecules to reach the CNS is the carrier mediated transport performed by the family of solute carrier transporters (SLCs). Transporters of the SLC superfamily with its 458 identified members (Pizzagalli et al., 2021) mediate transport across the BBB of essential polar nutrients like amino acids, fatty acids, carbohydrates, and nucleotides. Either located at the luminal or the basolateral side SLC expression is strictly regulated in its orientation, resulting in predetermined bidirectional transport of substrates in or out of the brain (Lin et al., 2015).

Transcytosis: Large molecules like neuroactive peptides, growth factors or hormones can cross the BBB at a low rate via transcytosis. This vesicular transport mechanism includes on the one hand receptor mediated transcytosis (RMT) and on the other hand adsorptive mediated transcytosis (AMT). In RMT a macromolecule like a protein binds to its specific receptor located in the luminal membrane of the endothelial cell and both receptor and ligand are internalized. A vesicle containing the ligand-receptor complex is formed and directed to the opposite side of the cell. The ligand is then released via exocytosis into the CNS. In contrast to this, AMT requires positively charged substrates, which bind to the surface of endothelial membrane resulting in endocytosis and subsequent transcytosis of the substrate (Abbott et al., 2010).

1.2.2.1 Transduction of proteins via TAT domain

Proteins are not able to cross the cell membrane of cerebral endothelial cells without any kind of transport mechanism. Therefore, protein transduction domains (PTDs) can be a helpful tool to attain sufficient protein delivery into cells. One of the most studied PTD is the TAT-domain (transactivator of transcription), originally found in human immunodeficiency virus (HIV). The TAT-sequence is comprised of 11, primarily positively charged amino acids and can be cross linked to heterologous proteins. TAT-fusion proteins can be incorporated by cells by classical endocytosis,

providing a method for protein replacement therapy (Nagahara et al., 1998). In 1999, Schwarze et al. provided proof that recombinant TAT-β-galactosidase protein could cross the BBB and reach the CNS of mice by preserving its biological activity (Schwarze et al., 1999).

1.2.3 Dysfunction of the Blood-Brain Barrier in diseases

In many neurological disorders the blood-brain barrier properties are disrupted (Daneman & Prat, 2015). For example, BBB dysfunction was observed in multiple sclerosis (Correale & Villa, 2007), vasogenic edema (Rosenberg & Yang, 2007), Alzheimer's disease (Zlokovic, 2008), epilepsy (Remy & Beck, 2006), tumors (Bronger et al., 2005) and Parkinson's disease (Desai et al., 2007). Pathological changes in the BBB can range from increased permeability due to tight junction breakdown to interruption of transport protein mechanisms (Persidsky et al., 2006). In addition to this, enhanced migration of inflammatory cells into the CNS is attributed to BBB disruption (Takeshita & Ransohoff, 2012). However, the underlying molecular mechanisms of BBB disturbance are still not completely known leading to the conclusion that more research regarding the BBB needs to be done (Profaci et al., 2020).

2 Aims

The aims of this work were on the one hand identifying new possible MeCP2 dependent genes and on the other hand if exogenous TAT-MeCP2 substitution can restore aberrant expression levels of predetermined targets.

As a first step to identify possible MeCP2 targets, primer pairs for selected genes should be designed and tested with cDNA samples of the used immortalized mouse cerebellar capillary endothelial cell line. PCR and gel electrophoresis should be performed to confirm suitability for real time quantitative PCR (qPCR).

To display differences in the protein expression of the well described MeCP2 dependent targets BDNF and Kir4.1, western blot with corresponding antibodies should be performed to test their suitability as a quantification method for the used immortalized mouse astrocyte cell line.

Previous experiments showed upregulation of the BBB marker Pgp and Bcrp in MeCP2 deficient mouse cerebellar capillary endothelial cells. In order to investigate if TAT-MeCP2 addition can rescue RTT phenotype, single cell substitution experiments with immortalized mouse cerebellar capillary endothelial cells should be performed. Consequently, expression of predetermined targets had to be quantified and compared between wildtype, HDR control and MeCP2 knock-out cells. Western blot and qPCR should elucidate regulation of blood-brain barrier markers under TAT-MeCP2 substitution. Different applied concentrations of TAT-MeCP2 addition should also provide reference point for an optimal treatment concentration.

3 Material and Methods

3.1 Material

3.1.1 Antibodies

3.1.1.1 Primary Antibodies

Antigen	Class	Host	Product Number	Supplier	Dilution for Western Blot
Anti-BCRP/ABCG2	monoclonal	rat	[BXP-53] (ab24115)	Abcam	1:100
Anti-BDNF	polyclonal	rabbit	ANT-010	Alomone Labs	1:200
Anti-BDNF	polyclonal	rabbit	AB1534SP	Sigma	1:500
Anti-Cldn5	polyclonal	rabbit	34-1600	Invitrogen	1:200
Anti-DNMT3a	monoclonal	mouse	(A-10): sc-373905	Santa Cruz	1:250
Anti-GAPDH	monoclonal	mouse	MAB374	Sigma	1:300
Anti-Kir4.1	polyclonal	rabbit	APC-035	Alomone Labs	1:400
Anti-MeCP2	monoclonal	rabbit	D4F3	Cell Signaling	1:400
Anti-P-glycoprotein	monoclonal	mouse	C219	Enzo	1:50
Anti-β-Tubulin	monoclonal	mouse	T4026	Sigma	1:1,500

3.1.1.2 Secondary Antibodies

Antigen	Class	Host	Product Number	Supplier	Dilution for Western Blotting
Anti-Mouse IgG HRP-linked Antibody	-	horse	7076S	Cell Signaling	1:10,000
Anti-Rabbit IgG HRP-linked Antibody	-	goat	7074S	Cell Signaling	1:10,000
Anti-Rat IgG HRP-linked Antibody	polyclonal	rabbit	61-9520	Invitrogen	1:10,000

3.1.2 Primers

Target (mouse)	Name	Primer Sequence (5´->3')	Supplier	Source
mActb	mActb forw	TTTGAGACCTTCAACACCCC	Eurofins Genomics	(Berndt et al., 2019)
	mActb rev	ATAGCTCTTCTCCAGGGAGG	Eurofins Genomics	(Berndt et al., 2019)
mCdh5	mCdh5 forw	ATTGAGACAGACCCCAAACG	Eurofins Genomics	(Berndt et al., 2019)
	mCdh5 rev	TTCTGGTTTTCTGGCAGCTT	Eurofins Genomics	(Berndt et al., 2019)
mCldn1	mCldn1 forw	GATGTGGATGGCTGTCATTG	Eurofins Genomics	(Berndt et al., 2019)
	mCldn1 rev	CGTGGTGTTGGGTAAGAGGT	Eurofins Genomics	(Berndt et al., 2019)
mCldn2	mCldn2 forw	ATGGTGACGTCCAGTGCAAT	Eurofins Genomics	(Berndt et al., 2019)
	mCldn2 rev	GGCGAGTAGAAGTCCCGAAG	Eurofins Genomics	(Berndt et al., 2019)
mCldn3	mCldn3 forw	GAGATGGGAGCTGGGTTGTA	Eurofins Genomics	(Berndt et al., 2019)
	mCldn3 rev	GTAGTCCTTGCGGTCGTAGG	Eurofins Genomics	(Berndt et al., 2019)
mCldn4	mCldn4 forw	CCCGAGCCCTTATGGTCATC	Eurofins Genomics	(Berndt et al., 2019)
	mCldn4 rev	GAGTAGGGCTTGTCGTTGCT	Eurofins Genomics	(Berndt et al., 2019)
mCldn5	mCldn5 forw	CTGGACCACAACATCGTGAC	Eurofins Genomics	(Berndt et al., 2019)
	mCldn5 rev	GCCGGTCCAGGTAACAAAGA	Eurofins Genomics	(Berndt et al., 2019)
mCldn6	mCldn6 forw	GAGCCAAGTGCACTACCTGT	Eurofins Genomics	(Berndt et al., 2019)
	mCldn6 rev	TGGTGGGATATTCGGAGGGT	Eurofins Genomics	(Berndt et al., 2019)
mCldn7	mCldn7 forw	GCGACAACATCATCACAGCC	Eurofins Genomics	(Berndt et al., 2019)
	mCldn7 rev	TACCAAGGCAGCAAGACCTG	Eurofins Genomics	(Berndt et al., 2019)
mCldn8	mCldn8 forw	TTGCTGACAGCCGGAATCAT	Eurofins Genomics	(Berndt et al., 2019)
	mCldn8 rev	TCGGAGATCTCTTTTCGGCG	Eurofins Genomics	(Berndt et al., 2019)
mCldn9	mCldn9 forw	CCAAGGCCCGTATCGTACTC	Eurofins Genomics	(Berndt et al., 2019)
	mCldn9 rev	GGACACGTACAGCAGAGGAG	Eurofins Genomics	(Berndt et al., 2019)
mCldn10	mCldn10 forw	GCTAAAATTGCTTGCTTGGC	Eurofins Genomics	(Berndt et al., 2019)
	mCldn10 rev	TCCGTTGTATGTGTAGCCCA	Eurofins Genomics	(Berndt et al., 2019)
mCldn11	mCldn11 forw	TAGCCACTTGCCTTCAGGTG	Eurofins Genomics	(Berndt et al., 2019)
	mCldn11 rev	GAGCAGCAGACGATGACACA	Eurofins Genomics	(Berndt et al., 2019)

mCldn12	mCldn12 forw	AACTGGCCAAGTGTCTGGTC	Eurofins Genomics	(Berndt et al., 2019)
	mCldn12 rev	AGACCCCCTGAGCTAGCAAT	Eurofins Genomics	(Berndt et al., 2019)
mCldn13	mCldn13 forw	CCCTGTCCTGGGTAACACAC	Eurofins Genomics	(Berndt et al., 2019)
	mCldn13 rev	GGCTCCTGAAGGTCTAGCAC	Eurofins Genomics	(Berndt et al., 2019)
mCldn14	mCldn14 forw	GCACAGGCATCTACCAGTGT	Eurofins Genomics	(Berndt et al., 2019)
	mCldn14 rev	TGAGGAGATGAAGCCCAGGT	Eurofins Genomics	(Berndt et al., 2019)
mCldn15	mCldn15 forw	TGTCTACGGTCCATGGCAAC	Eurofins Genomics	(Berndt et al., 2019)
	mCldn15 rev	CCACGAGATAGCCACCATCC	Eurofins Genomics	(Berndt et al., 2019)
mCldn16	mCldn16 forw	CCTGCGATGAGTACGACTCC	Eurofins Genomics	(Berndt et al., 2019)
	mCldn16 rev	CTCCTGCCAAAAAGCAACCC	Eurofins Genomics	(Berndt et al., 2019)
mCldn17	mCldn17 forw	TCTCCCTCCGGTACTGGAAG	Eurofins Genomics	(Berndt et al., 2019)
	mCldn17 rev	GCTCCTCCAAGTTCTCGCTT	Eurofins Genomics	(Berndt et al., 2019)
mCldn18	mCldn18 forw	GTGTCCATCTTCGCCCTGAA	Eurofins Genomics	(Berndt et al., 2019)
	mCldn18 rev	GGTGTACCTGGTCTGAACGG	Eurofins Genomics	(Berndt et al., 2019)
mCldn19	mCldn19 forw	TTCTTCAACCCCAGCACTCC	Eurofins Genomics	(Berndt et al., 2019)
	mCldn19 rev	GCGGGCAACTTAACAACAGG	Eurofins Genomics	(Berndt et al., 2019)
mCldn20	mCldn20 forw	CTTTCATCCTGGCCGTGTCT	Eurofins Genomics	(Berndt et al., 2019)
	mCldn20 rev	GGCTTTCCGGAATGGTCAGA	Eurofins Genomics	(Berndt et al., 2019)
mCldn22	mCldn22 forw	GGGCTTAGTCTTCCGAACG	Eurofins Genomics	(Berndt et al., 2019)
	mCldn22 rev	CTTCAAGTGCGGCAAGTAGT	Eurofins Genomics	(Berndt et al., 2019)
mCldn23	mCldn23 forw	GGACATATGTCGCGAGCAGA	Eurofins Genomics	(Berndt et al., 2019)
	mCldn23 rev	CGAAAAACACCACGCCAGAG	Eurofins Genomics	(Berndt et al., 2019)
mCldn24	mCldn24 forw	CTGTCATTGCTGGGATGGGT	Eurofins Genomics	(Berndt et al., 2019)
	mCldn24 rev	TGCACAGGGACATCAAGACC	Eurofins Genomics	(Berndt et al., 2019)
mCldn25	mCldn25 forw	CTACATGGCGGCCTCCATAG	Eurofins Genomics	(Berndt et al., 2019)
	mCldn25 rev	CGATGCCGCTATTGTGGTTG	Eurofins Genomics	(Berndt et al., 2019)
mCldn26	mCldn26 forw	TGACCGGGTTCTTGAGCTTC	Eurofins Genomics	(Berndt et al., 2019)
	mCldn26 rev	CAGAGACCAGCCAAAGCGTA	Eurofins Genomics	(Berndt et al., 2019)
mCldn27	mCldn27 forw	GCCTGGAAGTTTCTCCCTCC	Eurofins Genomics	(Berndt et al., 2019)
	mCldn27 rev	ATGTAGATGCTGAGCCCTGC	Eurofins Genomics	(Berndt et al., 2019)

mOcln	mOcln forw	ACTCCTCCAATGGCAAAGTG	Eurofins Genomics	(Berndt et al., 2019)
	mOcln rev	CCCCACCTGTCGTGTAGTCT	Eurofins Genomics	(Berndt et al., 2019)
mTric	mTric forw	GAGAATCCTGGGTGTGGTGG	Eurofins Genomics	(Berndt et al., 2019)
	mTric rev	TTTCGATGACAACGACGGGT	Eurofins Genomics	(Berndt et al., 2019)
mZo1	mZo1 forw	CCCACCCCCATCTCAGAGTA	Eurofins Genomics	(Berndt et al., 2019)
	mZo1 rev	GGGACAGCTTTAGGCATGGT	Eurofins Genomics	(Berndt et al., 2019)
mKir 4.1	mKir 4.1 forw	GGAGGAAATGGGACACAGGG	Eurofins Genomics	(Berndt et al., 2019)
	mKir 4.1 rev	GGGAGCAGCCAGAATGAAGT	Eurofins Genomics	(Berndt et al., 2019)
mBDNF	mBDNF forw	AAGGACGCGGACTTGTACAC	Eurofins Genomics	(Fukuchi et al., 2017)
	mBDNF rev	CGCTAATACTGTCACACACGC	Eurofins Genomics	(Fukuchi et al., 2017)
mActb	mActb forw	CCTCCCTGGAGAAGAGCTATG	Eurofins Genomics	(Wu et al., 2017)
	mActb rev	TTACGGATGTCAACGTCACAC	Eurofins Genomics	(Wu et al., 2017)
mCldn1	mCldn1 forw	ATCGCAATCTTTGTGTCCACCATT	Eurofins Genomics	(Förster et al., 2005)
	mCldn1 rev	ATTCTGTTTCCATACCATGCTGTGG	Eurofins Genomics	(Förster et al., 2005)
mCldn3	mCldn3 forw	GCAAGGACTACGTCTGAGGG	Eurofins Genomics	NCBI Primer Blast
	mCldn3 rev	ACTGTGTGTCGTCTGTCACC	Eurofins Genomics	NCBI Primer Blast
mCldn4	mCldn4 forw	CCACTCTGTCCACATTGCCT	Eurofins Genomics	NCBI Primer Blast
	mCldn4 rev	CTTTGCACAGTCCGGGTTTG	Eurofins Genomics	NCBI Primer Blast
mCldn11	mCldn11 forw	ATGGTAGCCACTTGCCTTCAG	Eurofins Genomics	(Cai et al., 2011)
	mCldn11 rev	AGTTCGTCCATTTTTCGGCAG	Eurofins Genomics	(Cai et al., 2011)
mZO1	mZO1 forw	TGAACGCTCTCATAAGCTTCGTAA	Eurofins Genomics	(Bleau et al., 2015)
	mZO1 rev	ACCGTACCAACCATCATTCATTG	Eurofins Genomics	(Bleau et al., 2015)
mTric	mTric forw	GAAAATGTGTGAAGCGGCCA	Eurofins Genomics	(Takano et al., 2017)
	mTric rev	TTTTGCCACGTAGTCAGGCA	Eurofins Genomics	(Takano et al., 2017)
mKir4.1	mKir4.1 forw	TGCCCCGCGATTTATCAGAG	Eurofins Genomics	NCBI Primer Blast
	mKir4.1 rev	CCGTCTTTCGTGAGGACCC	Eurofins Genomics	NCBI Primer Blast
mPPIA	mPPIA forw	TTTCGAGCTCTGAGCACTGG	Eurofins Genomics	NCBI Primer Blast
	mPPIA rev	CACCCTGGCACATGAATCCT	Eurofins Genomics	NCBI Primer Blast
mB2M	mB2M forw	CTCGGTGACCCTGGTCTTTC	Eurofins Genomics	(Wu et al., 2017)
	mB2M rev	GGATTTCAATGTGAGGCGGG	Eurofins Genomics	(Wu et al., 2017)

mDNMT1	mDNMT1 forw	GATCACACTACCAGCCCATCC	Eurofins Genomics	(Watanabe et al., 2019)
	mDNMT1 rev	GTCACGCCAATCTGATCCTG	Eurofins Genomics	(Watanabe et al., 2019)
mDNMT3A	mDNMT3A forw	GTCTGGAGCACGGCAGAATAG	Eurofins Genomics	(Watanabe et al., 2019)
	mDNMT3A rev	AAATGCTGGTCTTTGCCCTG	Eurofins Genomics	(Watanabe et al., 2019)
mDNMT3B	mDNMT3B forw	ACTCCATCAGACAGGGCAAA	Eurofins Genomics	(Watanabe et al., 2019)
	mDNMT3B rev	CCGTGTAGTGAGCAGGGAA	Eurofins Genomics	(Watanabe et al., 2019)
mTET1	mTET1 forw	CTCCGAATCCTACGGGAAGC	Eurofins Genomics	NCBI Primer Blast
	mTET1 rev	CTGTGAGCCTGCCAAGATGA	Eurofins Genomics	NCBI Primer Blast
mTET2	mTET2 forw	GCCGAGCCTAGAGAACAGAC	Eurofins Genomics	NCBI Primer Blast
	mTET2 rev	CCGTAGCGGAACAGGAACAA	Eurofins Genomics	NCBI Primer Blast
mTET3	mTET3 forw	GAAGGAGAAACTGAGCACGC	Eurofins Genomics	(Watanabe et al., 2019)
	mTET3 rev	AATCCACCCTTCAGAGACAGG	Eurofins Genomics	(Watanabe et al., 2019)
mUHRF1	mUHRF1 forw	TCCAGAGCATGGAGTGGACA	Eurofins Genomics	NCBI Primer Blast
	mUHRF1 rev	TCATACCAGAAGCCGCGTTT	Eurofins Genomics	NCBI Primer Blast

3.1.3 TaqMan® Gene Expression Assays

Gene Name	Species	Assay ID	Supplier
Abcb1a (Pgp)	mouse	Mm00440761_m1	Thermo Scientific
Abcg2 (BCRP)	mouse	Mm00496364_m1	Thermo Scientific
PPIA	mouse	Mm02342429_g1	Thermo Scientific
Cldn5	mouse	Mm00727012_s1	Thermo Scientific
Actb (Actin beta)	mouse	Mm01205647_g1	Thermo Scientific
Gapdh	mouse	Mm99999915_g1	Thermo Scientific

3.1.4 Chemicals and Reagents

	Product Number	Supplier
2-Mercaptoethanol (β-Mercaptoethanol)	M3148	Sigma
Ammonium persulfate (APS)	A3678	Sigma
Boric acid	B6768	Sigma
Bovine Serum Albumin (=BSA)	A9647	Sigma
Clarity Western ECL Substrate	1705061	BIO-RAD
Dimethyl sulfoxide (DMSO)	D2650	Sigma
di-Sodium hydrogen phosphate dihydrate	106580	Merck
DPBS (Dulbecco's phosphate-buffered saline)	D8537	Sigma
DreamTaq Green PCR Master Mix (2X)	K1081	Thermo Scientific
Dulbecco′s Modified Eagle′s Medium (DMEM) - high glucose	D5796	Sigma
Ethanol	100983	Merck
Ethylenediaminetetraacetic acid disodium salt dihydrate	E5134	Sigma
Fetal Bovine Serum (FBS)	F9665	Sigma
GeneRuler 1 kb Plus DNA Ladder	SM1333	Thermo Scientific
Glycerol	G2025	Sigma
Glycine	50046	Sigma
Hydrochloric acid	258148	EMD Millipore
iTaq™ Universal Probes Supermix	1725131	BIO-RAD
LE Agarose	840004	Biozym
Methanol	106009	Merck
Midori Green Advance	617004	Biozym
N,N,N',N'-Tetramethylethylendiamin (TEMED)	110732	Merck

Nitrocellulose-Membrane 0,2µm	1620112	BIO-RAD
Paraformaldehyde	158127	Sigma
Penicillin-Streptomycin (PenStrep)	15140122	Gibco
peqGOLD-Protein-Marker V	27-2210	Peqlab
PerfeCTa SYBR Green FastMix ROX	733-1385	QIAGEN
Potassium chloride	104936	Merck
Potassium dihydrogen phosphate	104873	Merck
ProSieve™ 50 Gel Solution	50618	Lonza
Protease Inhibitor Cocktail (=PIC (100x))	P8340	Sigma
Puromycin dihydrochloride	P9620	Sigma
RIPA Buffer 10X	20-188	EMD Millipore
SDS-PAGE Sample Loading Buffer [6X]	786-701	G-Biosciences
Sodium azide	S8032	Sigma
Sodium chloride	S3014	Sigma
Sodium n-Dodecyl Sulfate	428023	Calbiochem
Tricine	T0377	Sigma
Trizma® base (= TRIS)	T6066	Sigma
Trypsin-EDTA (0.05%)	25300062	Gibco
TWEEN® 20	P9416	Sigma

3.1.5 Solutions and Buffers

PBS (10x), pH = 7.4

Substance	Weight portion
NaCl	80 g
KCl	2 g
Na2HPO4 · 2 H2O	9.6 g
KH2PO4	2 g
ddH2O	Ad 1 L

The pH was adjusted with 20 % HCl using a pH meter. After preparation the solution was autoclaved and stored at RT.

TBE (10x), pH = 8.3

Substance	Weight portion
TRIS	108 g
Boric acid	55 g
Na_2EDTA	9.3 g
ddH_2O	Ad 1 L

The pH was adjusted with 20 % HCl using a pH meter. After preparation the solution was autoclaved and stored at RT.

PBS-T (PBS + 0.1 % Tween 20)

Substance	Weight portion
PBS (10x)	100 mL
TWEEN® 20	1 mL
ddH_2O	Ad 1000 mL

After preparation the solution was stored at 4°C.

TRIS-Tricine (10x) Buffer

Substance	Weight portion
TRIS	121 g
Tricine	179 g
ddH_2O	Ad 1000 mL

After preparation the solution was autoclaved and stored at 4°C.

Electrophoresis Buffer

Substance	Weight portion
TRIS/Tricine (10x)	100 mL
10 % SDS solution	10 mL
ddH_2O	Ad 1000 mL

After preparation the solution was stored at 4°C.

TRIS-Glycin (10x) Buffer

Substance	Weight portion
TRIS	30 g
Glycine	144 g
ddH_2O	Ad 1000 mL

After preparation the solution was autoclaved and stored at 4°C.

Blotting Buffer

Substance	Weight portion
TRIS-Glycin (10x)	100 mL
Methanol	200 mL
10 % SDS-Solution	200 µL
ddH_2O	Ad 1000 mL

After preparation the solution was stored at 4°C.

TRIS-HCl (pH 6,8)

Substance	Weight portion
TRIS	121.14 g
HCl	*q.s.*
ddH_2O	Ad 1000 mL

First, TRIS was dissolved in 800 mL ddH2O, then pH was adjusted with 20 % HCl using a pH meter and finally the remaining amount of water was added.

Stripping Buffer

Concentration	Substance	Weight portion
62.5 mM	TRIS-HCl (pH 6.8)	3.79 g
2 %	SDS	10 g
	ddH_2O	Ad 500 mL

Additionally, β-mercaptoethanol had to be added freshly before use (71.6 µl β-mercaptoethanol per 10 mL buffer).

Lysis Buffer

Substance	Weight portion
RIPA (10x)	100 µl
PIC (100x)	1 µl
ddH_2O	Ad 1 mL

PIC (100x) was added freshly before use.

Cell Culture Medium DMEM++

Substance	Weight portion
DMEM	500 mL
FBS	50 mL
Pen Strep, 100X	5 mL

After preparation the medium was stored at 4°C.

Cell Culture Medium for CTRL and KO cell lines

DMEM++ (+2 µg/mL Puromycin)

Substance	Weight portion
DMEM	500 mL
FBS	50 mL
Pen Strep, 100X	5 mL
Puromycin (10 mg/mL)	0.1 mL

After preparation the medium was stored at 4°C.

0.5% Gelatine Solution

Substance	Weight portion
Gelatine	2.5 g
ddH_2O	500 mL

First the gelatine was dissolved under constant stirring conditions at 60°C for one hour and was then autoclaved and stored at RT.

TAT-MeCP2-Solution

	Buffer	Bulk (Date of manufacture)	Acknowledgement
Recombinant TAT-MeCP2 solution (3.3 mg/mL respectively 56.1568 µM)	DPBS + 200 mM NaCl + 10%Glycerin pH=7,2	11th July 2019	Many thanks go to Alexander V. Beribisky for providing the TAT-MeCP2 for this work.

3.1.6 Kits

	Product Number	Supplier
RNeasy Plus Mini Kit	74134	QIAGEN
Pierce™ BCA Protein Assay Kit	23227	Thermo Scientific
iScript™ gDNA Clear cDNA Synthesis Kit	172-5035	BIO-RAD

3.1.7 Used Cell Lines

Immortalized mouse cerebellar capillary endothelial cell line (cerebEND)	**AIT, grant of Carola Förster Universitätsklinikum Würzburg, Germany (Förster et al., 2005). Thanks to Kathrin Rose for preparing the cerebEND clones, used in this work.**
cerebEND wildtype (WT)	Wildtype phenotype cells.
cerebEND HDR control (CTRL) clone 11F16	Gene insertion of MeCP2 via homology directed repair (HDR).
cerebEND knock-out (KO) clone 11F12	Gene knockout of MeCP2 generated with the editing tool CRSPR/Cas9.

Immortalized mouse neuronal astrocyte cell line (C8D1A)	**AIT, thanks to Anna Gerhartl for providing the astrocyte cell line and Kathrin Rose for preparing the clones, used in this work.**
C8D1A wildtype (WT)	Wildtype phenotype cells.
C8D1A HDR control (CTRL) clones 3G2 and 2D5	Gene insertion of MeCP2 via homology directed repair (HDR).
C8D1A knock-out (KO) clones 3F12 and1B9	Gene knockout of MeCP2 generated with the editing tool CRSPR/Cas9.

3.2 Methods

3.2.1 Cell Culture

3.2.1.1 Cultivation of immortalized mouse cerebellar capillary endothelial cells

All steps in the cell culture were performed in the laminar air flow. Media and working solutions were prewarmed at 37°C in a bead bath before usage. Working steps in the cell culture were adapted from previous work of the research group (Reitner, 2018).

The cerebENDs were cultivated in either T25 or T75 gelatine coated cell culture flasks in an incubator at 37°C and 5% CO_2 + 95% humidity. DMEM++ was used as medium for the WT cell lines and DMEM++ (+2 µg/mL Puromycin) was used for the CTRL and KO cell lines. The medium was changed three times a week. The cells were usually subcultivated once a week since they reached confluence.

3.2.1.2 Coating

The cell culture flasks were coated before usage with 0.5% gelatine solution. 2 mL of the gelatine solution were filled into a T25 cell culture flask, respectively 5 mL were filled in a T75 flask, and the flask was swayed until the growth area was completely covered. The flask was then left for 30 minutes in the laminar air flow. Afterwards the gelatine solution was completely aspirated, and the flask was ready for cell seeding.

3.2.1.3 Splitting (Passaging) of the cerebENDs

After an average of one week the cerebellar capillary endothelial cells were assessed for confluency with a light microscope.

The morphological characteristics of confluent cerebENDs are narrow and elongated shape of the cells and the appearance of concentric circles shown in Figure 3.

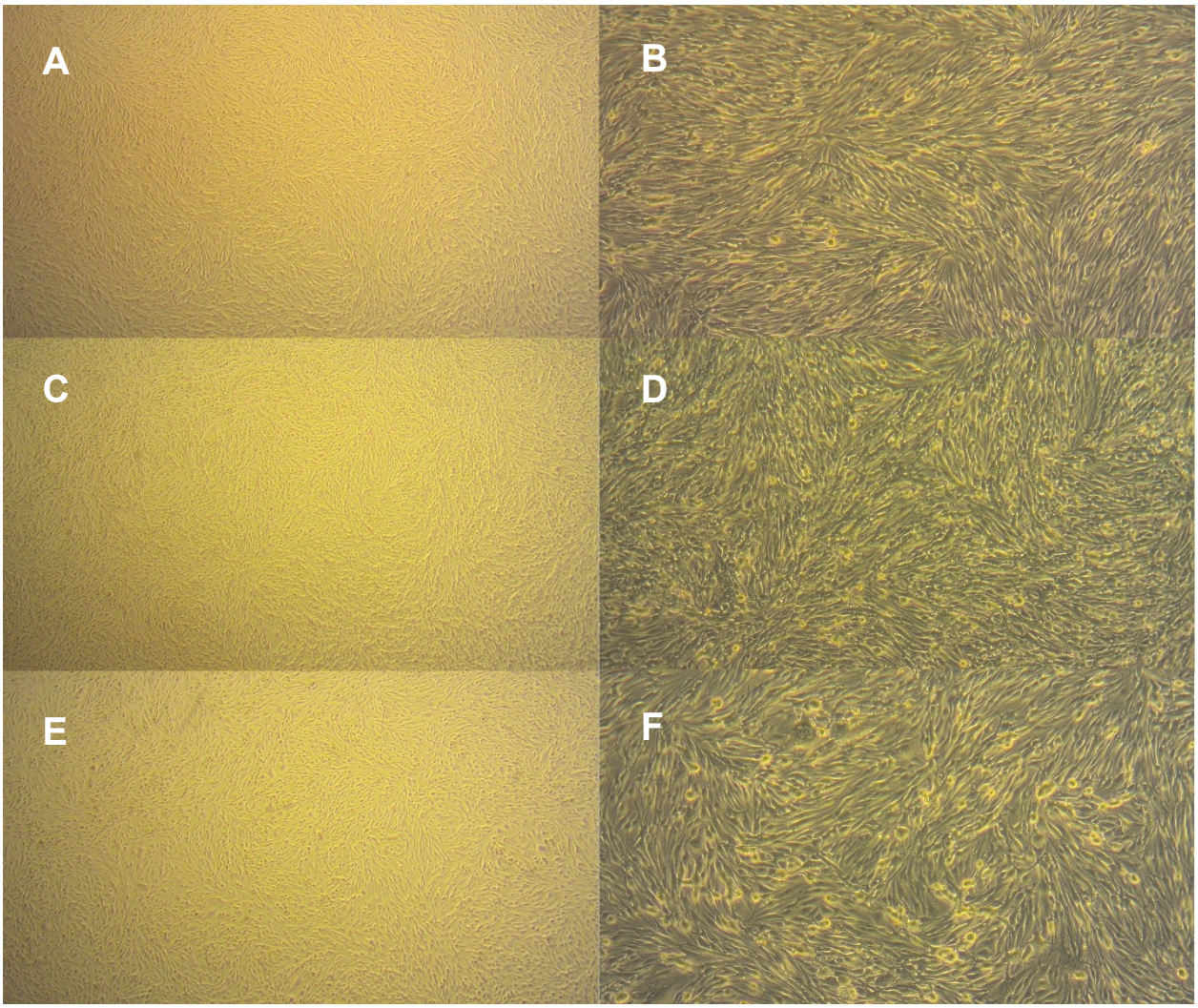

Figure 3: Confluent cerebENDs under a light microscope: ***A.*** *cerebENDs WT in 4x magnification,* ***B.*** *cerebENDs WT in 10x magnification,* ***C.*** *cerebENDs CTRL in 4x magnification,* ***D.*** *cerebENDs CTRL in 10x magnification,* ***E.*** *cerebENDs KO in 4x magnification,* ***F.*** *cerebENDs KO in 10x magnification.*

After the assessment of confluency, passaging of the cells was initiated. The medium (DMEM++) and Trypsin/EDTA were warmed in a bead bath. The cells were taken out of the incubator and the consumed medium was completely aspirated. Then the cell layer was washed with DPBS at least two times. Afterwards, the washing solution was aspirated and Trypsin/EDTA was added. To cover the whole cell layer the flask was gently shaken and was then left for incubation in the incubator at 37°C for four minutes. Afterwards, the flask was tapped on a hard surface to detach the cells. Detachment was verified with a light microscope. After that, fresh medium (DMEM++) was added to stop the enzymatic activity of trypsin. The medium was rinsed over the entire growth area and the cell suspension was resuspended at least ten times to disrupt the cerebENDs. Finally, an aliquot of one third (e.g., 2 mL of total 6 mL cell suspension) of the cell suspension was transferred into a new cell culture flask and the missing volume of DMEM++ was added. Consequently, the split ratio of the cerebENDs was 1:3. Table 3 shows the volumes of the two

sizes of cell culture flasks used in this work.

Table 3: Overview of the used volumes to passage cells grown in either a T25 or T75 cell culture flask.

Cell Culture Flask	Growth Medium (DMEM++)	Volume of Washing Solution (DPBS)	Trypsin/EDTA	Volume of added DMEM++ to stop trypsinization
T25	5 mL	2 mL	0.7 mL	5.3 mL
T75	15 mL	5 mL	2 mL	7 mL

3.2.1.4 Cultivation of immortalized mouse brain astrocyte cells (C8D1A)

All steps in the cell culture were performed in the laminar air flow. Media and working solutions were always prewarmed at 37°C in a bead bath before usage.

The astrocytes were cultivated in either T25 or T75 gelatine coated cell culture flasks in an incubator at 37°C and 5% CO_2 + 95% humidity. DMEM++ was used as medium for the WT cell lines and DMEM++ (+2 µg/mL Puromycin) was used for the CTRL and KO cell lines. The medium was changed three times a week. The cells were usually subcultivated once a week since they reached confluence.

3.2.1.5 Splitting (Passaging) of the C8D1A

After an average of one week the astrocytes were assessed for confluency with a light microscope.

The morphological characteristics of confluent astrocytes are narrow and elongated shape of the cells, the appearance of diffuse pattern of the cell layer and the beginning of detachment of the cells, as shown in Figure 4.

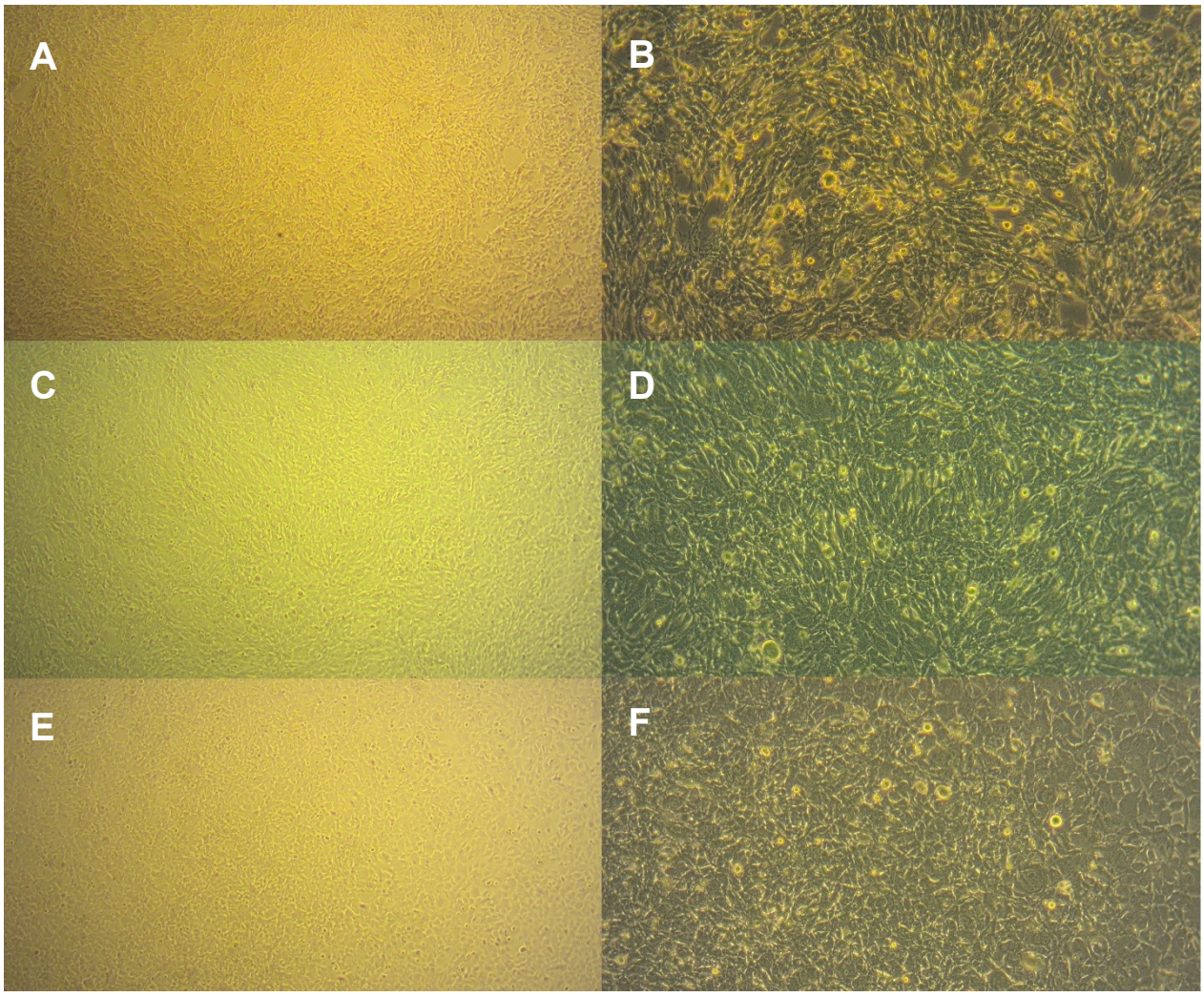

Figure 4: Confluent immortalized mouse neuronal astrocytes (C8D1A) under a light microscope: ***A.*** *C8D1A WT in 4x magnification,* ***B.*** *C8D1A WT in 10x magnification,* ***C.*** *C8D1A CTRL in 4x magnification,* ***D.*** *C8D1A CTRL in 10x magnification,* ***E.*** *C8D1A KO in 4x magnification,* ***F.*** *C8D1A KO in 10x magnification.*

Splitting of the C8D1A was performed the same way as passaging of the cerebENDs as described above with a difference in the splitting ratio, as the astrocytes exhibit a higher division rate. The aliquot which was transferred into a new cell culture flask after trypsinization was a sixth, resulting in a splitting ratio of 1:6 (e.g., 1 mL of 6 mL cell suspension).

3.2.2 TAT-MeCP2 substitution experiment

3.2.2.1 Cell Seeding in a 12-well plate

For the TAT-MeCP2 experiment the cerebEND cells and the astrocytes had to be seeded and grown in 12-well plates. Each of the three cell lines (WT, CTRL and KO) was seeded in 18 wells of two different 12-well plates.

To maintain optimum growing conditions, 40,000 cells/cm^2 were seeded in the wells. Each well of the 12-well plate had a surface area of 3.8 cm^2, requiring approximately 1.53x10^5 cells per well. After trypsinization during the weekly splitting process the cells obtained in a suspension were counted with an automatic cell counting system (TC20 Automated Cell Counter, BIO-RAD). Afterwards a suspension of 1.53x10^5 cells/mL was prepared in DMEM++. Then 1 mL of the suspension with 1.53x10^5 cells/mL was transferred in 18 different wells of two 12-well plates. After that 0.2 mL DMEM++ were added to the wells to achieve a volume of 1.2 mL medium per well. The medium was changed on the second and on the fifth day after seeding.

On the sixth day after the seeding different concentrations of DMEM++ with TAT-MeCP2 were prepared. TAT-MeCP2 was dissolved in a storage buffer (DPBS, 200mM NaCl, 10%Glycerin, pH=7,2) with a concentration of 3.3 mg/mL respectively 56.1568 µM. Table 4 shows an example of the preparation of the dilutions.

Table 4: Example of the preparation of a TAT-MeCP2 dilution series.

	DMEM++ (mL)	Storage Buffer (µL)	TAT-MeCP2 Stock-Solution (µL)
Baseline Control (BC)	22.7952	204.8	0.0
10 nM TAT-MeCP2	22.9959	200.7	4.1
30 nM TAT-MeCP2	22.9877	192.5	12.3
100 nM TAT-MeCP2	22.9590	163.8	41.0
500 nM TAT-MeCP2	22.7952	0.0	204.8

After the preparation of the various dilutions, the 12-well plates were taken out of the incubator and cells were assessed for confluency under a light microscope. When the cells appeared to be confluent the consumed medium was aspirated. Afterwards 1.2 mL of one of the prepared solutions were added per well and the 12-well plates were placed in the incubator again. The cells were treated with the TAT-MeCP2 media for either 24 or 48 hours.

After either 24 or 48 hours the cells were taken out of the incubator followed by transferring the consumed medium into 1.5 mL Eppendorf tubes. The used media were stored at -80°C. The cells were washed with 1 mL of DPBS and were prepared for cell lysis to collect RNA and protein samples.

3.2.3 Cell Lysis

3.2.3.1 Cell Lysis with RIPA Buffer to collect protein samples

All steps were performed on ice and the centrifuge was set up at 4°C. Working steps were adapted from previous work of the research group (Huber, 2019).

Lysis of cells on a 12-well plate

The 12-well plate was taken out of the incubator and was placed immediately on ice. The medium was aspirated, and each well was washed two times with 1 mL cold 1x PBS. After that, 50 µL lysis buffer (RIPA + PIC) was added dropwise to cover the whole monolayer. Cells were detached by using a cell scarper and the lysate was transferred into a 1.5 mL Eppendorf tube. The tubes were incubated afterwards for 15 minutes on ice. Then the tubes were centrifuged at 10,000 g at 4°C, followed by transferring the supernatant into another 1.5 mL Eppendorf tube. Finally, the samples were briefly immersed into liquid nitrogen to snapfreeze them. Protein samples were stored at -80°C.

Lysis of cells grown in a cell-culture flask

First, the T25 cell-culture flask was taken out of the incubator and the cell layer was washed two times with DPBS. Then, 0.7 mL Trypsin-EDTA (0.05%) was added, and the flask was incubated for four minutes in the incubator. After the cells detached from the flask, 5.3 mL DMEM was added, and the medium was resuspended several times in the flask. The cell suspension was then transferred into a 15 mL Falcon Tube and the tube was centrifuged for five minutes at 300 g at 4°C. Afterwards the medium was aspirated, the cell pellet was resuspended in 5 mL cold DPBS and the tube was again centrifuged for five minutes at 300 g at 4°C. This washing procedure was repeated a second time. After the second washing step the cell pellet was resuspended in 250 µL lysis buffer (RIPA+PIC) and the whole lysate was transferred into a cold 1.5 mL Eppendorf tube. The tube was incubated afterwards for 15 minutes on ice. Then the tube was centrifuged at 10,000 g at 4°C, followed by transferring the supernatant into another 1.5 mL Eppendorf tube. Finally, the sample was briefly immersed into liquid nitrogen to snapfreeze them. Protein samples were stored at -80°C.

3.2.3.2 Cell Lysis to extract and purify RNA

The extraction and purification of RNA samples were performed with RNeasy Plus Mini Kit (#74134, QIAGEN) (QIAGEN, 2020).

Before starting the extraction β-mercaptoethanol (β-ME) had to be added to buffer RLT Plus. 10 µL β-ME were added per 1 mL Buffer RLT Plus. Additionally, buffer RPE was supplied as a concentrate, so four volumes of ethanol 96% must be added prior to application to obtain a working solution. The medium of the cells grown on a monolayer in a 12-well plate was completely

aspirated and the wells were washed two times with 1 mL cold 1x PBS. Because the diameter of the growth surface area of a well was below 10 cm^2, the cells could be lysed directly in the well. For disrupting the cells, 350 µL buffer RLT Plus were added dropwise on the cell layer of each well. Cells were detached by using a cell scarper and the lysate was transferred into a 1.5 mL Eppendorf tube. The lysate was then homogenized by resuspending it through a 0.9 mm needle (Sterican® ø 0,90 x 40 mm, #4657519 BRAUN) fitted on a syringe for at least five times. The homogenized lysate was transferred into a gDNA Eliminator spin column placed in a 2 mL collection tube and the tube was centrifuged for 30 seconds at 8,000 g at RT. Afterwards the column was discarded, 350 µL 70% ethanol were added to the flowthrough and mixed by pipetting. The sample was then transferred into a RNeasy spin column placed in a 2 mL collection tube and the tube was centrifuged for 15 seconds at 8,000 g at RT. The flowthrough was discarded and 700 µL Buffer RW1 were added to the RNeasy spin column. The tube was centrifuged again for 15 seconds at 8,000 g at RT and the flowthrough was discarded. After that 500 µL buffer RPE were added to the RNeasy spin column, the tube was centrifuged for 15 seconds at 8,000 g at RT to wash the spin column membrane and the flowthrough was discarded. Then 500 µL buffer RPE were added again to the RNeasy spin column and the tube was centrifuged for 2 minutes at 8,000 g at RT. The RNeasy spin column was placed in a new 2 mL collection tube and the tube was centrifuged for one minute at 16,000 g at RT. Afterwards the RNeasy spin column was placed in a new 1.5 mL collection tube, 30 µL RNase-free water were added and the tube was centrifuged for one minute at 8,000 g at RT to elute the RNA. Finally, the 30 µL eluted RNA were pipetted again on the RNeasy spin column and the tube was centrifuged for one minute at 8,000 g at RT. RNA samples were stored at -80°C (QIAGEN, 2020).

3.2.4 Nucleic Acid Quantification

The quantification of the nucleic acid samples was performed with the NanoDrop® ND-1000 Spectrophotometer.

The measurement of the nucleic acid samples was carried out by selecting the ‘Nucleic Acid’ application module. RNase free water was applied as blank and 1.5 µL of the sample was measured.

3.2.5 cDNA Synthesis

The cDNA synthesis was performed with the iScript™ gDNA Clear cDNA Synthesis Kit #172-5035, BIO-RAD (BIO-RAD, 2023). All steps were performed on ice and nuclease free tubes were used (QPCR Tube Strips 0.2 mL #82-1502-A, PeqLab).

Before starting with the cDNA synthesis, the RNA samples had been diluted with RNase free water to achieve a concentration of 1 µg RNA in 14 µL. For removing any genomic DNA, a DNase

Master Mix was made by mixing 0.5 µL iScript DNase and 1.5µL iScript DNase Buffer per reaction. After that, 2 µL DNase Master Mix were added to 14 µL RNA sample by pipetting up and down several times. A thermal cycler was used to incubate the reaction with the settings shown in Table 5 (BIO-RAD, 2023).

Table 5: Thermal cycler setup for DNA digestion (BIO-RAD, 2023).

Step	Temperature (°C)	Time (min)
DNA digestion	25	5
DNase inactivation	75	5
Storage conditions	4; ice	Until RT step

Afterwards 4 µL iScript Reverse Transcription Supermix were added to the 16 µL DNase-treated RNA template. The sample was mixed by pipetting up and down. Reverse transcription was performed by using a thermal cycler with the setup shown in Table 6 (BIO-RAD, 2023).

Table 6: Thermal cycler setup for reverse transcription (BIO-RAD, 2023).

Step	Temperature (°C)	Time (min)
Priming	25	5
Reverse transcription	46	20
RT inactivation	95	1
Hold (optional)	4	-

After the reaction was finished, cDNA samples were stored at -20°C.

3.2.6 Protein Quantification

Protein quantification was performed with the Pierce™ BCA Protein Assay Kit #23227, Thermo Scientific™(Thermo-Fisher-Scientific, 2020). Working steps were adapted from previous work of the research group (Huber, 2019)

First a stock solution of BSA with a concentration of 2 mg/mL using the lysis buffer (RIPA + PIC) as solvent was prepared. Then a standard series of BSA solutions was established in 1.5 mL Eppendorf tubes (Table 7) (Thermo-Fisher-Scientific, 2020).

Table 7: Dilution scheme for establishing the BSA standard series (Thermo-Fisher-Scientific, 2020).

Tube	Solvent / Lysis Buffer	BSA-stock solution	BSA concentration
A	75 µL	225 µL	1,500 µg/mL
B	250 µL	250 µL	1,000 µg/mL
C	175 µL	175 µL of tube A	750 µg/mL
D	325 µL	325 µL of tube B	500 µg/mL
E	325 µL	325 µL of tube D	250 µg/mL
F	325 µL	325 µL of tube E	125 µg/mL
G	400 µL	100 µL of tube F	25 µg/mL
H	400 µL		0 µg/mL

For quantification the protein samples were thawed and diluted 1:15 with RIPA Buffer. Samples and standard solutions (tubes A-H) were pipetted as triplicates into a 96-well plate using a volume of 25 µL per well. Afterwards the BCA working reagent was prepared by mixing Reagent A and Reagent B in a 50:1 ratio. 200 µL of the BCA working reagent was added with a multichannel pipette to each well of the plate. Finally, the plate was shaken gently and left for incubation at 37°C for 30 minutes (Thermo-Fisher-Scientific, 2020).

Due to the lack of a suitable filter for 562 nm, the absorbance was measured at 570 nm wavelength at RT with an UV/Vis- spectrophotometer. The standard curve for determining the concentration of the protein samples was created with the program GraphPad PRISM.

3.2.7 SDS Polyacrylamide Gel Electrophoresis and Western Blot

Gel Electrophoresis and Western Blotting were performed with the BIO-RAD Mini-PROTEAN® Tetra System. Working steps were adapted from previous work of the research group (Huber, 2019)

3.2.7.1 Gel Preparation

For two gels, all reagents (table 8 provides an overview of the two used gel recipes) were mixed in a 50 mL Falcon tube. TEMED was added right before use. After vortexing, the separating gel was poured between the two glass plates of the Mini-PROTEAN® casting module. The gel was then overlayed with 1 mL isopropanol and left for polymerization for 30 minutes. After solidification isopropanol was removed and the stacking gel was poured onto the polymerized separating gel. Combs were inserted air bubble-free, and the gel was left for another 20 minutes. The gels were normally used on the day of preparation; however, they could be stored between wet paper towels in the fridge for several days.

Table 8: Gel recipe for 10% separating gel and 5% stacking gel.

10% Separating Gel	
ddH_2O	10.6 mL
ProSieve™ 50 Gel Solution	4 mL
1.5 M Tris/HCl	5 mL
10% SDS-Solution	200 µL
10% APS	200 µL
TEMED	8 µL

5% Stacking Gel	
ddH_2O	3.75 mL
ProSieve™ 50 Gel Solution	0.5 mL
1 M Tris/HCl	0.65 mL
10% SDS-Solution	50 µL
10% APS	50 µL
TEMED	5 µL

3.2.7.2 Sample Preparation

The protein solutions were diluted with ddH_2O achieving a defined concentration of 10 to 20 µg protein per 20 µL solution. Then 4 µL of SDS-PAGE Sample Loading Buffer [6x] and 5% 2-mercaptoethanol were added and the samples were incubated for denaturation at 95°C for 5 minutes.

3.2.7.3 Gel electrophoresis

The gel was placed into the electrophoresis cell and the unit was filled up with Electrophoresis Buffer until the gel was covered. Combs were removed and the wells of the stacking gel were washed with electrophoresis buffer. 5 µL peqGOLD-Protein-Marker V and 24 µL of the samples were loaded into the wells of the gel. The gel was running at 130 V at 4°C for an average of one hour.

3.2.7.4 Transfer

The gel was taken out of the electrophoresis cell, electrophoresis buffer was discarded, and the stacking gel was cut off. Afterwards a blotting sandwich was formed: The sandwich contained the separating gel, a nitrocellulose-membrane (#1620112, BIO-RAD), two layers of blotting paper and a sponge. The whole sandwich was moistened with blotting buffer and air bubbles were removed by flattening it with a plastic roller. Then, the blotting sandwich was placed into the electrophoresis unit and the unit was filled up with blotting buffer. Additionally, an ice rack was added to ensure cooling during the process. Electroblotting was performed with 0.35 A for one hour in the fridge at 4°C. The nitrocellulose membrane was taken out of the cell and was stained with Ponceau S to visualize the protein bands. After that the membrane was cut into strips containing the proteins of interest.

3.2.7.5 Blocking

The membrane was washed after staining with 15 mL PBS-T (PBS + 0.1% TWEEN 20). Afterwards blocking was performed with 15 mL 5%-milk powder solution in PBS-T for at least one hour at RT on a shaker.

3.2.7.6 Primary Antibody Incubation

For the primary antibody solution, a 50 mL Falcon tube was filled with 5 mL cold 5% milk powder solution in PBS-T and 0.002% NaN_3 was added for microbial preservation. Then the primary antibody was added in the intended dilution and the Falcon tube was vortexed. The membrane strip with the protein of interest was placed into the Falcon tube. For incubation the strips in the Falcon tubes were rolled on a shaker overnight in a 4°C temperature room.

3.2.7.7 Secondary Antibody Incubation

The next day the membrane strips were taken out of the Falcon tube and washed for three times with PBS-T for five minutes each. The secondary antibody, diluted in 5% milk powder in PBS-T was applied to the strips for one hour under constant shaking conditions. After the incubation the membranes were washed again with PBS-T for five minutes for three times.

3.2.7.8 Detection

Detection was performed with the ChemiDoc™ Touch Imaging System.

BIO-RAD Clarity™ Western ECL Substrate was prepared freshly and 200-400 µL of the substrate, depending on the size of the membrane were applied for five minutes. Then, each strip was recorded in two different settings. First a colorimetric image was taken and afterwards the bands were visualized by chemiluminescence. Exposure times of the chemiluminescence image were additionally noted. After detection the strips could be stored in PBS-T at 4°C for reusage for several days. Densitometric evaluation was performed with the program Image Lab™ by Bio-Rad.

3.2.7.9 Stripping

For reusing the membranes “Stripping” could be performed. During this process primary and secondary antibodies which were bound to the membrane were removed.

The strip was taken out of the storage solution and was washed with fresh PBS-T three times for ten minutes. For each strip 30 mL Stripping Buffer were prepared in a glass with screw cap. Before use 215 µL 2-mercaptoethanol were added to the Stripping Buffer. The strip was placed into the glass and the lid was closed. The glass was left in a 56°C water bath for 20 minutes under constantly shaking conditions. After the removal of the antibodies the strip was washed three times with PBS-T for ten minutes. Blocking was performed with 5 % milk powder in PBS-T solution for one hour. Afterwards the membrane could be incubated with a primary antibody again.

3.2.8 PCR

The PCR was performed with the Bioer LifeTouch™ Thermal Cycler 96 Well TC-96/G/H(b)B. Table 9 shows the reagents used in a 20 µL reaction mix and Table 10 shows the adjusted cycling setup. Working steps were adapted from previous work of the research group (Huber, 2019).

Table 9: PCR 20 µL reaction mix.

20 µL reaction setup	
Nuclease-free water	6 µL
DreamTaq Green PCR MasterMix	10 µL
Forward-Primer	1 µL
Reverse-Primer	1 µL
cDNA template	2 µL

Table 10: PCR cycling setup.

PCR cycling setup		
95°C	3 min	
95°C	30 sec	35x
60°C	30 sec	repeated
72°C	45 sec	
72°C	5 min	
4°C	∞	

3.2.8.1 Agarose Gel preparation

For 100 mL gel, 2 g of agarose was weighed in an Erlenmeyer flask and was completely dissolved in 100 mL 0.5x TBE Buffer by boiling the solution in a microwave. Then 5 µL Midori Green were added to the 2% agarose solution and dissolved by gentle shaking. After that, the solution was poured into the gel trays with inserted combs of the Mupid™-One Electrophoresis System and the gel was left for 30 minutes for solidification.

3.2.8.2 Electrophoresis

The electrophoresis was performed with the Mupid™-One Electrophoresis System.

After the gel had been solidified, combs were removed, and the gel was placed in the electrophoresis unit. Then, the unit was filled with 0.5x TBE Buffer until the gel was completely covered. Next 5 µL of the sample and 5 µL of GeneRuler 1 kb Plus DNA Ladder were loaded on the gel. The electrophoresis ran 45 minutes at 100 V. The gel was then taken out of the unit and was visualized with the FluorChem™ HD2 System (Biozym).

3.2.8.3 Primer Design

Primers were designed using the NCBI Primer Blast Website (Ye et al., 2012).

A refseq record of the corresponding mouse gene was inserted into the tool and following settings were adapted:

- PCR-Product Size: 70-200 bp
- Primer melting temperatures (Tm): 57.0 – 63.0°C
- Database: Refseq mRNA

- Organism: Mus musculus (taxid:10090)

Received forward and reverse primer sequences were checked on appropriate product length, transcript variants and melting temperatures. Selected DNA olignucleotides were ordered from a supplier and analyzed with cDNA samples from wildtype cerebENDs. After the amplification the PCR products were applied on an agarose gel and an electrophoresis were initiated.

3.2.9 qPCR gene expression analysis

In this work gene expression of selected targets was analyzed by two different fluorescence detection methods: SYBR Green and Primer-Probe Detection.

Regardless of the used method, the cDNA samples, which contained 1 µg transcribed RNA in 20 µL were diluted with nuclease free water to a total volume of 200 µL cDNA template solution. Then, a Multiplate™ 96-Well PCR Plate (#MLL9601, BIORAD) was placed on ice and the following reaction components given in Table 11 were pipetted into each well.

Table 11: Overview of the used reagents for a SYBR Green Assay and a Taqman Assay.

SYBR Green Assay:		TaqMan Assay:	
5 µL	PerfeCTa SYBR Green FastMix ROX	7.5 µL	iTaq Universal Probes Supermix
0.2 µL	Forward-Primer	0.75 µL	TaqMan® Gene Expression Assay
0.2 µL	Reverse-Primer	4.75 µL	Nuclease free water
2.6 µL	Nuclease free water	2 µL	cDNA template
2 µL	cDNA template		

After the components were pipetted into the wells, a Microseal® 'C' PCR Plate Sealing Film (#MSC1001, BIORAD) was placed onto the 96-well plate. Then, the plate was centrifuged at 1,000 g at 4°C for five minutes.

Real-Time PCR was performed with the StepOnePlus™ Real-Time PCR System (Thermo Scientific). The mode Quantitative Comparative Ct (ΔΔ Ct) was selected with the software program (StepOne). Following thresholds were set to produce consistent comparable Ct values:

SYBR Green Assay:		TaqMan Assay:	
Ppia	1.3 ΔRn	Ppia	0.4 ΔRn
Dnmt1	2.4 ΔRn	Bcrp	0.5 ΔRn
Cldn5	2.5 ΔRn	Pgp	0.1 ΔRn

Evaluation was done with Microsoft Excel using equations 1-3.

$$\Delta Ct = Ct\,(\text{mean gene}) - Ct\,(\text{mean endogenous control}) \quad \text{(eq.1)}$$

$$\Delta\Delta Ct = \Delta Ct\,(\text{treated cells}) - \Delta Ct\,(\text{control cells untreated}) \quad \text{(eq.2)}$$

$$\text{Relative Quantification (RQ)} = 2\text{^}(-\Delta\Delta Ct) \quad \text{(eq.3)}$$

Table 12 shows an example for the evaluation of the mRNA expression of the two selected targets Dnmt1 and Claudin5, analyzed with a SYBR Green Assay.

Table 12: Example for the evaluation of a SYBR Green gene expression assay. PPIA was used as endogenous control. DNMT1 and Claudin-5 (Cldn5) were genes of interest. Data are represented as mean ± standard deviation.

	cerebENDs WT #0828	untreated	24h 100 nM TAT-MeCP2 treated	24h 500 nM TAT-MeCP2 treated
	Ppia Average CT	16.86±0.06	16.66±0.11	16.68±0.19
DNMT1	**Dnmt1 Average CT**	25.23±0.31	26.64±1.54	25±0.56
	ΔCT Dnmt1-Ppia	8.37±0.31	9.98±1.54	8.32±0.59
	ΔΔCT **($\Delta C_{T\,treated} - \Delta C_{T\,untreated}$)**	0±0.31	1.61±1.54	-0.05±0.59
	Relative Quantification 2^(-ΔΔCT)	1 (0.8-1.2)	0.3 (0.1-1)	1 (0.7-1.6)
Cldn5	**Cldn5 Average CT**	22.79±0.36	24.71±1.65	23.04±0.85
	ΔCT Cldn5-Ppia	5.93±0.37	8.05±1.65	6.36±0.87
	ΔΔCT **$\Delta C_{T\,treated} - \Delta C_{T\,untreated}$**	0±0.37	2.12±1.65	0.43±0.87
	Relative Quantification 2^(-ΔΔCT)	1 (0.8-1.3)	0.2 (0.1-0.7)	0.7 (0.4-1.4)

4 Results

4.1 Identifying possible MeCP2 dependent targets

4.1.1 Selection of targets for RT-qPCR analysis

Previous work with MeCP2 deficient immortalized mouse cerebellar capillary endothelial cells (cerebENDs) has shown that a loss of MeCP2 can alter the properties of the BBB. As cell-cell junctions determine paracellular tightness (Abbott et al., 2010) several tight junction proteins were taken into consideration for the identification of makers, that may be influenced by MeCP2. Additionally, because MeCP2 plays a main role in DNA modification (Chahrour et al., 2008) various enzymes involved in gene regulation were selected as possible MeCP2 dependent targets. Following genes were taken into consideration:

- All members of the TJ family of the Claudins (Cldn1 to Cldn27) and the TJ protein ZO-1
- The TJ associated marvel proteins (TAMPs) Occludin (Ocln) and Tricellulin (Tric)
- The adherens junction protein Cadherin5 (Cdh5)
- The inward rectifying potassium channel Kir4.1 and the brain-derived neurotrophic factor (BDNF)
- The DNA-methyltransferases DNMT1, DNMT3A, DNMT3B
- The Ten-eleven translocation methylcytosine dioxygenases TET1, TET2 and TET3
- The Ubiquitin-like, containing PHD and RING finger domains 1 (UHRF1)
- The genes commonly used as endogenous control actin beta (Actb), the peptidylprolyl isomerase A (PPIA) and beta-2 microglobulin (B2M)

Primer pairs, which target the nucleotide sequence of the aforementioned mouse genes, were either self-designed with the NCBI Primer Blast Website or adopted from literature.

4.1.2 Verification of Primer-Pairs for possible readout candidates

Confluent cells of the mouse cerebEND cell line were lysed and RNA samples were collected. RNA was then transcribed into cDNA. Afterwards PCR with cDNA and the primer pairs was performed. Amplified PCR products were applied on an agarose gel and were visualized. Suitable primer pairs had to show a distinct isolated band with the correct product length without displaying any alternative products. Figures 5 to 7 show the agarose gels with the visualized products of the tested primer pairs.

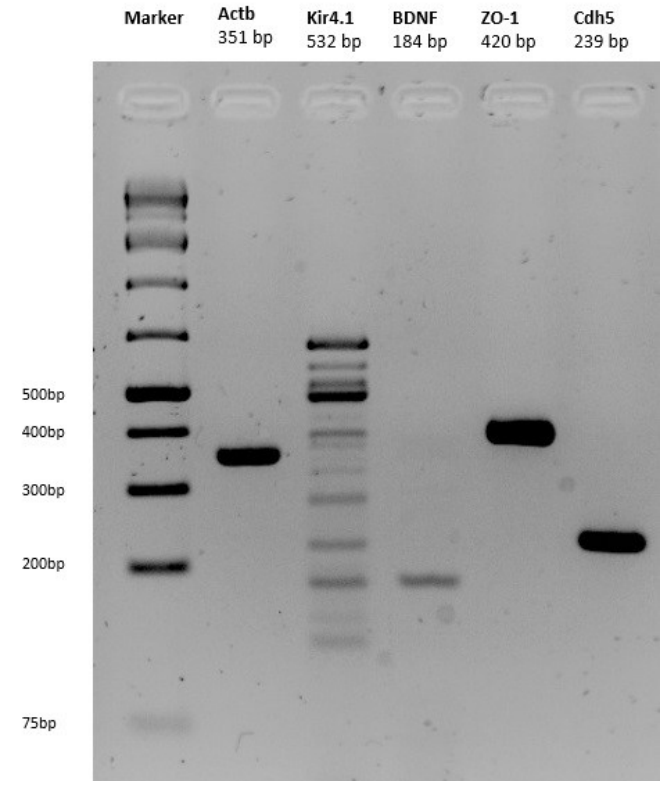

Figure 6: Agarose gel of cDNA samples of cerebENDs amplified with different primers. Below the gene of interest, the proper length of the corresponding PCR product is displayed. Actb=Actin beta; Kir4.1=Inward rectifier potassium channel 10; BDNF=Brain-derived neurotrophic factor; ZO-1=Zonula occludens-1; Cdh5=Cadherin5

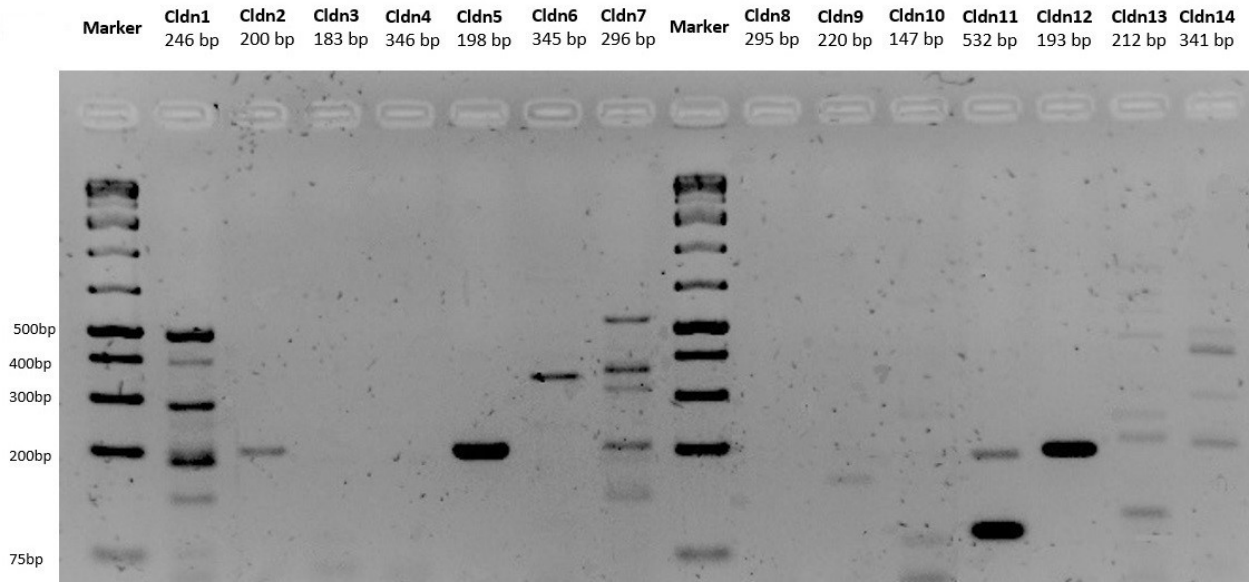

Figure 5: Agarose gel of cDNA samples of cerebENDs amplified with different primers. Below the gene of interest, the proper length of the corresponding PCR product is presented. Cldn1=Claudin-1; Cldn2=Claudin-2; Cldn3=Claudin-3; Cldn4=Claudin-4; Cldn5=Claudin-5; Cldn6=Claudin-6; Cldn7=Claudin-7; Cldn8=Claudin-8; Cldn9=Claudin-9; Cldn10=Claudin-10; Cldn11=Claudin-11; Cldn12=Claudin-12; Cldn13=Claudin-13; Cldn14=Claudin-14.

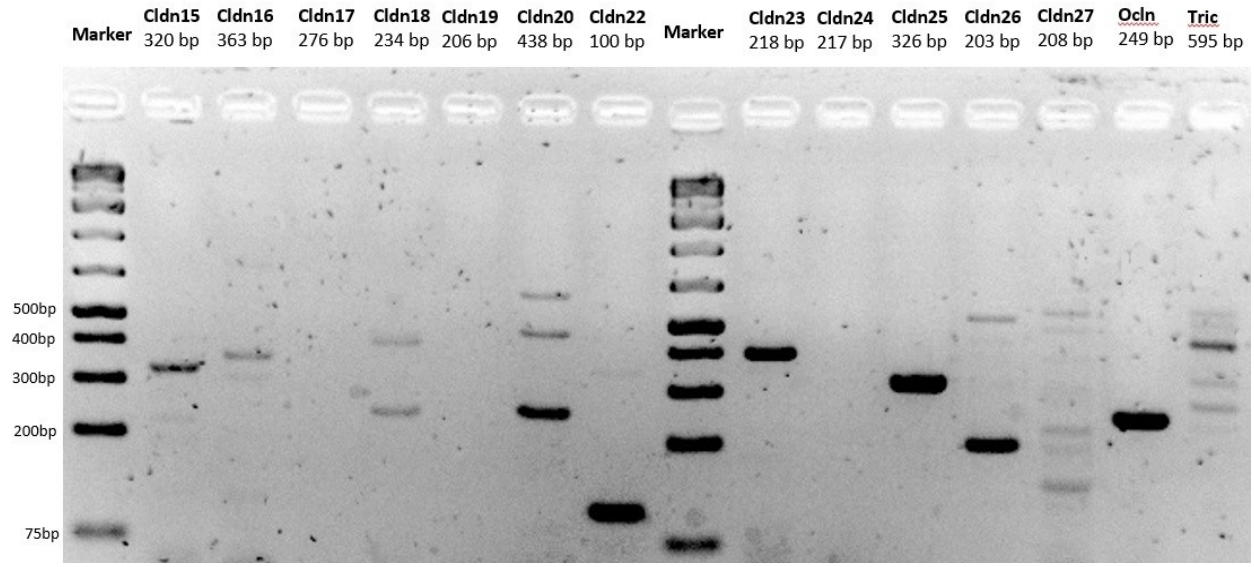

Figure 7: Agarose gel of cDNA samples of cerebENDs amplified with different primers. Below the gene of interest, the proper length of the corresponding PCR product is presented. Cldn15=Claudin-15; Cldn16=Claudin-16; Cldn17=Claudin-17; Cldn18=Claudin-18; Cldn19=Claudin-19; Cldn20=Claudin-20; Cldn22=Claudin-22; Cldn23=Claudin-23; Cldn24=Claudin-24; Cldn25=Claudin-25; Cldn26=Claudin-26; Cldn27=Claudin-27; Ocln=Occludin; Tric=Tricellulin.

Based on the results the primers for Cldn1, Cldn3, Cldn4, Cldn11, ZO-1, Tric and Kir4.1 seemed to be inappropriate and needed to be reconsidered, as they did not show a distinct isolated band on the gel. Furthermore, PCR product length of Actb was found to be too high for reliable qPCR, so an additional primer pair for Actb was ordered and had been tested. Figures 8 and 9 display the reconsidered primer pairs with the addition of the genes for the DNA modification enzymes and the endogenous control genes PPIA and B2M.

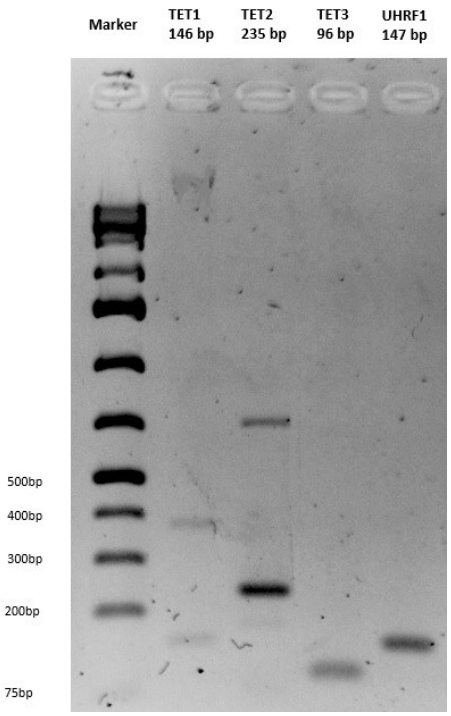

Figure 8: Agarose gel of cDNA samples of cerebENDs amplified with different primers. Below the gene of interest, the proper length of the corresponding PCR product is presented. TET1=Ten-eleven translocation methylcytosine dioxygenase 1; TET2=Ten-eleven translocation methylcytosine dioxygenase 2; TET3=Ten-eleven translocation methylcytosine dioxygenase 3; UHRF1=Ubiquitin-like, containing PHD and RING finger domains 1.

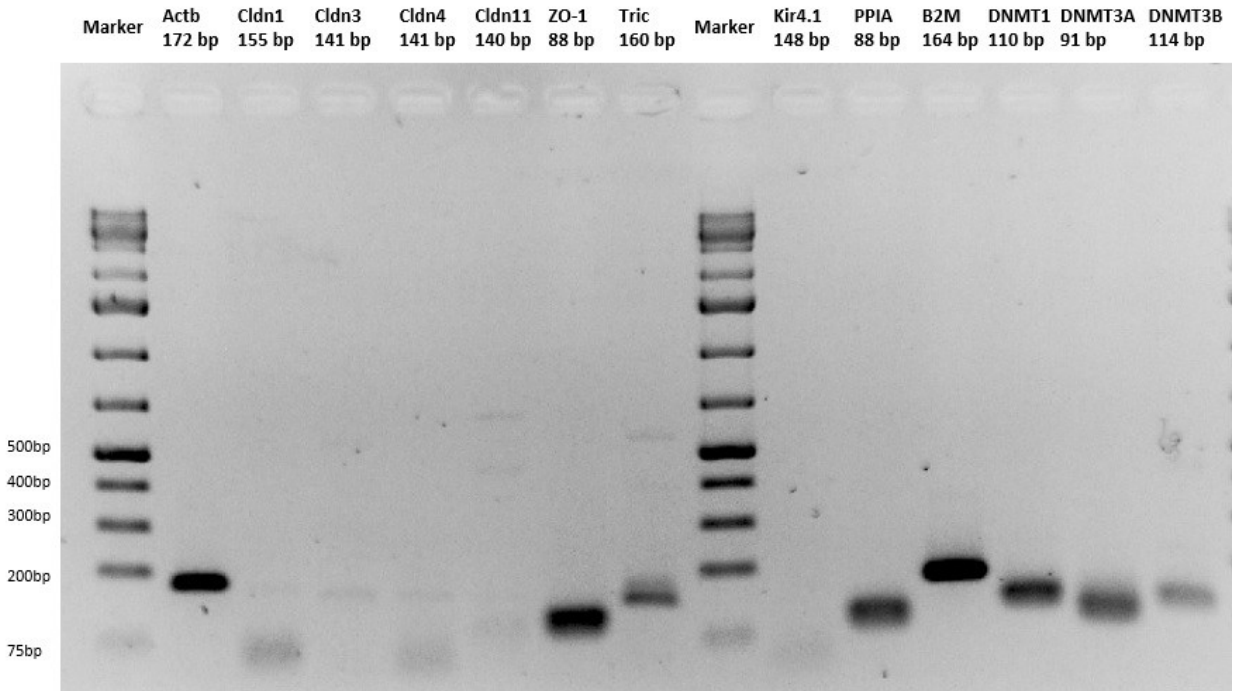

Figure 9: Agarose gel of cDNA samples of cerebENDs amplified with different primers. Below the gene of interest, the proper length of the corresponding PCR product is presented. Actb=Actin beta; Cldn1=Claudin-1; Cldn3=Claudin-3; Cldn4=Claudin-4; Cldn11=Claudin-11; ZO-1=Zonula occludens-1; Tric=Tricellulin; Kir4.1=inward rectifier potassium channel 10; PPIA= Peptidylprolyl isomerase A; B2M=Beta-2 microglobulin; DNMT1=DNA methyltransferase 1; DNMT3A=DNA methyltransferase 3A; DNMT3B=DNA methyltransferase 3B.

The results of the preceding agarose gels were taken to evaluate, whether a primer pair was suitable for the cerebEND cell line as a possible target for mRNA quantification. Table 13 provides an overview of the tested primer pairs and their suitability.

Table 13: Overview of tested primer pairs to check if they are suitable with the cerebEND cell line as possible readouts.

Primer product	Amplicon length (bp)	Distinct isolated band (+/-)	Comment	Readout candidate (+/-)
mActb	172	+		+
mPPIA	88	+		+
mB2M	164	+		+
mCldn1	155	+		+
mCldn2	200	+		+
mCldn3	141	-	No signal was detectable.	-
mCldn4	141	-	No signal was detectable.	-
mCldn5	198	+		+
mCldn6	345	+	Amplicon length might be too high for reliable qPCR.	-
mCldn7	296	-	Alternative products were detected.	-
mCldn8	295	-	No signal was detectable.	-
mCldn9	220	-	Band was detected in the wrong length.	-
mCldn10	147	-	No signal was detectable.	-
mCldn11	140	-	Alternative products were detected.	-
mCldn12	193	+		+
mCldn13	212	-	Alternative products were detected.	-
mCldn14	341	-	Alternative products were detected.	-
mCldn15	320	+	Amplicon length might be too high for reliable qPCR.	-
mCldn16	363	+	Amplicon length might be too high for reliable qPCR.	-
mCldn17	276	-	No signal was detectable.	-
mCldn18	234	-	Alternative products were detected.	-
mCldn19	206	-	No signal was detectable.	-
mCldn20	438	-	Alternative products were detected.	-
mCldn22	100	+		+
mCldn23	218	-	Band was detected in the incorrect length.	-
mCldn24	217	-	No signal was detectable.	-
mCldn25	326	+	Amplicon lenght might be too high for reliable qPCR.	-
mCldn26	203	-	Alternative products were detected.	-
mCldn27	208	-	Alternative products were detected.	-
mCdh5	239	+		+
mOcln	249	+		+
mTric	160	-	Alternative products were detected.	-
mZO1	88	+		+

mKir4.1	148	-	No signal was detectable.	-
mBDNF	184	+		+
mDNMT1	110	+		+
mDNMT3A	91	+		+
mDNMT3B	114	+		+
mTET1	146	-	Alternative products were detected.	-
mTET2	235	-	Alternative products were detected.	-
mTET3	96	+		+
mUHRF1	147	+		+

4.1.3 Verification of astrocyte readouts for western blot analysis

Since brain-derived neurotrophic factor BDNF (Chang et al., 2006) and the ATP-sensitive inward rectifier potassium channel 10 (Kir 4.1) (Kahanovitch et al., 2018) were published as MeCP2 dependent targets the aim was to find reliable antibodies for western blot analysis to display differences in the protein expression of the used mouse astrocyte (C8D1A) cell lines. For this purpose, antibodies for BDNF (#AB1534, Sigma) and for Kir4.1 (#APC-035, Alomone Labs) were purchased and tested with the astrocyte cell lines. Western blot with protein lysate samples from wildtype (WT), HDR control (CTRL) and knock out (KO) cells was performed. Two different clones of CTRL and KO astrocyte cells were applied for the two following blots.

The antibody for Kir4.1 seemed to work well, as the corresponding band was visualized at the correct molecular weight (~40 kDa), although CTRL and KO cells showed a slightly higher band than expected. This could indicate different protein modifications in the CTRL and KO cell lines. All in all, the antibody was found to be appropriate for Kir4.1 quantification (Figures 10 and 11).

Using the BDNF antibody however did not show an assignable band pattern. Mature BDNF should be displayed at ~14 kDa and pro BDNF can be visualized at 20-35 kDa according to the supplier. The bands on both blots could not be assigned properly (Figures 10 and 11), so an alternative antibody was ordered.

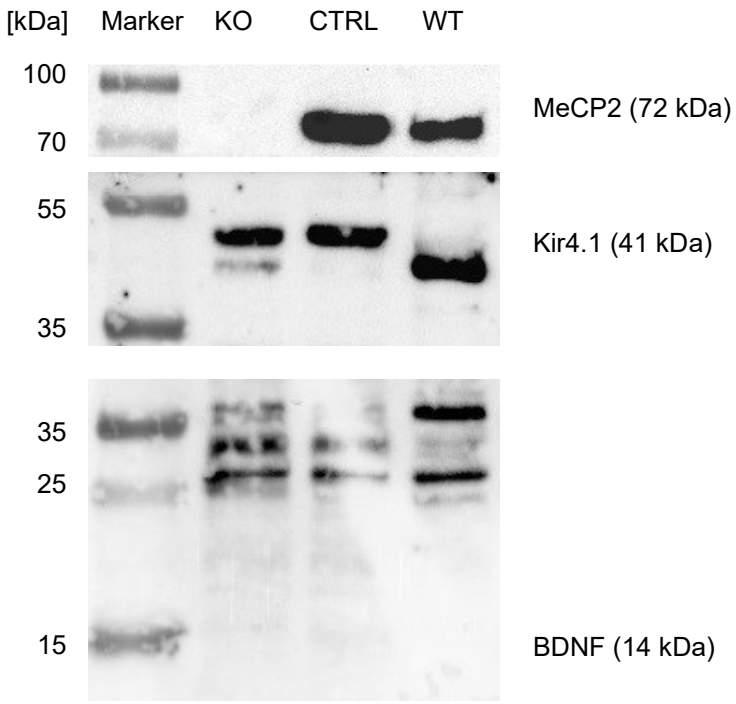

Figure 10: Western blot of immortalized mouse astrocytes (C8D1A). WT=wildtype cells, CTRL= HDR control cells (clone 2D5), KO=knock out cells (clone 1B9).

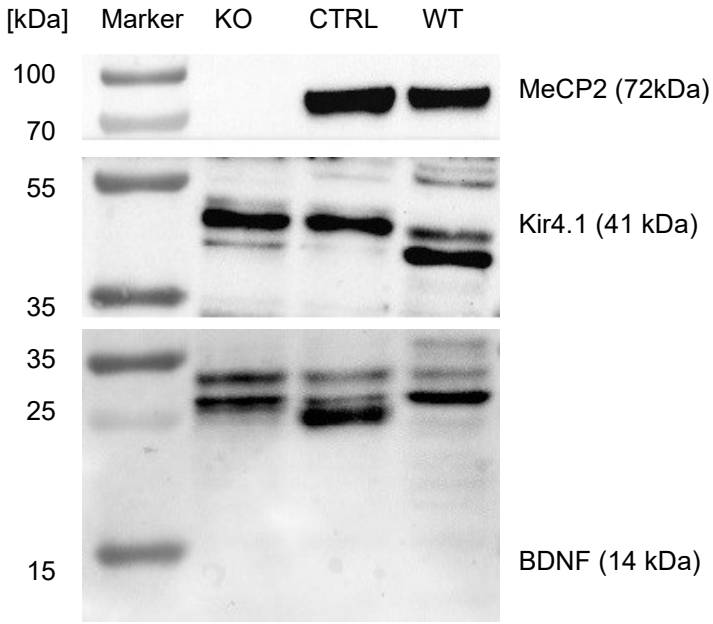

Figure 11: Western blot of immortalized mouse astrocytes (C8D1A). WT=wildtype cells, CTRL= HDR control cells (clone 3G2), KO=knock out cells (clone 3F12).

The second tested antibody for BDNF (#ANT-010, Alomone Labs) displayed a consistent band pattern. The most concise band around 20 kDa can be interpreted as a variant of proBDNF, which can be found between 20 to 35 kDa according to the manufacturer. However, a significant, but weak band around 14 kDa is also displayed in all three cell lines, therefore the antibody was deemed to be appropriate for BDNF quantification (Figure 12).

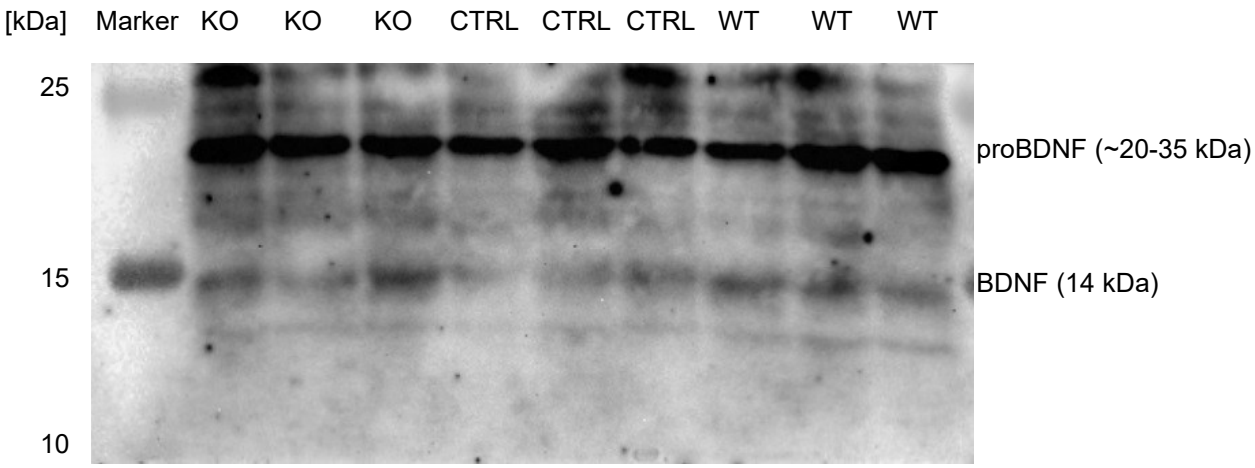

Figure 12: Western blot analysis of immortalized mouse astrocytes (C8D1A). WT=wildtype cells, CTRL= HDR control cells (clone 3G2), KO=knock out cells (clone 3F12).

One aim of this work was to find new possible MeCP2 dependent targets on the mRNA level, as well as to receive reliable antibodies for the identified MeCP2 dependent targets Kir4.1 and BDNF to be analyzed in mouse astrocytes. Further work with the astrocyte cell lines needs to be continued to investigate differences in the expression between the WT, CTRL and KO cell lines of the aforementioned targets and subsequently if treatment with TAT-MeCP2 can revert alterations in MeCP2 deficient cells. For this work it was decided to focus on brain endothelial cell lines, since previous data already showed regulation of the BBB targets such as Pgp in MeCP2 KO mouse brain endothelial cells (Neuhaus, 2018).

4.2 TAT-MeCP2 substitution experiment

Previous work with MeCP2 deficient immortalized mouse cerebellar capillary endothelial cells showed an increase in the protein levels of the ABC-transporters Pgp and Bcrp compared to wildtype cells (Neuhaus, 2018). Interestingly, recent studies showed that expression of the most present tight junction protein Cldn5 is decreased in MeCP2 deficient mice in the cortex and the striatum (Pepe et al., 2023). Based on these findings, the two ABC-transporters Pgp and Bcrp and the tight junction protein Cldn5 were chosen as target genes for the TAT-MeCP2 substitution experiment. Additionally, to investigate whether the DNA methyltransferases are possible MeCP2 dependent targets, DNMT1 was added to the genes of interest.

The substitution experiment with exogenous TAT-MeCP2 should on the one hand demonstrate, if addition of exogenous TAT-MeCP2 can alter the expression of predetermined readouts and on the other hand provide a reference point for the optimal concentration to reverse RTT phenotype. Finding the proper settings and concentration is crucial, because overexpression as well as knock-down or knock-out of MeCP2 can lead to abnormal cell function (Van Esch et al., 2005).

Based on previous experiments of the research group concentrations of 10 nM, 30 nM, 100 nM, and 500 nM TAT-MeCP2 were chosen, and cells were treated for 24 hours. Additionally, a 100 nM TAT-MeCP2 substitution experiment with a treatment duration of 48 hours was performed. Recombinant TAT-MeCP2 protein was added to the three used cerebEND cell lines (WT, CTRL and KO) grown on 12-well plates. After the treatment period, the cells were lysed, RNA was collected and transcribed into cDNA. Then, mRNA expression of four readout genes was analyzed with RT-qPCR. The four genes of interest included the ABC-transporters P-gp and Bcrp, the tight junction protein Cldn5 and the DNA methyl transferase DNMT1. Normalization was done with the housekeeping gene PPIA.

4.2.1 Comparison of target genes of untreated WT, CTRL and KO cerebENDs

In a first step, untreated samples of the 24h substitution experiments were compared to display differences in the mRNA expression of the readouts between the WT, the CTRL, and the KO cell lines. One-way ANOVA was performed to calculate mean differences between the three cell lines. DNMT1 mRNA expression was significantly lowered ($P<0.01$) in MeCP2 KO cells compared to wildtype cells (Figure 13). Furthermore, CTRL and KO cells exhibited reduced expression of Bcrp ($P<0.01$) compared to wildtype cerebENDs (Figure 15). While quantitative comparative qPCR analysis revealed an increase in the expression of Pgp ($P<0.01$) in CTRL and KO cells (Figure 16), no significant difference of Cldn5 could be observed between the three cell-lines (Figure 14).

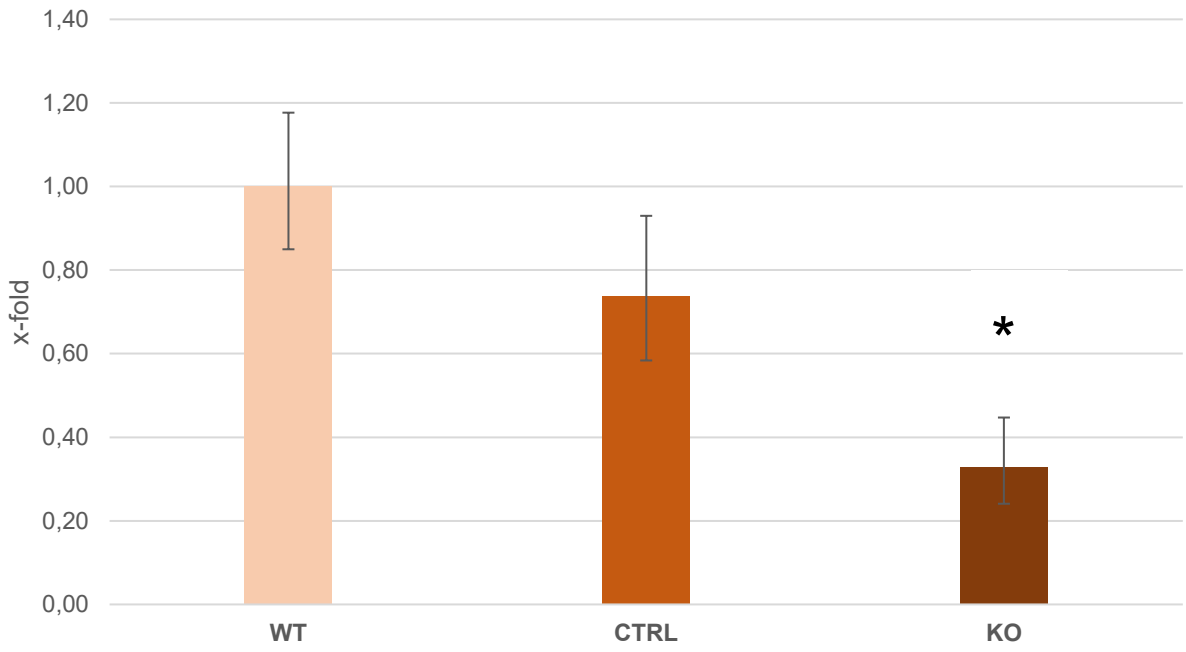

*Figure 13: Relative quantification of mRNA expression of DNMT1 of cerebEND cells. The signals were normalized to the endogenous control PPIA. Data are represented as mean ± SEM (n=12 biological replicants; N=4 experiments). Quantitative comparative qPCR analysis indicates statistically significant differences of DNMT1 between the displayed cell-lines P<0.05 (One-way ANOVA). Comparison between WT and KO cells showed a significant reduction (*P<0.01) (One-way ANOVA). WT=wildtype cells; CTRL=HDR control cells; KO=knock-out cells.*

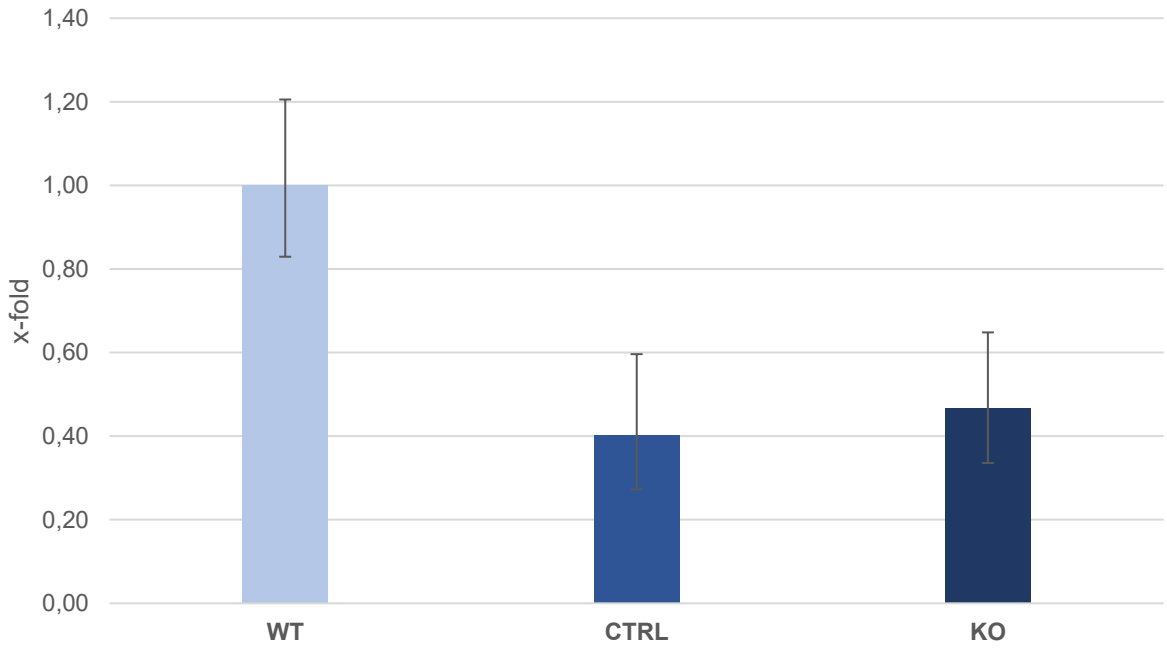

Figure 14: Relative quantification of mRNA expression of Cldn5 of cerebEND cells. The signals were normalized to the endogenous control PPIA. Data are represented as mean ± SEM (n=12 biological replicants; N=4 experiments). Quantitative comparative qPCR analysis indicates no statistically significant differences of Cldn5 between the displayed cell-lines P>0.05 (One-way ANOVA) WT=wildtype cells; CTRL=HDR control cells; KO=knock-out cells.

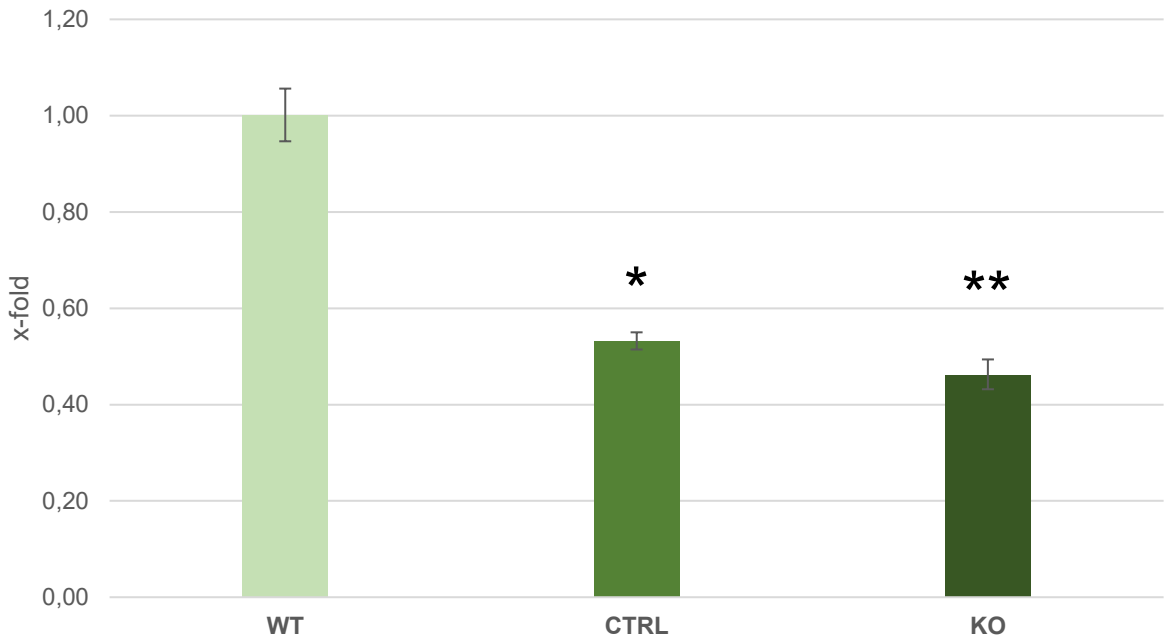

*Figure 15: Relative quantification of mRNA expression of Bcrp of cerebEND cells. The signals were normalized to the endogenous control PPIA. Data are represented as mean ± SEM (n=12 biological replicants; N=4 experiments). Quantitative comparative qPCR analysis indicates statistically significant difference of Bcrp between the displayed cell-lines P<0.01 (One-way ANOVA). Comparison between WT and CTRL (*P<0.01) cerebENDs and between WT and KO (**P<0.01) cerebENDs showed a significant reduction (One-way ANOVA). WT=wildtype cells; CTRL=HDR control cells; KO=knock-out cells.*

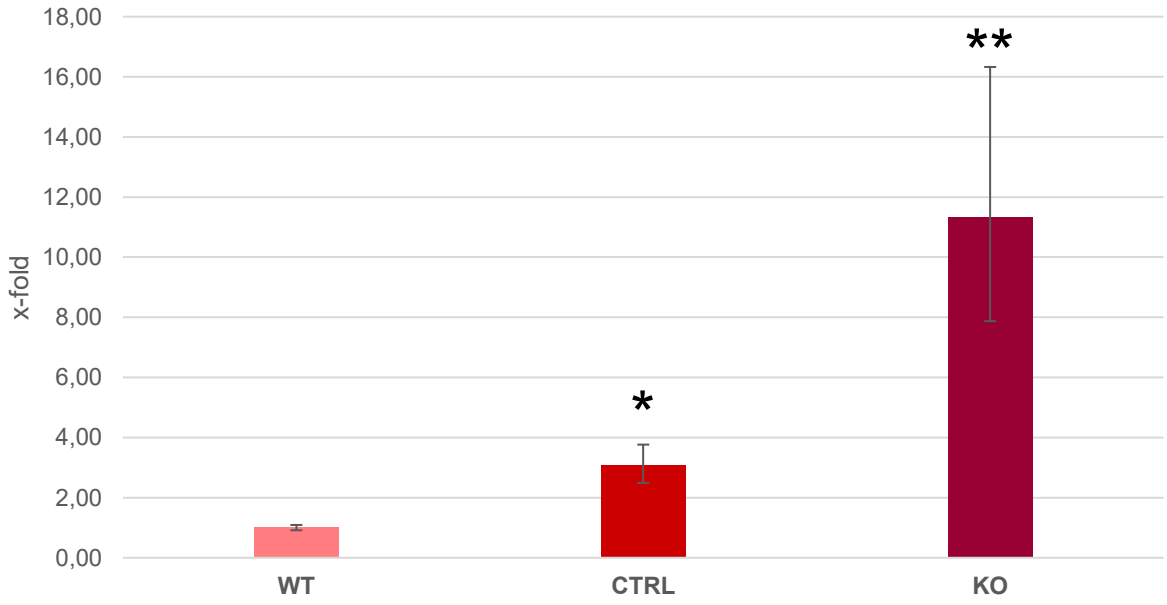

*Figure 16: Relative quantification of mRNA expression of Pgp of cerebEND cells. The signals were normalized with the endogenous control PPIA. Data are represented as mean ± SEM (WT: n=8; CTRL: n=11; KO: n=11; N=4 experiments). Quantitative comparative qPCR analysis indicates statistically significant difference of Pgp between the displayed cell-lines P<0.01 (One-way ANOVA). Comparison between WT and CTRL (*P<0.01) cerebENDs and between WT and KO (**P<0.01) cerebENDs showed a significant increase (One-way ANOVA). WT=wildtype cells; CTRL=HDR control cells; KO=knock-out cells.*

4.2.2 RT-qPCR analysis of TAT-MeCP2 treated cerebENDs

To find a reference point for an optimal TAT-MeCP2 treatment concentration four different concentrations of TAT-MeCP2 addition (10 nM, 30 nM, 100 nM, and 500 nM) were chosen and treatment duration was set to 24 hours. The 24-hour treatment experiments consisted of three biological replicants (n=3) per cell line (WT, CTRL and KO) and were repeated under the same conditions for a second time (N=2). Furthermore, a 100 nM TAT-MeCP2 substitution experiment with a treatment duration of 48 hours was performed. Based on the RT-qPCR analysis no significant regulation under the treatment of TAT-MeCP2 of any of the four target genes (DNMT1, Cldn5, Bcrp and Pgp) was detectable.

Although not significantly noticeable, DNMT1 mRNA expression showed a trend to be reduced in WT cerebENDs under TAT-MeCP2 treatment. While DNMT1 seemed to be upregulated in CTRL cells, which was more pronounced in the 48-hour treatment experiment, KO cells did not seem to be affected by TAT-MeCP2 addition (Figures 17-19).

Cldn5 seemed to be reduced in WT cells when treated with TAT-MeCP2, while substitution indicated an upregulation in KO cells, when treated with 10 nM TAT-MeCP2. However, since comparison of untreated WT, CTRL and KO cerebENDs displayed no significant alteration in Cldn5 mRNA expression, no prediction if TAT-MeCP2 can rescue RTT phenotype can be made (Figures 20-22).

TAT-MeCP2 addition in any concentration or treatment duration had no observable effect on Bcrp mRNA expression in all of the three used cell lines (Figures 23-25).

Due to low concentration, Pgp was not detectable in several samples, leading to difficulties in the interpretation of the presented data. However, based on valid qPCR data, TAT-MeCP2 treatment did not seem to revert the observed upregulation of Pgp mRNA expression in KO cells, as TAT-MeCP2 addition appeared to increase Pgp mRNA expression (Figures 26-28).

4.2.2.1 Relative mRNA expression of DNMT1 of cerebENDs treated with TAT-MeCP2

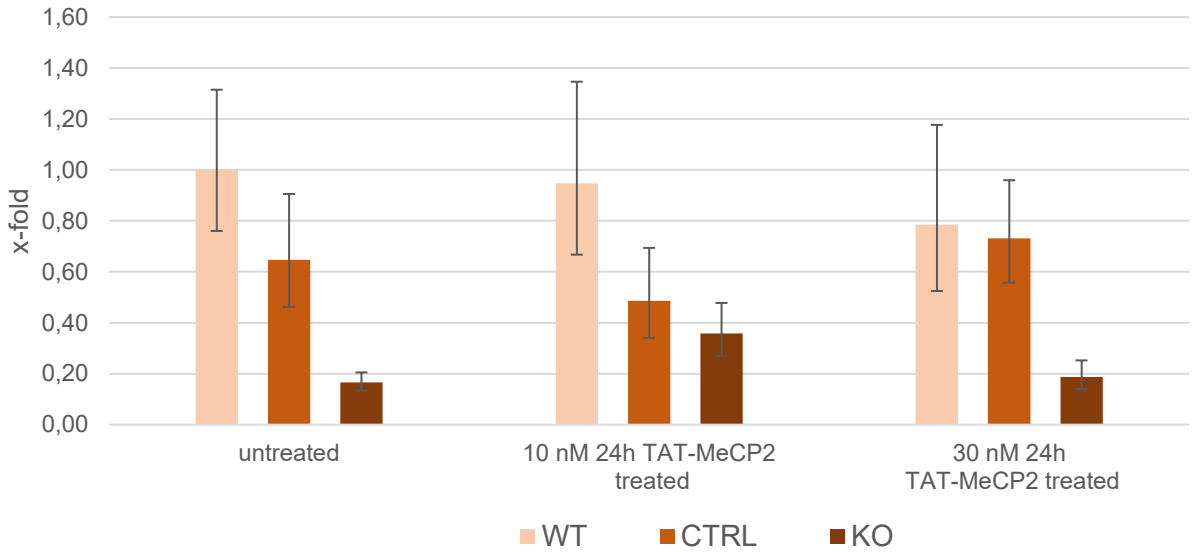

Figure 17: Relative quantification of mRNA expression of DNMT1 of with TAT-MeCP2 treated cerebEND cells referred to untreated WT cells. The duration of treatment was 24 hours. The signals were normalized to the endogenous control PPIA. Data are represented as mean ± SEM (n=6 biological replicants; N=2 experiments). WT=wildtype cells; CTRL=HDR control cells; KO=knock-out cells.

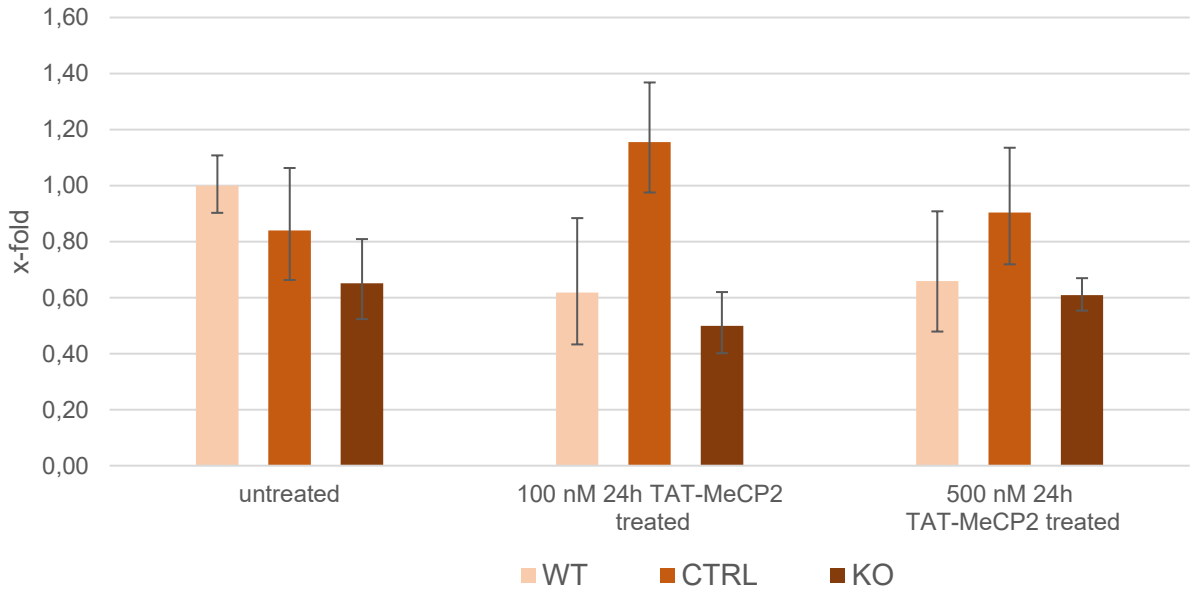

Figure 18: Relative quantification of mRNA expression of DNMT1 of with TAT-MeCP2 treated cerebEND cells referred to untreated WT cells. The duration of treatment was 24 hours. The signals were normalized to the endogenous control PPIA. Data are represented as mean ± SEM (n=6 biological replicants; N=2 experiments). WT=wildtype cells; CTRL=HDR control cells; KO=knock-out cells.

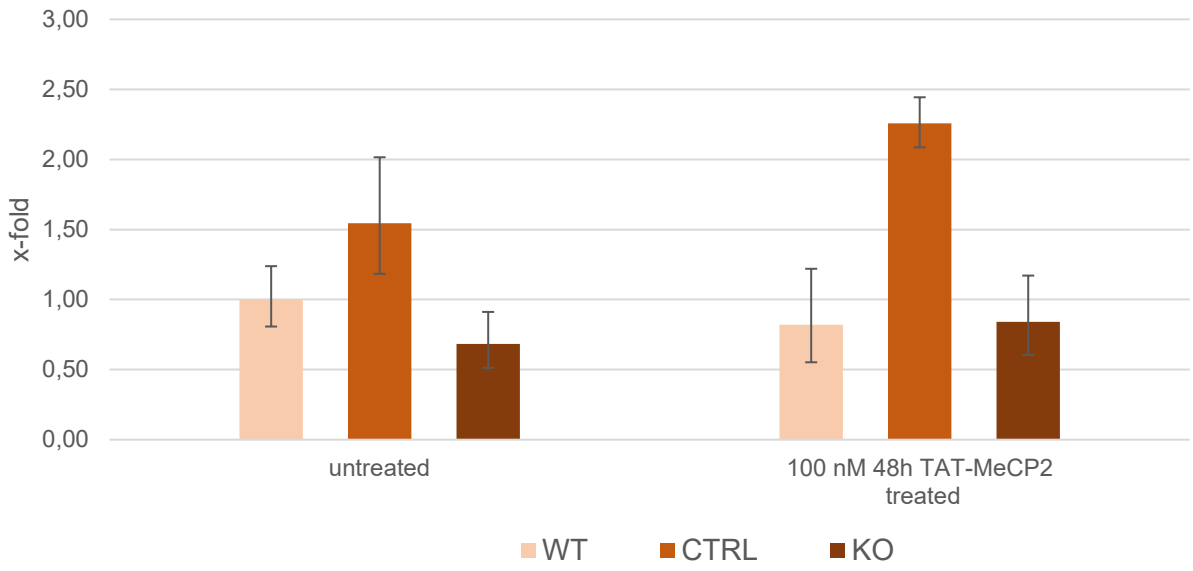

Figure 19: Relative quantification of mRNA expression of DNMT1 of with TAT-MeCP2 treated cerebEND cells referred to untreated WT cells. The duration of treatment was 48 hours. The signals were normalized to the endogenous control PPIA. Data are represented as mean ± SEM (n=3 biological replicants). WT=wildtype cells; CTRL=HDR control cells; KO=knock-out cells.

4.2.2.2 Relative mRNA expression of Cldn5 of cerebENDs treated with TAT-MeCP2

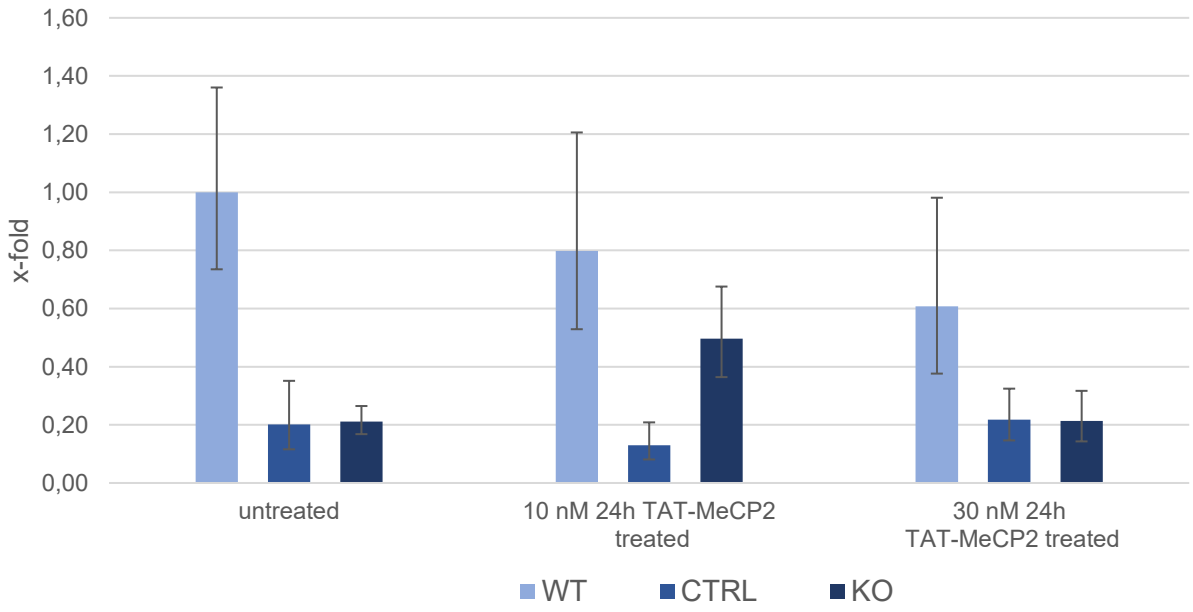

Figure 20: Relative quantification of mRNA expression of Cldn5 of with TAT-MeCP2 treated cerebEND cells referred to untreated WT cells. The duration of treatment was 24 hours. The signals were normalized to the endogenous control PPIA. Data are represented as mean ± SEM (n=6 biological replicants; N=2 experiments). WT=wildtype cells; CTRL=HDR control cells; KO=knock-out cells.

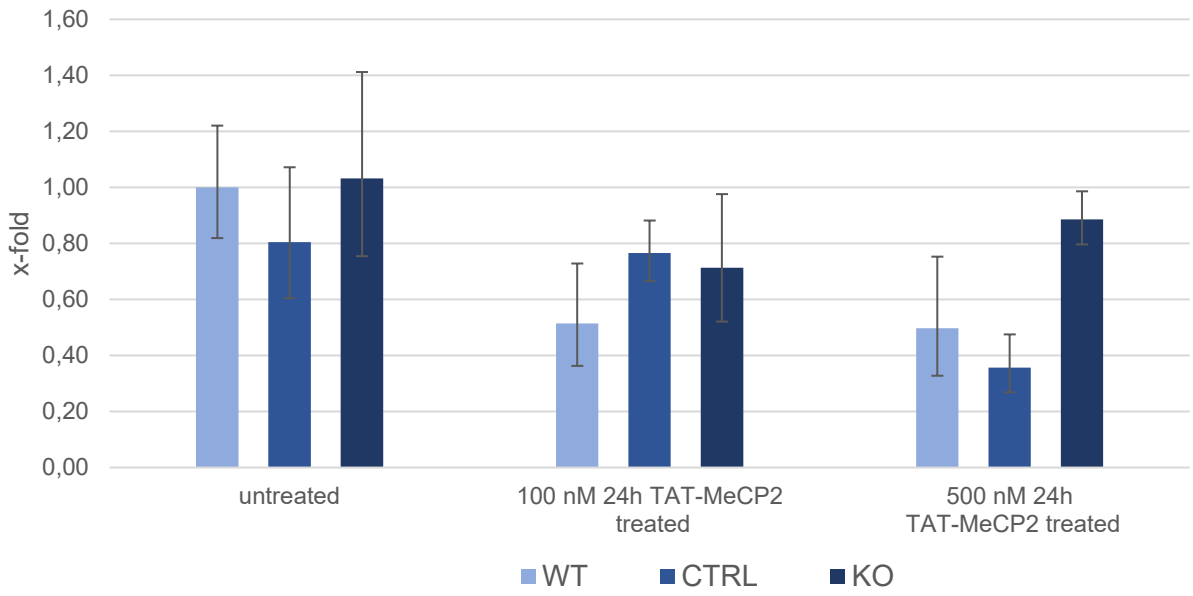

Figure 21: Relative quantification of mRNA expression of Cldn5 of with TAT-MeCP2 treated cerebEND cells referred to untreated WT cells. The duration of treatment was 24 hours. The signals were normalized to the endogenous control PPIA. Data are represented as mean ± SEM (n=6 biological replicants; N=2 experiments). WT=wildtype cells; CTRL=HDR control cells; KO=knock-out cells.

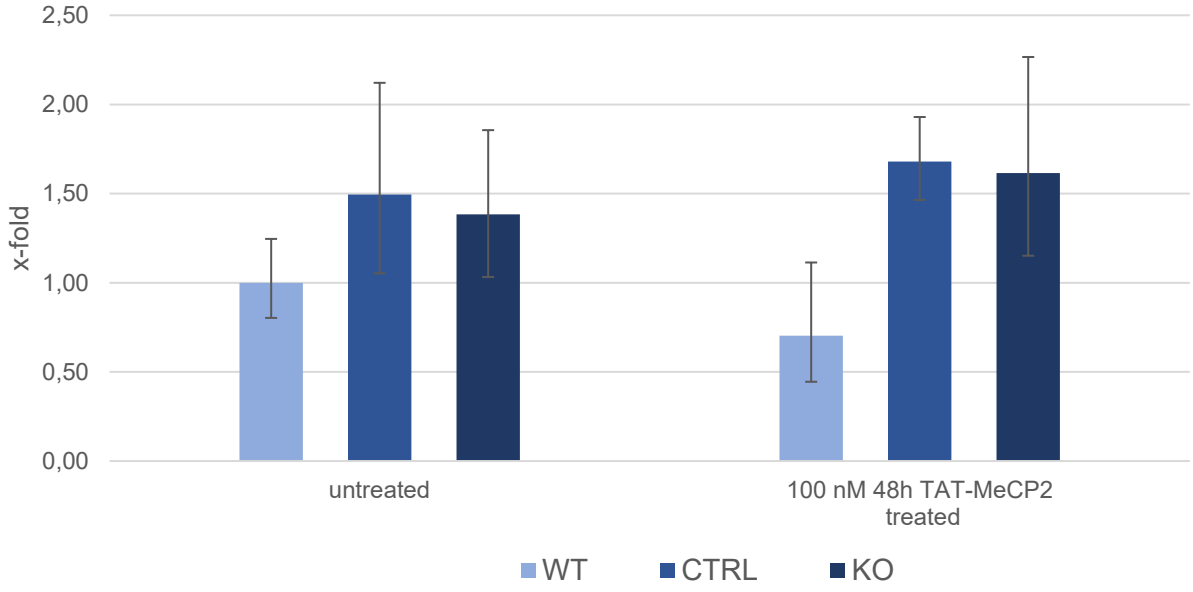

Figure 22: Relative quantification of mRNA expression of Cldn5 of with TAT-MeCP2 treated cerebEND cells referred to untreated WT cells. The duration of treatment was 48 hours. The signals were normalized to the endogenous control PPIA. Data are represented as mean ± SEM (n=3 biological replicants). WT=wildtype cells; CTRL=HDR control cells; KO=knock-out cells.

4.2.2.3 Relative mRNA expression of Bcrp of cerebENDs treated with TAT-MeCP2

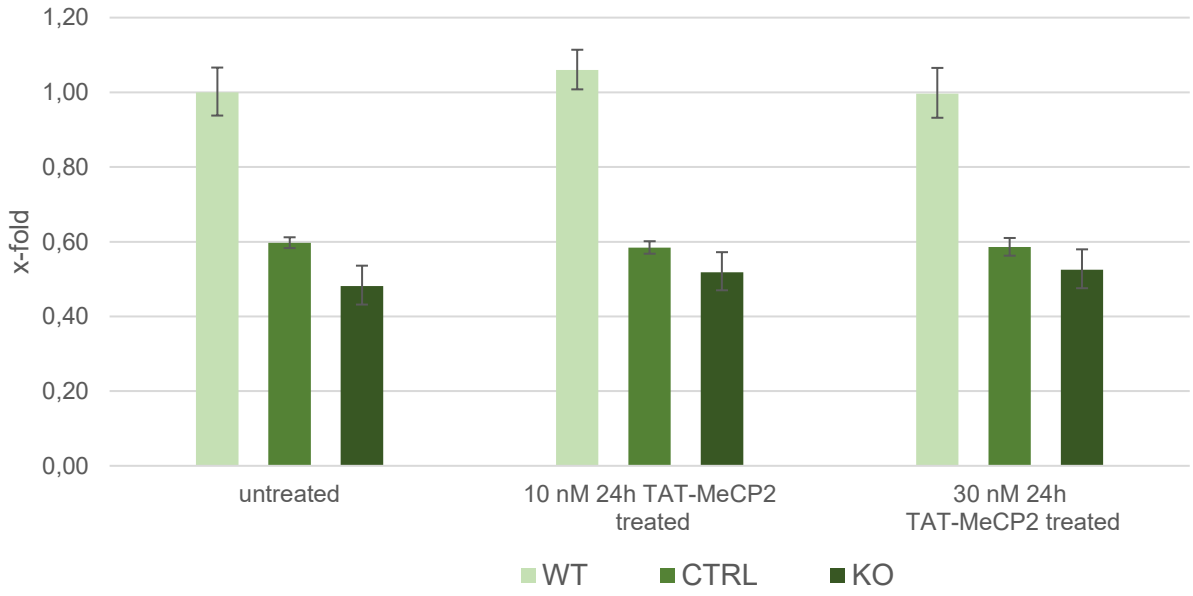

Figure 23: Relative quantification of mRNA expression of Bcrp of with TAT-MeCP2 treated cerebEND cells referred to untreated WT cells. The duration of treatment was 24 hours. The signals were normalized to the endogenous control PPIA. Data are represented as mean ± SEM (n=6 biological replicants; N=2 experiments). WT=wildtype cells; CTRL=HDR control cells; KO=knock-out cells.

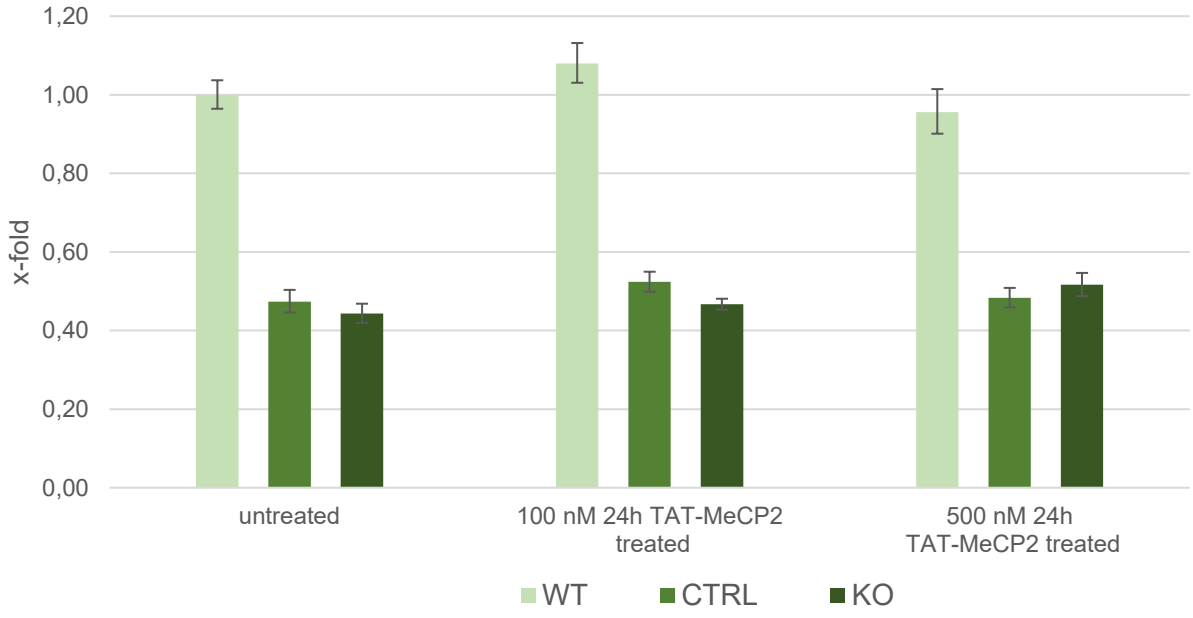

Figure 24: Relative quantification of mRNA expression of Bcrp of with TAT-MeCP2 treated cerebEND cells referred to untreated WT cells. The duration of treatment was 24 hours. The signals were normalized to the endogenous control PPIA. Data are represented as mean ± SEM (n=6 biological replicants; N=2 experiments). WT=wildtype cells; CTRL=HDR control cells; KO=knock-out cells.

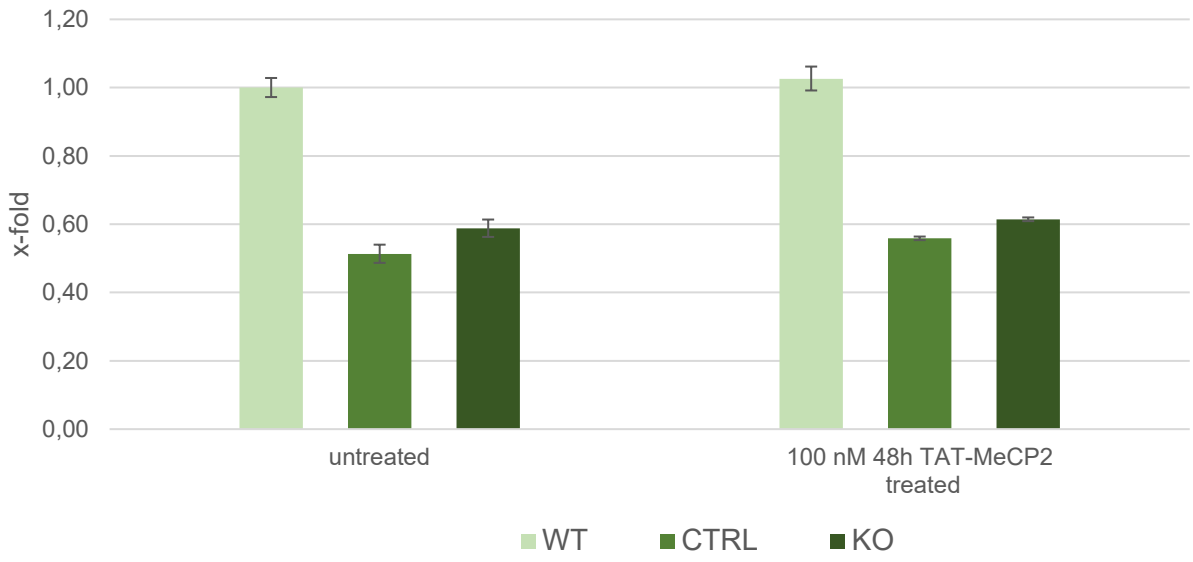

Figure 25: Relative quantification of mRNA expression of Bcrp of with TAT-MeCP2 treated cerebEND cells referred to untreated WT cells. The duration of treatment was 48 hours. The signals were normalized to the endogenous control PPIA. Data are represented as mean ± SEM (n=3 biological replicants). WT=wildtype cells; CTRL=HDR control cells; KO=knock-out cells.

4.2.2.4 Relative mRNA expression of Pgp of cerebENDs treated with TAT-MeCP2

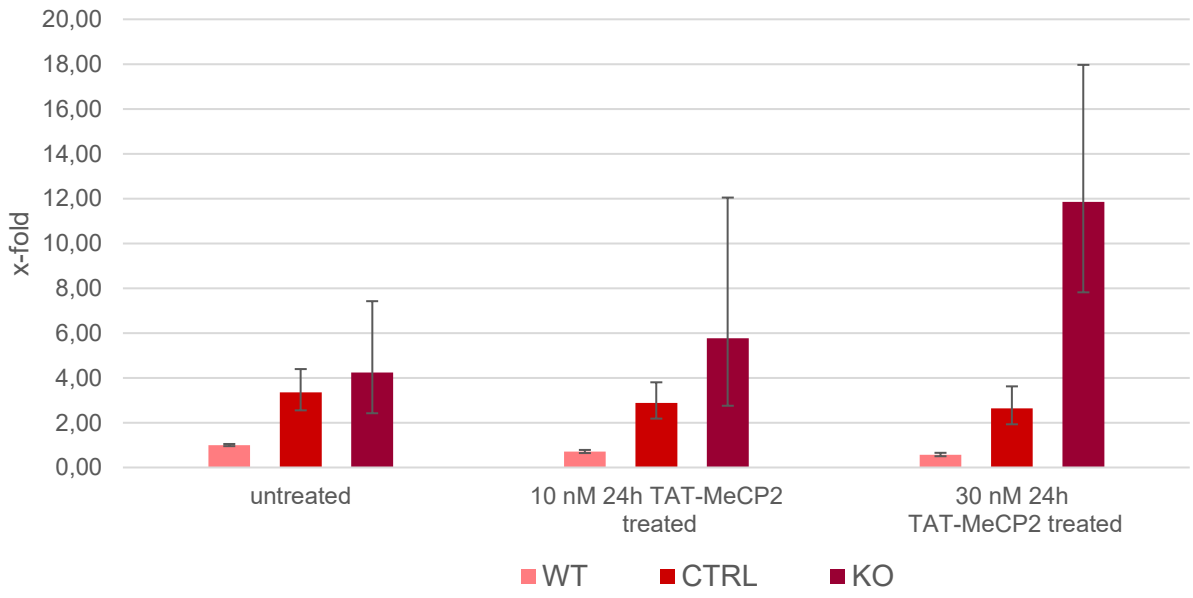

Figure 26: Relative quantification of mRNA expression of Pgp of with TAT-MeCP2 treated cerebEND cells referred to untreated WT cells. The duration of treatment was 24 hours. The signals were normalized to the endogenous control PPIA. Data are represented as mean ± SEM (WT: n=4; CTRL: n=5; KO: n=4 biological replicants; N=2 experiments). WT=wildtype cells; CTRL=HDR control cells; KO=knock-out cells.

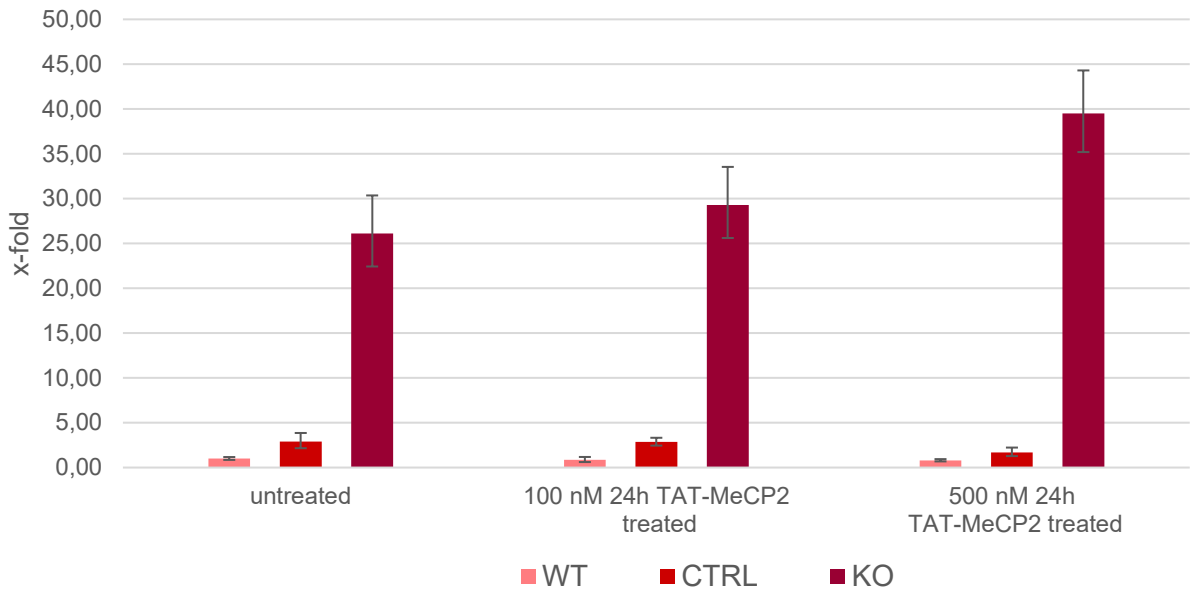

Figure 27: Relative quantification of mRNA expression of Pgp of with TAT-MeCP2 treated cerebEND cells referred to untreated WT cells. The duration of treatment was 24 hours. The signals were normalized to the endogenous control PPIA. Data are represented as mean ± SEM (WT: n=5; CTRL: n=6; KO: n=6 biological replicants; N=2 experiments). WT=wildtype cells; CTRL=HDR control cells; KO=knock-out cells.

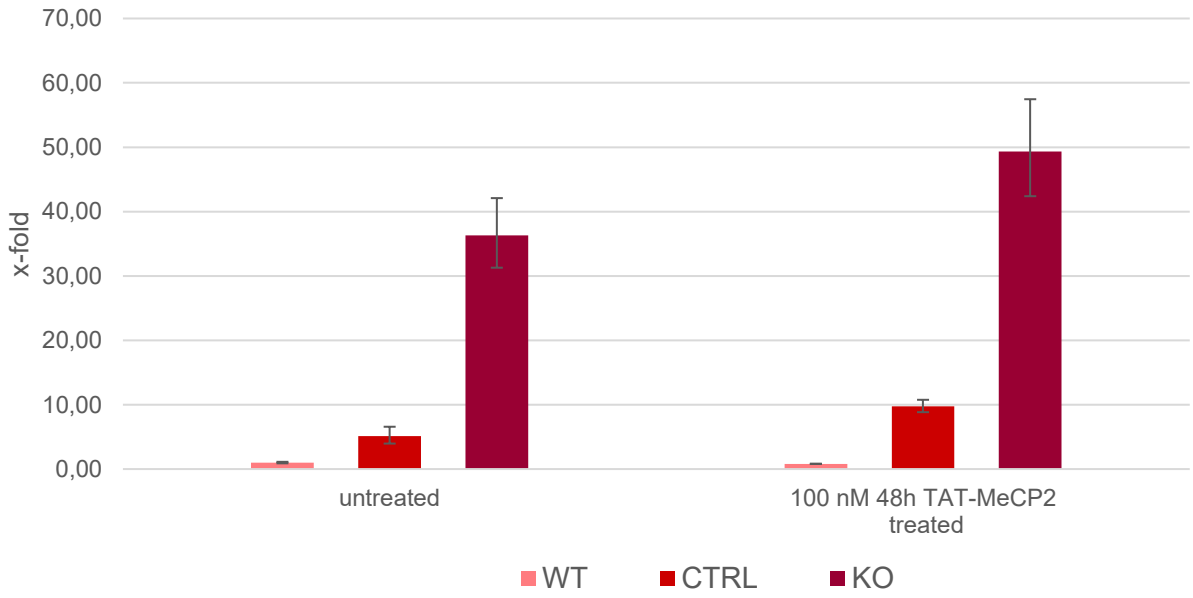

Figure 28: Relative quantification of mRNA expression of Pgp of with TAT-MeCP2 treated cerebEND cells referred to untreated WT cells. The duration of treatment was 48 hours. The signals were normalized to the endogenous control PPIA. Data are represented as mean ± SEM (n=3 biological replicants). WT=wildtype cells; CTRL=HDR control cells; KO=knock-out cells.

4.2.3 Western blot analysis of TAT-MeCP2 treated cerebENDs

Since analysis of mRNA expression of the 10/30 nM TAT-MeCP2 substitution experiments displayed no significant changes but promising trends, western blot was performed to investigate possible effects in the protein expression of the selected targets. Antibodies for the ABC-transporters Pgp and Bcrp and the tight junction protein Cldn5 were used for western blotting (Figures 29 to 34) and densitometric analysis was accomplished using endogenous control GAPDH for normalization. However, Bcrp could not be displayed and evaluated in the CTRL (Figure 31) and KO (Figure 33) cell lines due to band intensity issues of experiment #1002.

4.2.3.1 Western blot gels

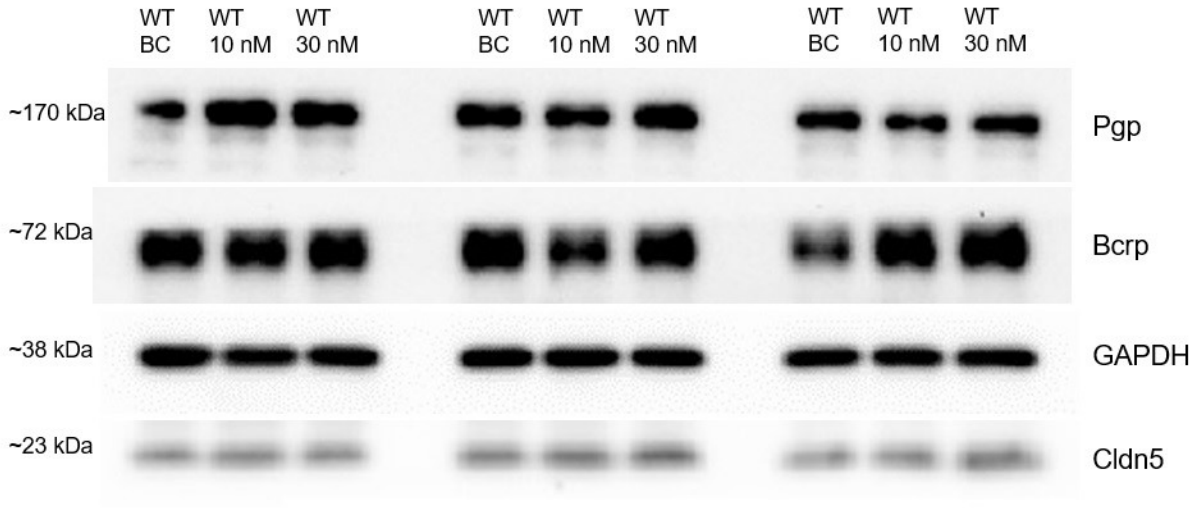

Figure 29: Western blot of cerebEND wildtype (WT) samples of experiment #1002. Baseline control (BC) were non-treated samples, compared to with 10 nM and 30 nM TAT-MeCP2 treated cerebENDs.

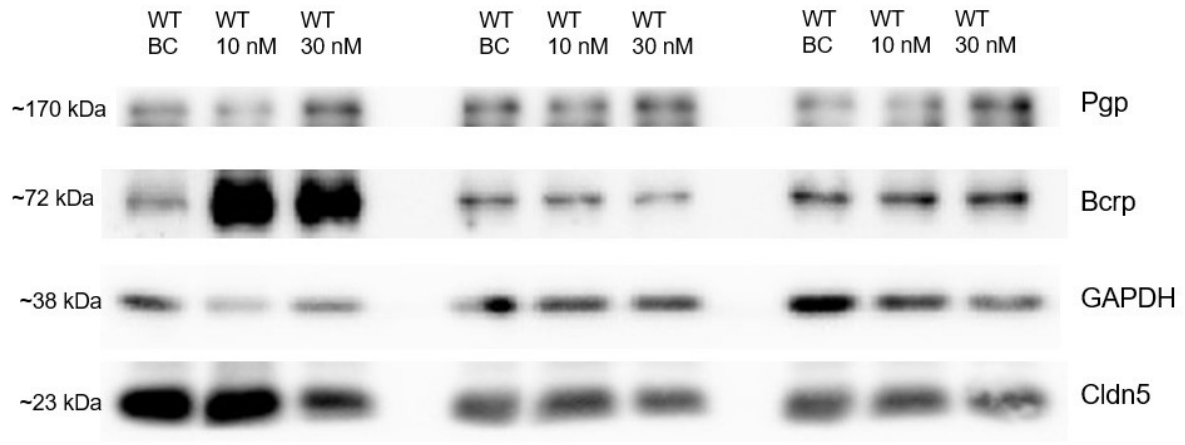

Figure 30: Western blot of cerebEND wildtype (WT) samples of experiment #1127. Baseline control (BC) were non-treated samples, compared to with 10 nM and 30 nM TAT-MeCP2 treated cerebENDs.

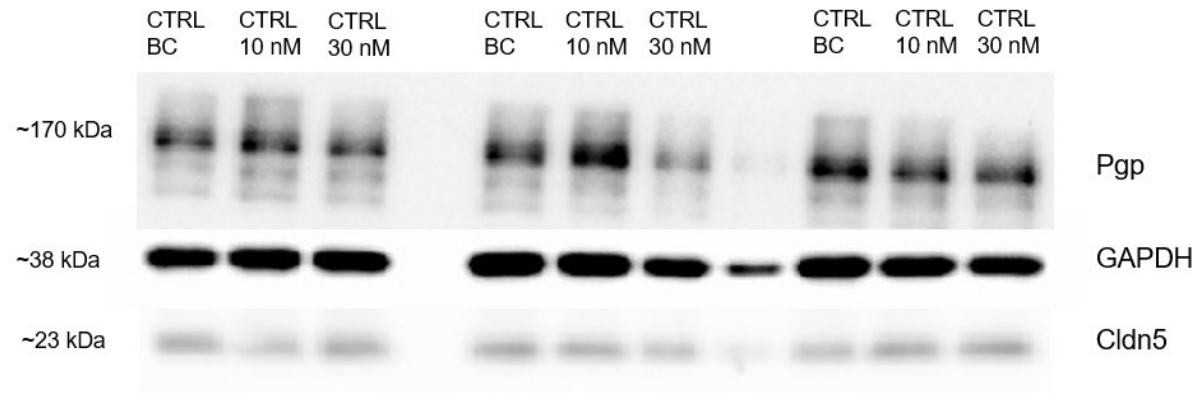

Figure 31: Western blot of cerebEND HDR control (CTRL) samples of experiment #1002. Baseline control (BC) were non-treated samples, compared to with 10 nM and 30 nM TAT-MeCP2 treated cerebENDs. Due to detection issues Bcrp was not representable in this blot.

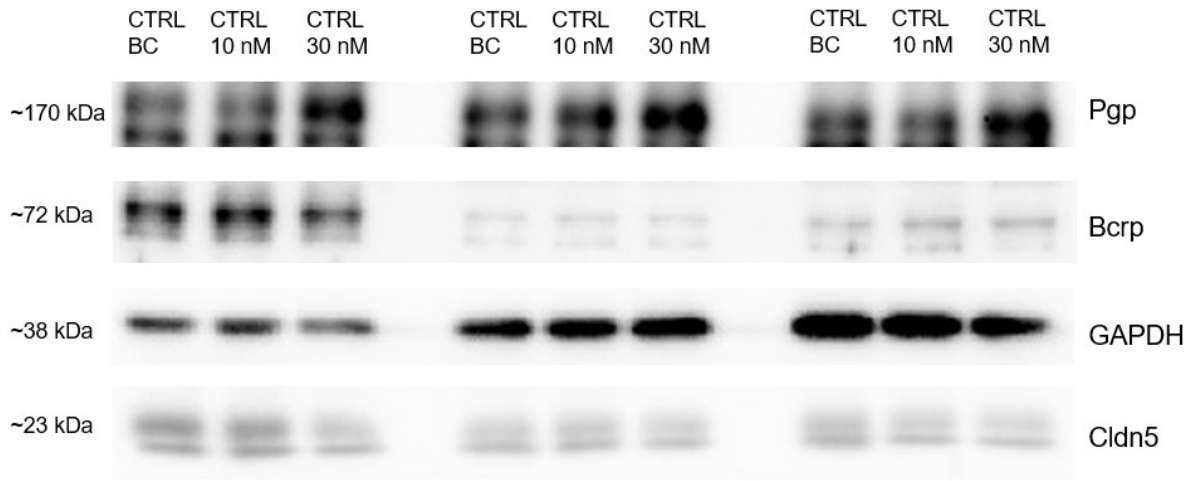

Figure 32: Western blot of cerebEND HDR control (CTRL) samples of experiment #1127. Baseline control (BC) were non-treated samples, compared to with 10 nM and 30 nM TAT-MeCP2 treated cerebENDs.

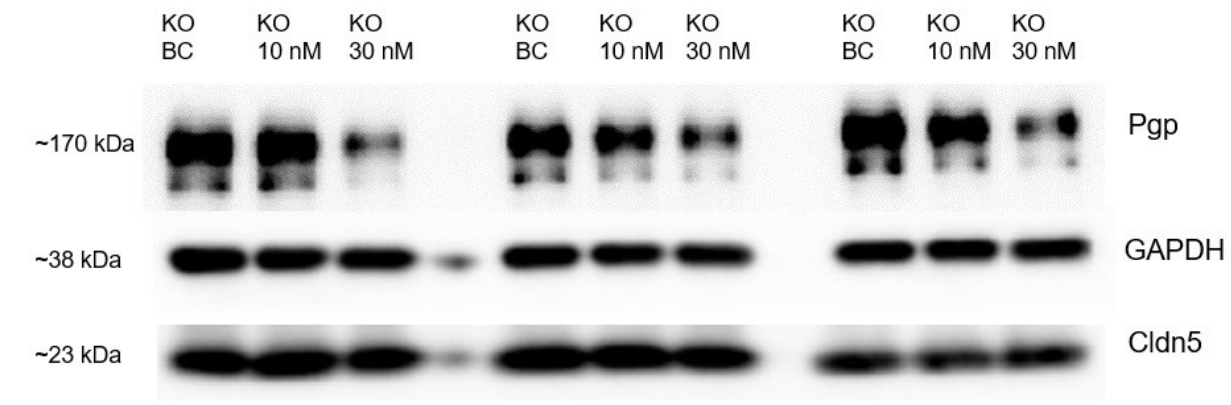

Figure 33: Western blot of cerebEND knock out (KO) samples of experiment #1002. Baseline control (BC) were non-treated samples, compared to with 10 nM and 30 nM TAT-MeCP2 treated cerebENDs. Due to detection issues Bcrp was not representable in this blot.

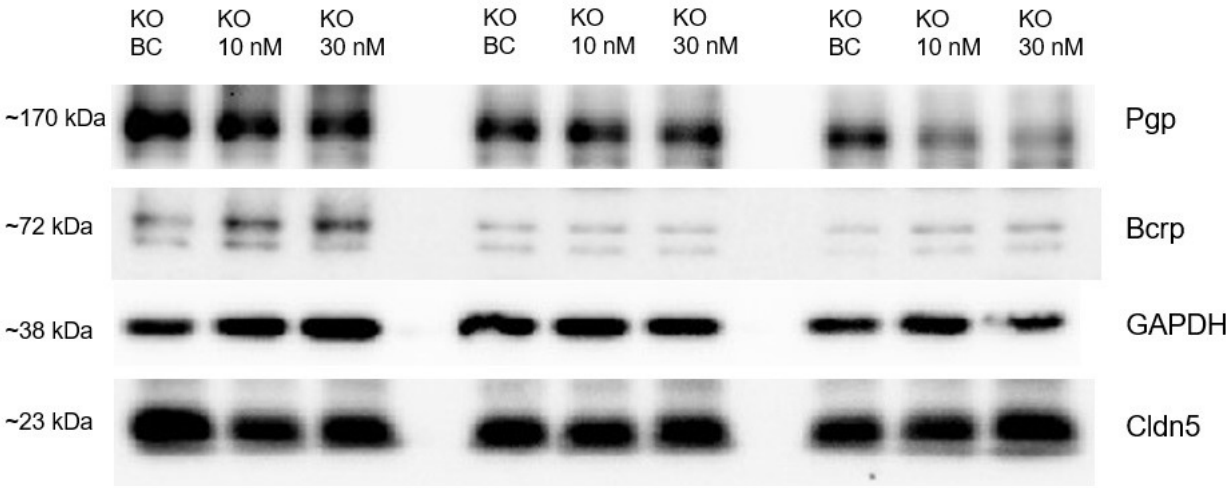

Figure 34: Western blot of cerebEND knock out (KO) samples of experiment #1127. Baseline control (BC) were non-treated samples, compared to with 10 nM and 30 nM TAT-MeCP2 treated cerebENDs.

4.2.3.2 Densitometric analysis

Densitometric analysis displayed no significant difference in all three cerebEND cell lines in the expression of the targets Cldn5 (Figure 36) and Bcrp (Figure 37) after treatment with 10 nM or 30 nM TAT-MeCP2. However, Pgp was regulated by TAT-MeCP2 addition. WT and CTRL cerebENDs showed a tendency to be increased, when treated with TAT-MeCP2 (Figure 35). The increase by ~1.7-fold of Pgp was statistically significant in WT samples with 30 nM TAT-MeCP2 addtion ($P < 0.05$; Student´s t-test). Furthermore, TAT-MeCP2 caused a decrease in Pgp expression of KO cells treated with 30 nM to ~ 55 % ($P < 0.01$; Student´s t-test). The reduction of Pgp in MeCP2 knock out cells indicated that exogenous TAT-MeCP2 was capable of reversing RTT phenotype in cerebENDs.

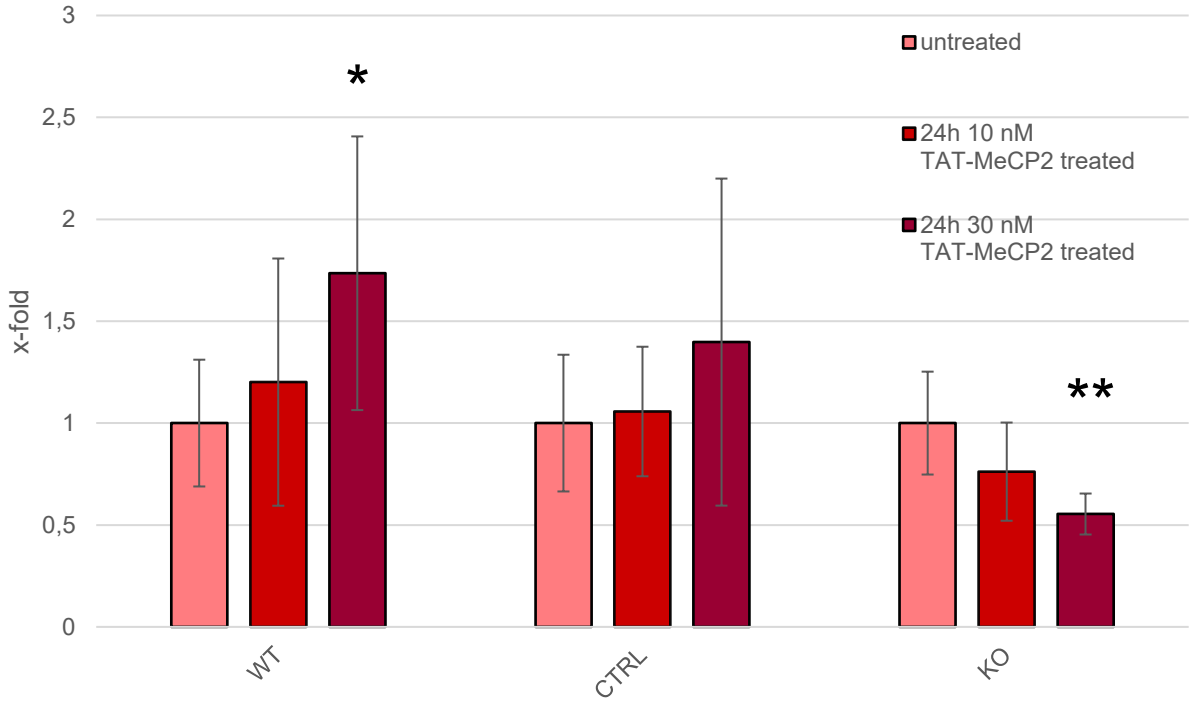

*Figure 35: Densitometric analysis of relative Pgp expression of with TAT-MeCP2 treated cerebEND cells. WT = wildtype cerebENDs (n = 5); CTRL = HDR control cerebENDs (n = 6); KO = MeCP2 knock out cells (n = 6). Signal intensity of Pgp was normalized to the endogenous control GAPDH. Data are represented as mean ± standard deviation. The increase to 170 % of Pgp in WT cells treated with 30 nM TAT-MeCP2 compared to untreated cells was statistically significant (*P < 0.05; Student´s t-test), as well as the reduction to 60 % of with 30 nM TAT-MeCP2 treated KO cells compared to untreated cerebENDs (**P < 0.01; Student´s t-test).*

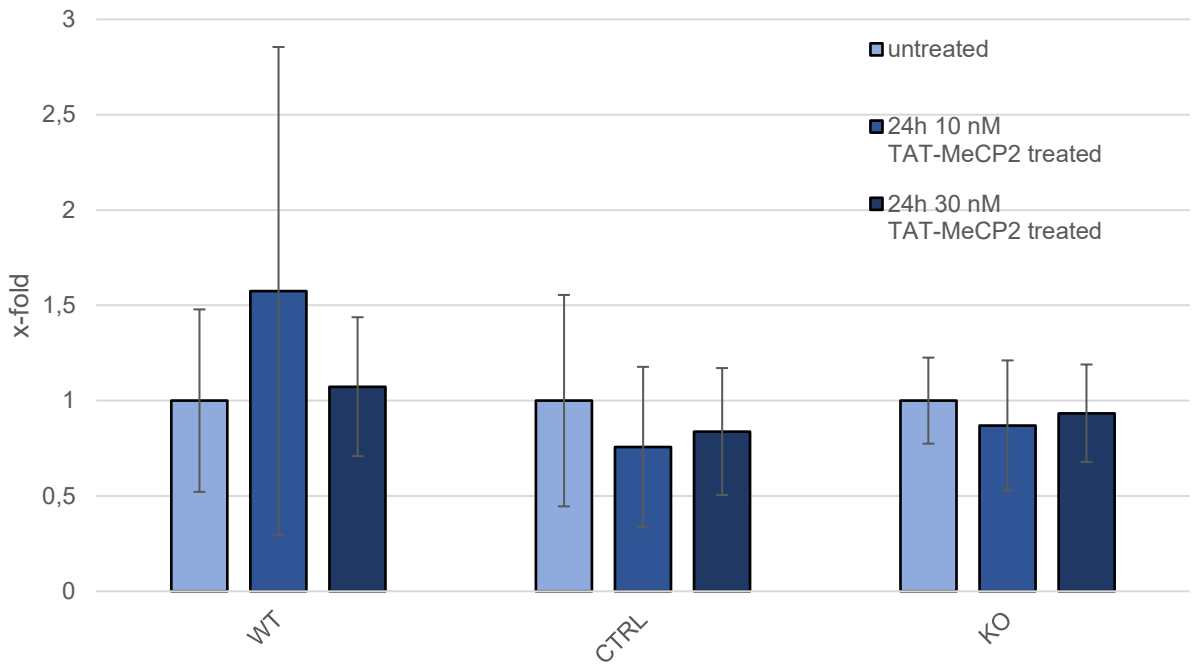

Figure 36: Densitometric analysis of relative Cldn5 expression of with TAT-MeCP2 treated cerebEND cells. WT = wildtype cerebENDs (n = 6); CTRL = HDR control cerebENDs (n = 6); KO = MeCP2 knock out cells (n = 6). Signal intensity of Pgp was normalized to the endogenous control GAPDH. Data are represented as mean ± standard deviation.

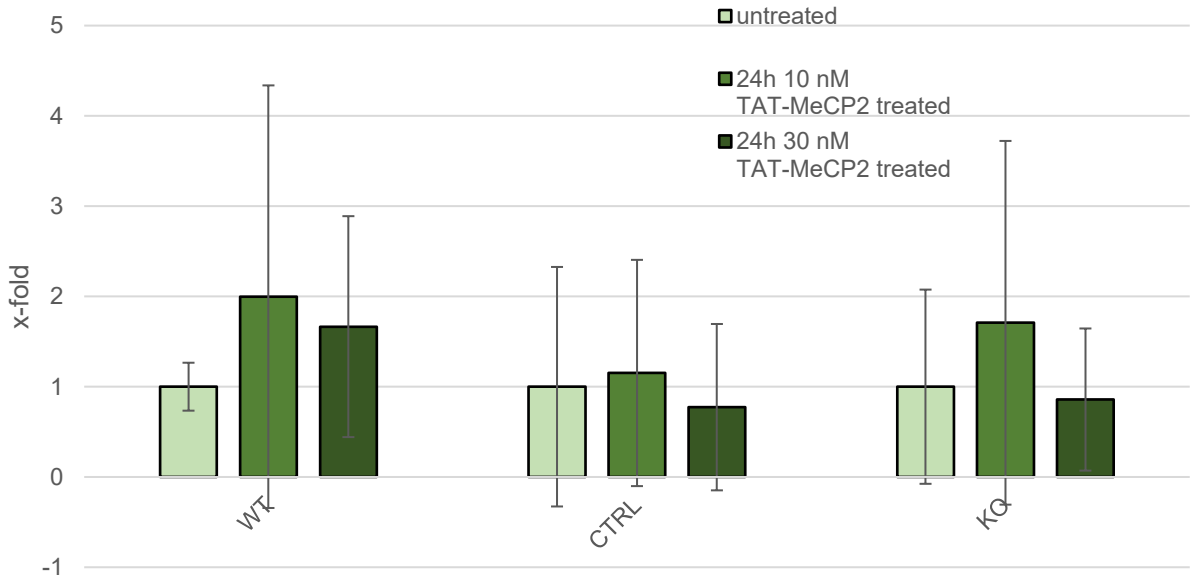

Figure 37: Densitometric analysis of relative Bcrp expression of with TAT-MeCP2 treated cerebEND cells. WT = wildtype cerebENDs (n = 6); CTRL = HDR control cerebENDs (n = 3); KO = MeCP2 knock out cells (n = 3). Signal intensity of Pgp was normalized to the endogenous control GAPDH. Data are represented as mean ± standard deviation.

5 Discussion

5.1 MeCP2 and the complexity of identifying downstream targets

Mutations in the MeCP2 gene are the main cause of Rett syndrome (Amir et al., 1999). Since MeCP2 acts as an epigenetic regulator, it can alter the expression of hundreds of genes (Chahrour et al., 2008). These regulatory mechanisms include transcriptional activation and repression (Nan et al., 1998), remodeling of chromatin structures (Horike et al., 2005), RNA splicing (Young et al., 2005) and the expression of regulatory RNAs (Szulwach et al., 2010). Due to this broad range of possibilities of gene regulation, identification of downstream targets is a challenging process. Additionally, MeCP2 expression levels vary dramatically between different types of tissue and their stages of differentiation (Shahbazian et al., 2002). For instance, during brain development, MeCP2 levels are lowest prenatally and increase progressively after birth (Samaco et al., 2004), leading to complicated prediction which genes are under control of MeCP2.

To date, many MeCP2 dependent targets remain unknown, so one aim of this work was to find a sufficient method of quantification for possible unidentified downstream targets as well as for well-known targets for the mouse cerebEND and astrocyte cell-line used in this work.

5.1.1 Tight Junction proteins play an essential role in BBB permeability

Disturbance of the blood-brain barrier is observed in neurological diseases like multiple sclerosis (Correale & Villa, 2007), Alzheimer's disease (Zlokovic, 2008), epilepsy (Remy & Beck, 2006), and Parkinson's disease (Desai et al., 2007). Interestingly, recent studies suggest, that BBB breakdown is an early biomarker for human cognitive dysfunction (Nation et al., 2019). The formation of unique tight junctions and adherens junctions between brain endothelial cells is responsible for the paracellular tightness of the BBB. Therefore, to investigate possible changes in MeCP2 deficient cerebENDs, one focus of this work was the tight junction protein family.

Tight junctions are formed by the protein family of claudins, occludin and junctional adhesion proteins (Abbott et al., 2010). The mammalian tight junction protein family of claudins comprises 27 members (Cldn1-Cldn27). Proper formation of the different claudins is essential for the integrity of the BBB. While some claudins are responsible for tightening cell-cell contact (e.g., Cldn1, Cldn3, Cldn5, Cldn11), others form ion pores between endothelial cells (e.g., Cldn2, Cldn10, Cldn16). Assembly and interplay of the various claudins are crucial for maintaining BBB properties and their expression is highly dependent on the neurovascular environment (Haseloff et al., 2015). Cldn5 is, by far, the most dominant member of the claudin family in brain endothelial cells. In Cldn5 knock-out mice paracellular permeability of small molecules (<800 Da) is dramatically increased, leading to disruption of BBB properties (Nitta et al., 2003). Interestingly, expression

pattern of claudins vary between *in vivo* and *in vitro* situation as microdissected brain capillaries showed higher mRNA expression levels of Clnd -11, -12, -25 compared to primary mouse brain capillary endothelial cells. These findings highlight the importance of the interplay between cells of the neurovascular unit (Berndt et al., 2019).

Recent work with MeCP2 null mice showed an altered expression of tight junction proteins Cldn5 and occludin resulting in enhanced BBB permeability. Cldn5 protein expression was decreased in RTT symptomatic knock-out mice. However, these findings were only observable in particular brain regions, namely the cortex and the striatum (Pepe et al., 2023). In this work, we investigated if there is a difference in Cldn5 transcript expression between wildtype immortalized mouse cerebellar capillary endothelial cells (WT cerebENDs), HDR control cerebENDs and MeCP2 knock-out cerebENDs. No significant reduction of Cldn5 mRNA expression between WT and KO cells was detectable in our performed experiments. Additionally, TAT-MeCP2 substitution showed no significant regulation in all three of the used cell-lines of this work. Thus, leading to the hypothesis, that the lack of neurovascular environment in *in vitro* single-cell experiments might have an impact on Cldn5 expression pattern. Therefore, further research with co-culture experiments may be needed to display aberrant tight junction expression patterns to confirm enhanced BBB permeability in MeCP2-KO cerebENDs.

5.1.2 MeCP2 and its role epigenetic regulation mechanisms

Epigenetic regulation is characterized by altering gene expression without changes in the nucleotide sequence. The underlying mechanisms of epigenetic regulation comprises DNA methylation, chromatin remodeling, RNA modification and activation of regulatory RNAs (Pejhan & Rastegar, 2021). DNA methylation pattern is crucial for maturation and development and is established in early embryogenesis. The process of DNA methylation is mediated by specific enzymes called DNA-methyl transferases (DNMT), which attach a methyl group at the 5^{th} carbon of the DNA base cytosine, resulting in 5-methyl cytosine (5-mC). Methylation of cytosine occurs preferably on DNA, containing CpG dinucleotides. The responsible enzymes are divided into *de novo* DNA methyltransferases (DNMT3A and DNMT3B) and the maintenance DNA methyltransferase DNMT1 (Hamidi et al., 2015). While DNA methylation pattern is commonly seen as a relatively stable modification, DNA demethylation can occur passively and actively mediated by the enzyme family of Ten-eleven translocation dioxygenases (TET). The TET protein family comprises three members (TET1, TET2 and TET3) which are capable of transforming 5-mC into 5-hydroxymethylcytosine, resulting after multiple downstream steps in unmethylated cytosine (Delcuve et al., 2009). Aberrant activity and mutations of DNA methyltransferases and TETs are associated with hereditary sensory neuropathy (Klein et al., 2011), acute myeloid leukemia (AML) (Ley et al., 2010), the immunodeficiency, centromeric region instability, and facial

anomalies syndrome (ICF) (Ehrlich et al., 2008) and Myelodysplastic syndrome (MDS) (Oh et al., 2020).

One of the most studied “reader”-proteins of methylated DNA is MeCP2 (Amir et al., 1999). As a first step in this work the aim was to find sufficient primer pairs for mRNA quantification for the DNA methyltransferases (DNMT1, DNMT3A and DNMT3B) and the Ten-eleven translocation dioxygenases (TET1-TET3). Since there is to date no evidence of aberrant expression of these epigenetic enzymes in RTT syndrome, the impact of a MeCP2 knock-out needs to be elucidated. Our findings imply that MeCP2 KO cerebENDs exhibit reduced DNMT1 mRNA expression ($P<0.05$ one-way ANOVA). However, mRNA expression does not necessarily correlate with activity or protein expression (Buccitelli & Selbach, 2020). Furthermore, the performed TAT-MeCP2 substitution experiments did not show significant regulation of DNMT1 and subsequently no restoration of abnormal DNMT1 mRNA levels found in MeCP2 knock-out cells. In order to get more accurate data if DNA methyltransferases are MeCP2 dependent, *in vivo* quantification of DNMT1 in MeCP2 deficient mice may underline the preceding *in vitro* regulation of KO cerebENDs.

5.1.3 BDNF and Kir4.1 as well-known downstream targets of MeCP2 in RTT syndrome

Proper function of MeCP2 in astrocytes is essential for accurate neurodevelopment. Even though MeCP2 expression in astrocytes is lower compared to neurons, glial astrocytic cells contribute massively to RTT pathophysiology. MeCP2 deficiency in astrocytes can cause abnormal dendritic morphology of neighboring neurons due to aberrant secretion of soluble factors (Ballas et al., 2009). Probably one of the best studied MeCP2 dependent targets of such a soluble factor is the brain-derived neurotrophic growth factor BDNF (Pejhan & Rastegar, 2021). BDNF plays a fundamental role in the central nervous system by regulating differentiation, maturation, survival, and plasticity of neurons. Several downstream pathways of BDNF signaling are described, after BDNF binds to its target the tropomyosin-related kinase B (TrkB). This binding activates various signal transduction cascades including the mitogen-activated protein kinase (MAPK) pathway, the phosphatidylinositol 3-kinase (PI3K) pathway, and the phospholipase C (PLC) pathway, resulting in regulation of transcription of hundreds of different genes (Chao, 2003). Additionally, recent studies suggest biological activity of precursor pro-BDNF by activating p75NTR, which leads to neuronal programmed cell death (Mizui et al., 2016). Today there is an ongoing debate about BDNF regulation by MeCP2. Earlier studies suggested MeCP2 as a transcriptional repressor as it binds selectively to BDNF promotor region to prevent transcription. After membrane depolarization MeCP2 is phosphorylated and released from BDNF promotor, resulting in BDNF transcription (Chen et al., 2003). However, there is also a BDNF activation model

described in the literature. MeCP2 deficient mice exhibit lower levels of BDNF in brain tissue compared to wildtype individuals, indicating upregulation mechanism by MeCP2 (Li & Pozzo-Miller, 2012). In addition to this, overexpression of MeCP2 results in increased BDNF levels in the hypothalamus (Chahrour et al., 2008). The aforementioned findings suggest a dynamic BDNF regulation, where MeCP2 can switch between an activator and a repressor. While most studies focused on BDNF expression in neurons in RTT pathophysiology, we wanted to investigate BDNF mRNA and protein expression levels in our used cerebral endothelial as well as our astrocyte cell lines as both cell types exhibit physiological noticeable BDNF expression pattern (Pejhan et al., 2020).

Another well described MeCP2 dependent target is the inward rectifying potassium channel 4.1 (Kir4.1), which is essential for astrocytic potassium membrane properties. Influx of K^+ in astrocytes contributes to normal neuronal electrical stimulation as glial cells restore K^+ levels in synapses after repolarization (Djukic et al., 2007; Kinboshi et al., 2020). Loss of function of glial Kir4.1 is associated with seizures, epilepsy, neurodevelopmental delay, and ataxia, which are all symptoms of RTT syndrome (Kofuji et al., 2000). The expression of Kir4.1 protein and mRNA transcripts were found to be significantly reduced in MeCP2 deficient mice, as well as Kir4.1 mediated currents were impaired in MeCP2 null animals. The decrease of Kir4.1 correlated with occurrence of RTT phenotype, as symptomatic MeCP2 deficient mice never reached wildtype Kir4.1 levels during postnatal neurodevelopment (Kahanovitch et al., 2018). These findings provide evidence for the important role of Kir4.1 and how aberrant astrocytic function can contribute to RTT syndrome.

In this work antibodies for protein quantification and primer pairs for mRNA quantification of BDNF and Kir4.1 were checked for suitability with the astrocyte cell lines. The antibodies for BDNF and Kir4.1 were deemed to be appropriate for quantification, as well as the primer pair for BDNF. However, both of the designed Kir4.1 primer pairs were not suitable for mRNA quantification as they did not show a distinct isolated band without displaying any alternative products on the agarose gel. Further work with the astrocyte cell lines needs to be continued to investigate differences in the expression between the WT, CTRL and KO cell lines of the astrocytic targets BDNF and Kir4.1 and subsequently if treatment with TAT-MeCP2 can revert alterations in MeCP2 deficient cells. For this work it was decided to focus on brain endothelial cell lines, since previous data showed regulation of the BBB targets such as Pgp and Bcrp in MeCP2-KO mouse brain endothelial cells (Neuhaus, 2018).

5.2 ABC-Transporters and their contribution to BBB properties

Previous work of the group has demonstrated that MeCP2 knock-out in cerebral endothelial cells leads to increase in the protein levels of ABC-transporters Bcrp (Abcg2) and Pgp (Abcb1) (Neuhaus, 2018). ATP binding-cassette transporter are responsible for active efflux of substances using ATP. Divided into seven subgroups (Abca to Abcg), the ABC-transporter family comprises 49 known members. Mainly located on the luminal side of endothelial cells, ABC-transporters act as a gatekeeper for xenobiotics, massively contributing to the restricting barrier properties of the BBB (Vasiliou et al., 2009). Due to their high affinity to lipophilic substances approximately 98% of all small molecule drugs cannot cross the BBB and reach the CNS (Pardridge, 2005).

One of the best described efflux transporter is the ABC-transporter P-glycoprotein, also known as multidrug resistance protein 1 (MDR). Pgp is highly expressed in enterocytes, brain capillary endothelial cells, hepatocytes, and renal proximal tubular cells and facilitates drug excretion. A variety of drugs are Pgp substrates including fexofenadine (Matsushima et al., 2008), dabigatran etexilate (Moj et al., 2019) or digoxin (Troutman & Thakker, 2003) whose pharmacokinetics can be massively influenced by agents inducing or inhibiting Pgp activity (Elmeliegy et al., 2020).

Another well studied multidrug resistance transporter is the breast cancer resistance protein (Bcrp/Abcg2). Originally cloned from a multidrug resistant cell line, Bcrp mediates efflux of a large number of chemotherapeutics, such as methotrexate, mitoxantrone, imatinib or irinotecan (Mao & Unadkat, 2005). However, substrates of Bcrp are not limited to chemotherapeutics, as Bcrp also transports chemical toxicants and conjugated organic anions. Interestingly, some of the substrates of BCRP are overlapping with other ABC-transporters like Pgp (Mao & Unadkat, 2015).

ABC-transporter function was found to be perturbed in neurological diseases like Alzheimer's Disease (van Assema & van Berckel, 2016) and epilepsy (Eleonora Aronica et al., 2012). Over expression of efflux transporters in the BBB is often seen in patients who suffer from epilepsy, thus leading to multidrug resistance (E. Aronica et al., 2012). Today it is still unclear if epilepsy progression itself, genetic polymorphisms, transporter up-regulation after induction by antiepileptic drugs or consequence of repeated seizures are responsible for increased ABC-transporter activity (Tang et al., 2017). Since about 80 % of RTT patients suffer from epilepsy (Jian et al., 2006), ABC-transporter expression pattern in cells of the neurovascular unit ask for elucidation.

As stated above MeCP2 knock-out cerebENDs exhibited an increase in Pgp and Bcrp expression (Neuhaus, 2018). In this work, increase of Pgp transcript variants in KO cerebENDs could be observed (11.34 ± 4.99 x-fold) compared to WT cerebENDs. This finding underlines MeCP2 dependent regulation of Pgp. However, Bcrp analysis of mRNA expression displayed significant

reduction in MeCP2 deficient cerebENDs (0.46 ± 0.03 x-fold). Further investigation is required to clarify these discrepancies between protein and mRNA expression of Bcrp.

5.3 TAT-MeCP2 and its potential as protein replacement therapy to revert RTT phenotype

So far, there is no cure for Rett syndrome. Existing therapies are limited to alleviate occurring symptoms during RTT progression targeting neurotropic factors, neurotransmitters, and metabolic effects like increased serum cholesterol (Vashi & Justice, 2019). One promising treatment approach is protein replacement therapy, where malfunctioned protein is substituted exogenously. However, protein delivery across the BBB can be a challenging obstacle. Therefore, protein transduction domains (PTDs) can be a helpful tool to attain sufficient protein delivery into cells of the neurovascular unit. One of the most studied PTD is the TAT-domain (transactivator of transcription), originally found in human immunodeficiency virus (HIV) (Nagahara et al., 1998). Recent study has proven, that TAT-CDKL5 fusion protein was sufficient to treat CDKL5-null mice, who suffer from the severe neurodevelopmental disease Cyclin-dependent kinase like-5 (CDKL5) disorder. TAT-CDKL5 was injected systemically and successfully reached the CNS by crossing the BBB (Trazzi et al., 2018). Another proof of concept was provided by our research group in 2022. In a RTT mouse model administered TAT-MeCP2e1 and TAT-MeCP2e2 fusion protein variants were able to rescue RTT phenotype. The hypothesis of this study was confirmed by *in vitro* experiments, where TAT-MeCP2 could reverse pathological hyperacetylation of histones H3K9 and H4K16 and *in vivo* mouse model, wherein MeCP2-null mice exhibited prolonged life spans after treatment with TAT-MeCP2 (Steinkellner et al., 2022).

In this work, the performed TAT-MeCP2 substitution experiments did not show any significant regulation at the mRNA levels of the four predetermined targets DNMT1, Cldn5, Bcrp and Pgp. A factor, which should not be ignored was the detection issue in the quantification of Pgp transcript variants. Some of the used samples displayed fluorescence signals in RT-PCR below detection limits, resulting in reduced significance of the findings. Repeating the experiment with increased concentration of used cDNA may lead to more adequate results. However, TAT-MeCP2 addition did show significant reduction (0.55 ± 0.1 x-fold compared to wildtype cells) in the protein levels of Pgp in MeCP2 knock-out cerebENDs, when treated with 30 nM TAT-MeCP2 for 24 hours. Because TAT-MeCP2 substitution was able to reduce previously noted pathophysiological upregulation of Pgp protein levels in MeCP2 deficient cerebENDs, the hypothesis, if TAT-MeCP2 is suitable for rescuing RTT phenotype, can be considered as confirmed.

5.4 Interplay between cells of the neurovascular unit is crucial for maintaining BBB-integrity

It is a well-known fact, that physiological blood-brain barrier integrity can only be maintained by correct interplay between cells of the neurovascular unit (NVU) (Yu et al., 2020). The specific anatomic structure of the NVU is formed by different cell types: endothelial cells, neurons, pericytes and nerve glial cells (e.g., astrocytes), and the extracellular matrix (Saili et al., 2017). These cell types are in close contact with each other, resulting in mutual influence of gene expression. For example, astrocytes, which cover most of the surface of endothelial cells with their “end-feet”, communicate via release of cytokines and neurotrophic factors with their neighboring cells. Astrocytic glial cells show high density of ionic transporters in the contact areas between cells of the NVU, implicating their role as neurovascular couplers (Abbott et al., 2006). Ballas et al. (2009), suggested that MeCP2 deficient astrocytes exhibit disturbances in their secretion pattern of growth factors, leading to abnormal dendritic morphology in adjacent wildtype neurons (Ballas et al., 2009). Furthermore, pericytes play an integral role in the formation of tight junctions indicating endothelial-pericyte cell interaction is crucial for regulating paracellular tightness. Interestingly, pericytes are not able to induce gene expression in cerebral endothelial cells, they rather inhibit expression of factors which increase BBB permeability. Moreover, cerebral endothelial cells, that are co-cultured with pericytes show a four-fold increased trans-endothelial cell electrical resistance (TEER), which is a marker for paracellular tightness (Daneman et al., 2010).

All the prementioned factors elucidate the importance of the crosstalk between cells of the NVU. Consequently, single cell experiments performed in the current work fail to depict physiological NVU homeostasis and their extensive effects. Further research with co-culture experiments is required to examine functional abnormalities in MeCP2 deficient cells.

5.5 Conclusion

In summary, discovering MeCP2 dependent targets and elucidating their influence in RTT progression is a challenging field of research. In the current work various unexplored possible targets had been suggested, as well as further investigation of well known MeCP2 dependent genes was advanced. Moreover, the performed TAT-MeCP2 substitution experiment revealed possibility to reverse RTT phenotype, contributing to the potential of protein replacement therapy for RTT patients.

References

Abbott, N. J. (2005). Dynamics of CNS barriers: evolution, differentiation, and modulation. *Cell Mol Neurobiol*, *25*(1), 5-23. https://doi.org/10.1007/s10571-004-1374-y

Abbott, N. J., Patabendige, A. A., Dolman, D. E., Yusof, S. R., & Begley, D. J. (2010). Structure and function of the blood-brain barrier. *Neurobiol Dis*, *37*(1), 13-25. https://doi.org/10.1016/j.nbd.2009.07.030

Abbott, N. J., Rönnbäck, L., & Hansson, E. (2006). Astrocyte-endothelial interactions at the blood-brain barrier. *Nat Rev Neurosci*, *7*(1), 41-53. https://doi.org/10.1038/nrn1824

Abdala, A. P., Lioy, D. T., Garg, S. K., Knopp, S. J., Paton, J. F., & Bissonnette, J. M. (2014). Effect of Sarizotan, a 5-HT1a and D2-like receptor agonist, on respiration in three mouse models of Rett syndrome. *Am J Respir Cell Mol Biol*, *50*(6), 1031-1039. https://doi.org/10.1165/rcmb.2013-0372OC

Amir, R. E., Van den Veyver, I. B., Wan, M., Tran, C. Q., Francke, U., & Zoghbi, H. Y. (1999). Rett syndrome is caused by mutations in X-linked MECP2, encoding methyl-CpG-binding protein 2. *Nature Genetics*, *23*(2), 185-188. https://doi.org/10.1038/13810

Ariani, F., Hayek, G., Rondinella, D., Artuso, R., Mencarelli, M. A., Spanhol-Rosseto, A., Pollazzon, M., Buoni, S., Spiga, O., Ricciardi, S., Meloni, I., Longo, I., Mari, F., Broccoli, V., Zappella, M., & Renieri, A. (2008). FOXG1 is responsible for the congenital variant of Rett syndrome. *Am J Hum Genet*, *83*(1), 89-93. https://doi.org/10.1016/j.ajhg.2008.05.015

Armstrong, D. D. (1992). The neuropathology of the Rett syndrome. *Brain Dev*, *14 Suppl*, S89-98.

Armstrong, D. D. (2002). Neuropathology of Rett syndrome. *Ment Retard Dev Disabil Res Rev*, *8*(2), 72-76. https://doi.org/10.1002/mrdd.10027

Aronica, E., Sisodiya, S. M., & Gorter, J. A. (2012). Cerebral expression of drug transporters in epilepsy. *Adv Drug Deliv Rev*, *64*(10), 919-929. https://doi.org/10.1016/j.addr.2011.11.008

Aronica, E., Sisodiya, S. M., & Gorter, J. A. (2012). Cerebral expression of drug transporters in epilepsy. *Advanced Drug Delivery Reviews*, *64*(10), 919-929. https://doi.org/https://doi.org/10.1016/j.addr.2011.11.008

Bahi-Buisson, N., Guellec, I., Nabbout, R., Guet, A., Nguyen, G., Dulac, O., & Chiron, C. (2008). Parental view of epilepsy in Rett Syndrome. *Brain Dev*, *30*(2), 126-130. https://doi.org/10.1016/j.braindev.2007.07.002

Balaton, B. P., Dixon-McDougall, T., Peeters, S. B., & Brown, C. J. (2018). The eXceptional nature of the X chromosome. *Hum Mol Genet*, *27*(R2), R242-r249. https://doi.org/10.1093/hmg/ddy148

Ballas, N., Lioy, D. T., Grunseich, C., & Mandel, G. (2009). Non-cell autonomous influence of MeCP2-deficient glia on neuronal dendritic morphology. *Nat Neurosci*, *12*(3), 311-317. https://doi.org/10.1038/nn.2275

Begley, D. J. (2004). Delivery of therapeutic agents to the central nervous system: the problems and the possibilities. *Pharmacol Ther*, *104*(1), 29-45. https://doi.org/10.1016/j.pharmthera.2004.08.001

Berndt, P., Winkler, L., Cording, J., Breitkreuz-Korff, O., Rex, A., Dithmer, S., Rausch, V., Blasig, R., Richter, M., Sporbert, A., Wolburg, H., Blasig, I. E., & Haseloff, R. F. (2019). Tight junction proteins at the blood-brain barrier: far more than claudin-5. *Cell Mol Life Sci*, *76*(10), 1987-2002. https://doi.org/10.1007/s00018-019-03030-7

Bienvenu, T., Carrié, A., de Roux, N., Vinet, M. C., Jonveaux, P., Couvert, P., Villard, L., Arzimanoglou, A., Beldjord, C., Fontes, M., Tardieu, M., & Chelly, J. (2000). MECP2 mutations account for most cases of typical forms of Rett syndrome. *Hum Mol Genet*, *9*(9), 1377-1384. https://doi.org/10.1093/hmg/9.9.1377

BIO-RAD. (2023). *iScript™ gDNA Clear cDNA Synthesis Kit-Information Sheet*. Retrieved 11.09.2023 from https://www.bio-rad.com/sites/default/files/webroot/web/pdf/lsr/literature/10043078.pdf

Bleau, C., Filliol, A., Samson, M., & Lamontagne, L. (2015). Brain Invasion by Mouse Hepatitis Virus Depends on Impairment of Tight Junctions and Beta Interferon Production in Brain Microvascular Endothelial Cells. *J Virol*, *89*(19), 9896-9908. https://doi.org/10.1128/jvi.01501-15

Bronger, H., König, J., Kopplow, K., Steiner, H. H., Ahmadi, R., Herold-Mende, C., Keppler, D., & Nies, A. T. (2005). ABCC drug efflux pumps and organic anion uptake transporters in human gliomas and the blood-tumor barrier. *Cancer Res*, *65*(24), 11419-11428. https://doi.org/10.1158/0008-5472.Can-05-1271

Buccitelli, C., & Selbach, M. (2020). mRNAs, proteins and the emerging principles of gene expression control. *Nat Rev Genet*, *21*(10), 630-644. https://doi.org/10.1038/s41576-020-0258-4

Byard, R. W. (2006). Forensic issues and possible mechanisms of sudden death in Rett syndrome. *J Clin Forensic Med*, *13*(2), 96-99. https://doi.org/10.1016/j.jcfm.2005.08.013

Cai, H., Ren, Y., Li, X. X., Yang, J. L., Zhang, C. P., Chen, M., Fan, C. H., Hu, X. Q., Hu, Z. Y., Gao, F., & Liu, Y. X. (2011). Scrotal heat stress causes a transient alteration in tight junctions and induction of TGF-β expression. *Int J Androl*, *34*(4), 352-362. https://doi.org/10.1111/j.1365-2605.2010.01089.x

Chahrour, M., Jung, S. Y., Shaw, C., Zhou, X., Wong, S. T., Qin, J., & Zoghbi, H. Y. (2008). MeCP2, a key contributor to neurological disease, activates and represses transcription. *Science*, *320*(5880), 1224-1229. https://doi.org/10.1126/science.1153252

Chahrour, M., & Zoghbi, H. Y. (2007). The story of Rett syndrome: from clinic to neurobiology. *Neuron*, *56*(3), 422-437. https://doi.org/10.1016/j.neuron.2007.10.001

Chang, Q., Khare, G., Dani, V., Nelson, S., & Jaenisch, R. (2006). The disease progression of Mecp2 mutant mice is affected by the level of BDNF expression. *Neuron*, *49*(3), 341-348. https://doi.org/10.1016/j.neuron.2005.12.027

Chao, H. T., Chen, H., Samaco, R. C., Xue, M., Chahrour, M., Yoo, J., Neul, J. L., Gong, S., Lu, H. C., Heintz, N., Ekker, M., Rubenstein, J. L., Noebels, J. L., Rosenmund, C., & Zoghbi, H. Y. (2010). Dysfunction in GABA signalling mediates autism-like stereotypies and Rett syndrome phenotypes. *Nature*, *468*(7321), 263-269. https://doi.org/10.1038/nature09582

Chao, M. V. (2003). Neurotrophins and their receptors: a convergence point for many signalling pathways. *Nat Rev Neurosci*, *4*(4), 299-309. https://doi.org/10.1038/nrn1078

Chen, W. G., Chang, Q., Lin, Y., Meissner, A., West, A. E., Griffith, E. C., Jaenisch, R., & Greenberg, M. E. (2003). Derepression of BDNF transcription involves calcium-dependent phosphorylation of MeCP2. *Science*, *302*(5646), 885-889. https://doi.org/10.1126/science.1086446

Clarke, L. E., & Barres, B. A. (2013). Emerging roles of astrocytes in neural circuit development. *Nat Rev Neurosci*, *14*(5), 311-321. https://doi.org/10.1038/nrn3484

Correale, J., & Villa, A. (2007). The blood-brain-barrier in multiple sclerosis: functional roles and therapeutic targeting. *Autoimmunity*, *40*(2), 148-160. https://doi.org/10.1080/08916930601183522

Cuddapah, V. A., Pillai, R. B., Shekar, K. V., Lane, J. B., Motil, K. J., Skinner, S. A., Tarquinio, D. C., Glaze, D. G., McGwin, G., Kaufmann, W. E., Percy, A. K., Neul, J. L., & Olsen, M. L. (2014). Methyl-CpG-binding protein 2 (MECP2) mutation type is associated with disease severity in Rett syndrome. *J Med Genet*, *51*(3), 152-158. https://doi.org/10.1136/jmedgenet-2013-102113

Daneman, R., & Prat, A. (2015). The blood-brain barrier. *Cold Spring Harb Perspect Biol*, *7*(1), a020412. https://doi.org/10.1101/cshperspect.a020412

Daneman, R., Zhou, L., Kebede, A. A., & Barres, B. A. (2010). Pericytes are required for blood-brain barrier integrity during embryogenesis. *Nature*, *468*(7323), 562-566. https://doi.org/10.1038/nature09513

Delcuve, G. P., Rastegar, M., & Davie, J. R. (2009). Epigenetic control. *Journal of Cellular Physiology*, *219*(2), 243-250. https://doi.org/https://doi.org/10.1002/jcp.21678

Deogracias, R., Yazdani, M., Dekkers, M. P., Guy, J., Ionescu, M. C., Vogt, K. E., & Barde, Y. A. (2012). Fingolimod, a sphingosine-1 phosphate receptor modulator, increases BDNF levels and improves symptoms of a mouse model of Rett syndrome. *Proc Natl Acad Sci U S A*, *109*(35), 14230-14235. https://doi.org/10.1073/pnas.1206093109

Desai, B. S., Monahan, A. J., Carvey, P. M., & Hendey, B. (2007). Blood-brain barrier pathology in Alzheimer's and Parkinson's disease: implications for drug therapy. *Cell Transplant*, *16*(3), 285-299. https://doi.org/10.3727/000000007783464731

Djukic, B., Casper, K. B., Philpot, B. D., Chin, L. S., & McCarthy, K. D. (2007). Conditional knock-out of Kir4.1 leads to glial membrane depolarization, inhibition of potassium and glutamate uptake, and enhanced short-term synaptic potentiation. *J Neurosci*, *27*(42), 11354-11365. https://doi.org/10.1523/jneurosci.0723-07.2007

Ehrlich, M., Sanchez, C., Shao, C., Nishiyama, R., Kehrl, J., Kuick, R., Kubota, T., & Hanash, S. M. (2008). ICF, an immunodeficiency syndrome: DNA methyltransferase 3B involvement, chromosome anomalies, and gene dysregulation. *Autoimmunity*, *41*(4), 253-271. https://doi.org/10.1080/08916930802024202

Elmeliegy, M., Vourvahis, M., Guo, C., & Wang, D. D. (2020). Effect of P-glycoprotein (P-gp) Inducers on Exposure of P-gp Substrates: Review of Clinical Drug-Drug Interaction Studies. *Clin Pharmacokinet*, *59*(6), 699-714. https://doi.org/10.1007/s40262-020-00867-1

Farkas, E., & Luiten, P. G. (2001). Cerebral microvascular pathology in aging and Alzheimer's disease. *Prog Neurobiol*, *64*(6), 575-611. https://doi.org/10.1016/s0301-0082(00)00068-x

Förster, C., Silwedel, C., Golenhofen, N., Burek, M., Kietz, S., Mankertz, J., & Drenckhahn, D. (2005). Occludin as direct target for glucocorticoid-induced improvement of blood-brain barrier properties in a murine in vitro system. *J Physiol*, *565*(Pt 2), 475-486. https://doi.org/10.1113/jphysiol.2005.084038

Fukuchi, M., Izumi, H., Mori, H., Kiyama, M., Otsuka, S., Maki, S., Maehata, Y., Tabuchi, A., & Tsuda, M. (2017). Visualizing changes in brain-derived neurotrophic factor (BDNF) expression using bioluminescence imaging in living mice. *Sci Rep*, *7*(1), 4949. https://doi.org/10.1038/s41598-017-05297-x

Gadalla, K. K., Bailey, M. E., Spike, R. C., Ross, P. D., Woodard, K. T., Kalburgi, S. N., Bachaboina, L., Deng, J. V., West, A. E., Samulski, R. J., Gray, S. J., & Cobb, S. R. (2013). Improved survival and reduced phenotypic severity following AAV9/MECP2 gene transfer to neonatal and juvenile male Mecp2 knockout mice. *Mol Ther*, *21*(1), 18-30. https://doi.org/10.1038/mt.2012.200

Gold, W. A., Krishnarajy, R., Ellaway, C., & Christodoulou, J. (2018). Rett Syndrome: A Genetic Update and Clinical Review Focusing on Comorbidities. *ACS Chem Neurosci*, *9*(2), 167-176. https://doi.org/10.1021/acschemneuro.7b00346

Guideri, F., Acampa, M., Hayek, G., Zappella, M., & Di Perri, T. (1999). Reduced heart rate variability in patients affected with Rett syndrome. A possible explanation for sudden death. *Neuropediatrics*, *30*(3), 146-148. https://doi.org/10.1055/s-2007-973480

Hagberg, B. (1993). *Rett syndrome - clinical &amp: biological aspects* (1. publ.. ed.). Mac Keith Press [u.a.]. https://ubdata.univie.ac.at/AC02044635

Hagberg, B., Aicardi, J., Dias, K., & Ramos, O. (1983). A progressive syndrome of autism, dementia, ataxia, and loss of purposeful hand use in girls: Rett's syndrome: report of 35 cases. *Ann Neurol*, *14*(4), 471-479. https://doi.org/10.1002/ana.410140412

Hall, C. N., Reynell, C., Gesslein, B., Hamilton, N. B., Mishra, A., Sutherland, B. A., O'Farrell, F. M., Buchan, A. M., Lauritzen, M., & Attwell, D. (2014). Capillary pericytes regulate cerebral blood flow in health and disease. *Nature*, *508*(7494), 55-60. https://doi.org/10.1038/nature13165

Hamidi, T., Singh, A. K., & Chen, T. (2015). Genetic alterations of DNA methylation machinery in human diseases. *Epigenomics*, *7*(2), 247-265. https://doi.org/10.2217/epi.14.80

Hanefeld, F. (1985). The clinical pattern of the Rett syndrome. *Brain Dev*, *7*(3), 320-325. https://doi.org/10.1016/s0387-7604(85)80037-1

Haseloff, R. F., Dithmer, S., Winkler, L., Wolburg, H., & Blasig, I. E. (2015). Transmembrane proteins of the tight junctions at the blood-brain barrier: structural and functional aspects. *Semin Cell Dev Biol*, *38*, 16-25. https://doi.org/10.1016/j.semcdb.2014.11.004

Horike, S., Cai, S., Miyano, M., Cheng, J. F., & Kohwi-Shigematsu, T. (2005). Loss of silent-chromatin looping and impaired imprinting of DLX5 in Rett syndrome. *Nat Genet*, *37*(1), 31-40. https://doi.org/10.1038/ng1491

Huber, A. (2019). *Characterization of the blood-brain barrier of MeCP2-knockout mice* [Diplomarbeit, Universität Wien].

Itoh, M., Ide, S., Takashima, S., Kudo, S., Nomura, Y., Segawa, M., Kubota, T., Mori, H., Tanaka, S., Horie, H., Tanabe, Y., & Goto, Y. (2007). Methyl CpG-binding protein 2 (a mutation of which causes Rett syndrome) directly regulates insulin-like growth factor binding protein 3 in mouse and human brains. *J Neuropathol Exp Neurol*, *66*(2), 117-123. https://doi.org/10.1097/nen.0b013e3180302078

Jian, L., Nagarajan, L., de Klerk, N., Ravine, D., Bower, C., Anderson, A., Williamson, S., Christodoulou, J., & Leonard, H. (2006). Predictors of seizure onset in Rett syndrome. *J Pediatr*, *149*(4), 542-547. https://doi.org/10.1016/j.jpeds.2006.06.015

Justice, M. J., Buchovecky, C. M., Kyle, S. M., & Djukic, A. (2013). A role for metabolism in Rett syndrome pathogenesis: New clinical findings and potential treatment targets. *Rare Dis*, *1*, e27265. https://doi.org/10.4161/rdis.27265

Kadry, H., Noorani, B., & Cucullo, L. (2020). A blood-brain barrier overview on structure, function, impairment, and biomarkers of integrity. *Fluids Barriers CNS*, *17*(1), 69. https://doi.org/10.1186/s12987-020-00230-3

Kahanovitch, U., Cuddapah, V. A., Pacheco, N. L., Holt, L. M., Mulkey, D. K., Percy, A. K., & Olsen, M. L. (2018). MeCP2 Deficiency Leads to Loss of Glial Kir4.1. *eNeuro*, *5*(1). https://doi.org/10.1523/eneuro.0194-17.2018

Katz, D. M., Menniti, F. S., & Mather, R. J. (2016). N-Methyl-D-Aspartate Receptors, Ketamine, and Rett Syndrome: Something Special on the Road to Treatments? *Biol Psychiatry*, *79*(9), 710-712. https://doi.org/10.1016/j.biopsych.2016.03.1045

Kinboshi, M., Ikeda, A., & Ohno, Y. (2020). Role of Astrocytic Inwardly Rectifying Potassium (Kir) 4.1 Channels in Epileptogenesis. *Front Neurol*, *11*, 626658. https://doi.org/10.3389/fneur.2020.626658

Klein, C. J., Botuyan, M. V., Wu, Y., Ward, C. J., Nicholson, G. A., Hammans, S., Hojo, K., Yamanishi, H., Karpf, A. R., Wallace, D. C., Simon, M., Lander, C., Boardman, L. A., Cunningham, J. M., Smith, G. E., Litchy, W. J., Boes, B., Atkinson, E. J., Middha, S., . . . Dyck, P. J. (2011). Mutations in DNMT1 cause hereditary sensory neuropathy with dementia and hearing loss. *Nat Genet*, *43*(6), 595-600. https://doi.org/10.1038/ng.830

Kofuji, P., Ceelen, P., Zahs, K. R., Surbeck, L. W., Lester, H. A., & Newman, E. A. (2000). Genetic inactivation of an inwardly rectifying potassium channel (Kir4.1 subunit) in mice: phenotypic impact in retina. *J Neurosci*, *20*(15), 5733-5740. https://doi.org/10.1523/jneurosci.20-15-05733.2000

Leonard, H., Cobb, S., & Downs, J. (2017). Clinical and biological progress over 50 years in Rett syndrome. *Nat Rev Neurol*, *13*(1), 37-51. https://doi.org/10.1038/nrneurol.2016.186

Ley, T. J., Ding, L., Walter, M. J., McLellan, M. D., Lamprecht, T., Larson, D. E., Kandoth, C., Payton, J. E., Baty, J., Welch, J., Harris, C. C., Lichti, C. F., Townsend, R. R., Fulton, R. S., Dooling, D. J., Koboldt, D. C., Schmidt, H., Zhang, Q., Osborne, J. R., . . . Wilson, R. K. (2010). DNMT3A mutations in acute myeloid leukemia. *N Engl J Med*, *363*(25), 2424-2433. https://doi.org/10.1056/NEJMoa1005143

Li, W., & Pozzo-Miller, L. (2012). Beyond Widespread Mecp2 Deletions to Model Rett Syndrome: Conditional Spatio-Temporal Knockout, Single-Point Mutations and Transgenic Rescue Mice. *Autism Open Access*, *2012*(Suppl 1), 5. https://doi.org/10.4172/2165-7890.S1-005

Lin, L., Yee, S. W., Kim, R. B., & Giacomini, K. M. (2015). SLC transporters as therapeutic targets: emerging opportunities. *Nat Rev Drug Discov*, *14*(8), 543-560. https://doi.org/10.1038/nrd4626

Lipinski, C. A., Lombardo, F., Dominy, B. W., & Feeney, P. J. (2001). Experimental and computational approaches to estimate solubility and permeability in drug discovery and development settings. *Adv Drug Deliv Rev*, *46*(1-3), 3-26. https://doi.org/10.1016/s0169-409x(00)00129-0

Liu, X., Tu, M., Kelly, R. S., Chen, C., & Smith, B. J. (2004). Development of a computational approach to predict blood-brain barrier permeability. *Drug Metab Dispos*, *32*(1), 132-139. https://doi.org/10.1124/dmd.32.1.132

Mahringer, A., & Fricker, G. (2016). ABC transporters at the blood-brain barrier. *Expert Opin Drug Metab Toxicol*, *12*(5), 499-508. https://doi.org/10.1517/17425255.2016.1168804

Mao, Q., & Unadkat, J. D. (2005). Role of the breast cancer resistance protein (ABCG2) in drug transport. *Aaps j*, *7*(1), E118-133. https://doi.org/10.1208/aapsj070112

Mao, Q., & Unadkat, J. D. (2015). Role of the breast cancer resistance protein (BCRP/ABCG2) in drug transport--an update. *Aaps j*, *17*(1), 65-82. https://doi.org/10.1208/s12248-014-9668-6

Matsushima, S., Maeda, K., Hayashi, H., Debori, Y., Schinkel, A. H., Schuetz, J. D., Kusuhara, H., & Sugiyama, Y. (2008). Involvement of multiple efflux transporters in hepatic disposition of fexofenadine. *Mol Pharmacol*, *73*(5), 1474-1483. https://doi.org/10.1124/mol.107.041459

Mizui, T., Ishikawa, Y., Kumanogoh, H., & Kojima, M. (2016). Neurobiological actions by three distinct subtypes of brain-derived neurotrophic factor: Multi-ligand model of growth factor signaling. *Pharmacol Res*, *105*, 93-98. https://doi.org/10.1016/j.phrs.2015.12.019

Mnatzakanian, G. N., Lohi, H., Munteanu, I., Alfred, S. E., Yamada, T., MacLeod, P. J., Jones, J. R., Scherer, S. W., Schanen, N. C., Friez, M. J., Vincent, J. B., & Minassian, B. A. (2004). A previously unidentified MECP2 open reading frame defines a new protein isoform relevant to Rett syndrome. *Nat Genet*, *36*(4), 339-341. https://doi.org/10.1038/ng1327

Moj, D., Maas, H., Schaeftlein, A., Hanke, N., Gómez-Mantilla, J. D., & Lehr, T. (2019). A Comprehensive Whole-Body Physiologically Based Pharmacokinetic Model of Dabigatran Etexilate, Dabigatran and Dabigatran Glucuronide in Healthy Adults and Renally Impaired Patients. *Clin Pharmacokinet*, *58*(12), 1577-1593. https://doi.org/10.1007/s40262-019-00776-y

Montagne, A., Barnes, S. R., Sweeney, M. D., Halliday, M. R., Sagare, A. P., Zhao, Z., Toga, A. W., Jacobs, R. E., Liu, C. Y., Amezcua, L., Harrington, M. G., Chui, H. C., Law, M., & Zlokovic, B. V. (2015). Blood-brain barrier breakdown in the aging human hippocampus. *Neuron*, *85*(2), 296-302. https://doi.org/10.1016/j.neuron.2014.12.032

Moog, U., Smeets, E. E., van Roozendaal, K. E., Schoenmakers, S., Herbergs, J., Schoonbrood-Lenssen, A. M., & Schrander-Stumpel, C. T. (2003). Neurodevelopmental disorders in males related to the gene causing Rett syndrome in females (MECP2). *Eur J Paediatr Neurol*, *7*(1), 5-12. https://doi.org/10.1016/s1090-3798(02)00134-4

Motil, K. J., Caeg, E., Barrish, J. O., Geerts, S., Lane, J. B., Percy, A. K., Annese, F., McNair, L., Skinner, S. A., Lee, H. S., Neul, J. L., & Glaze, D. G. (2012). Gastrointestinal and nutritional problems occur frequently throughout life in girls and women with Rett

syndrome. *J Pediatr Gastroenterol Nutr*, *55*(3), 292-298. https://doi.org/10.1097/MPG.0b013e31824b6159

Nagahara, H., Vocero-Akbani, A. M., Snyder, E. L., Ho, A., Latham, D. G., Lissy, N. A., Becker-Hapak, M., Ezhevsky, S. A., & Dowdy, S. F. (1998). Transduction of full-length TAT fusion proteins into mammalian cells: TAT-p27Kip1 induces cell migration. *Nat Med*, *4*(12), 1449-1452. https://doi.org/10.1038/4042

Nagel-Wolfrum, K., Möller, F., Penner, I., Baasov, T., & Wolfrum, U. (2016). Targeting Nonsense Mutations in Diseases with Translational Read-Through-Inducing Drugs (TRIDs). *BioDrugs*, *30*(2), 49-74. https://doi.org/10.1007/s40259-016-0157-6

Nan, X., Ng, H. H., Johnson, C. A., Laherty, C. D., Turner, B. M., Eisenman, R. N., & Bird, A. (1998). Transcriptional repression by the methyl-CpG-binding protein MeCP2 involves a histone deacetylase complex. *Nature*, *393*(6683), 386-389. https://doi.org/10.1038/30764

Nation, D. A., Sweeney, M. D., Montagne, A., Sagare, A. P., D'Orazio, L. M., Pachicano, M., Sepehrband, F., Nelson, A. R., Buennagel, D. P., Harrington, M. G., Benzinger, T. L. S., Fagan, A. M., Ringman, J. M., Schneider, L. S., Morris, J. C., Chui, H. C., Law, M., Toga, A. W., & Zlokovic, B. V. (2019). Blood-brain barrier breakdown is an early biomarker of human cognitive dysfunction. *Nat Med*, *25*(2), 270-276. https://doi.org/10.1038/s41591-018-0297-y

Neuhaus, W., Gerhartl, A., Bounzina, N., Huber, A., Reitner, A., Steinkellner, H., Laccone, F. (2018). *Alterations of the blood-brain barrier in RETT syndrome.* YSA PhD Symposium 2018,

Neul, J. L., Fang, P., Barrish, J., Lane, J., Caeg, E. B., Smith, E. O., Zoghbi, H., Percy, A., & Glaze, D. G. (2008). Specific mutations in methyl-CpG-binding protein 2 confer different severity in Rett syndrome. *Neurology*, *70*(16), 1313-1321. https://doi.org/10.1212/01.wnl.0000291011.54508.aa

Neul, J. L., Kaufmann, W. E., Glaze, D. G., Christodoulou, J., Clarke, A. J., Bahi-Buisson, N., Leonard, H., Bailey, M. E., Schanen, N. C., Zappella, M., Renieri, A., Huppke, P., & Percy, A. K. (2010). Rett syndrome: revised diagnostic criteria and nomenclature. *Ann Neurol*, *68*(6), 944-950. https://doi.org/10.1002/ana.22124

Neul, J. L., Lane, J. B., Lee, H. S., Geerts, S., Barrish, J. O., Annese, F., Baggett, L. M., Barnes, K., Skinner, S. A., Motil, K. J., Glaze, D. G., Kaufmann, W. E., & Percy, A. K. (2014). Developmental delay in Rett syndrome: data from the natural history study. *J Neurodev Disord*, *6*(1), 20. https://doi.org/10.1186/1866-1955-6-20

Nitta, T., Hata, M., Gotoh, S., Seo, Y., Sasaki, H., Hashimoto, N., Furuse, M., & Tsukita, S. (2003). Size-selective loosening of the blood-brain barrier in claudin-5-deficient mice. *J Cell Biol*, *161*(3), 653-660. https://doi.org/10.1083/jcb.200302070

Oh, Y. J., Shin, D. Y., Hwang, S. M., Kim, S. M., Im, K., Park, H. S., Kim, J. A., Song, Y. W., Márquez, A., Martín, J., Lee, D. S., & Park, J. K. (2020). Mutation of ten-eleven translocation-2 is associated with increased risk of autoimmune disease in patients with myelodysplastic syndrome. *Korean J Intern Med*, *35*(2), 457-464. https://doi.org/10.3904/kjim.2018.247

Panayotis, N., Ehinger, Y., Felix, M. S., & Roux, J. C. (2023). State-of-the-art therapies for Rett syndrome. *Dev Med Child Neurol*, *65*(2), 162-170. https://doi.org/10.1111/dmcn.15383

Pardridge, W. M. (2005). The Blood-Brain Barrier: Bottleneck in Brain Drug Development. *NeuroRX*, *2*(1), 3-14. https://doi.org/https://doi.org/10.1602/neurorx.2.1.3

Paterson, D. S., Thompson, E. G., Belliveau, R. A., Antalffy, B. A., Trachtenberg, F. L., Armstrong, D. D., & Kinney, H. C. (2005). Serotonin transporter abnormality in the dorsal motor nucleus of the vagus in Rett syndrome: potential implications for clinical autonomic dysfunction. *J Neuropathol Exp Neurol*, *64*(11), 1018-1027. https://doi.org/10.1097/01.jnen.0000187054.59018.f2

Patrizi, A., Picard, N., Simon, A. J., Gunner, G., Centofante, E., Andrews, N. A., & Fagiolini, M. (2016). Chronic Administration of the N-Methyl-D-Aspartate Receptor Antagonist Ketamine Improves Rett Syndrome Phenotype. *Biol Psychiatry*, *79*(9), 755-764. https://doi.org/10.1016/j.biopsych.2015.08.018

Pejhan, S., & Rastegar, M. (2021). Role of DNA Methyl-CpG-Binding Protein MeCP2 in Rett Syndrome Pathobiology and Mechanism of Disease. *Biomolecules*, *11*(1). https://doi.org/10.3390/biom11010075

Pejhan, S., Siu, V. M., Ang, L. C., Del Bigio, M. R., & Rastegar, M. (2020). Differential brain region-specific expression of MeCP2 and BDNF in Rett Syndrome patients: a distinct grey-white matter variation. *Neuropathol Appl Neurobiol*, *46*(7), 735-750. https://doi.org/10.1111/nan.12619

Pepe, G., Fioriniello, S., Marracino, F., Capocci, L., Maglione, V., D'Esposito, M., Di Pardo, A., & Della Ragione, F. (2023). Blood-Brain Barrier Integrity Is Perturbed in a Mecp2-Null Mouse Model of Rett Syndrome. *Biomolecules*, *13*(4). https://doi.org/10.3390/biom13040606

Percy, A. K., Lane, J. B., Childers, J., Skinner, S., Annese, F., Barrish, J., Caeg, E., Glaze, D. G., & MacLeod, P. (2007). Rett syndrome: North American database. *J Child Neurol*, *22*(12), 1338-1341. https://doi.org/10.1177/0883073807308715

Persidsky, Y., Ramirez, S. H., Haorah, J., & Kanmogne, G. D. (2006). Blood-brain barrier: structural components and function under physiologic and pathologic conditions. *J Neuroimmune Pharmacol*, *1*(3), 223-236. https://doi.org/10.1007/s11481-006-9025-3

Pfrieger, F. W., & Ungerer, N. (2011). Cholesterol metabolism in neurons and astrocytes. *Prog Lipid Res*, *50*(4), 357-371. https://doi.org/10.1016/j.plipres.2011.06.002

Pintaudi, M., Calevo, M. G., Vignoli, A., Parodi, E., Aiello, F., Baglietto, M. G., Hayek, Y., Buoni, S., Renieri, A., Russo, S., Cogliati, F., Giordano, L., Canevini, M., & Veneselli, E. (2010). Epilepsy in Rett syndrome: clinical and genetic features. *Epilepsy Behav*, *19*(3), 296-300. https://doi.org/10.1016/j.yebeh.2010.06.051

Pizzagalli, M. D., Bensimon, A., & Superti-Furga, G. (2021). A guide to plasma membrane solute carrier proteins. *Febs j*, *288*(9), 2784-2835. https://doi.org/10.1111/febs.15531

Profaci, C. P., Munji, R. N., Pulido, R. S., & Daneman, R. (2020). The blood-brain barrier in health and disease: Important unanswered questions. *J Exp Med*, *217*(4). https://doi.org/10.1084/jem.20190062

QIAGEN. (2020). *RNeasy Plus Mini Handbook*. Retrieved 31.08.2023 from https://www.qiagen.com/us/resources/download.aspx?id=16b8f578-d192-4613-ae32-8e02e0b0fa77&lang=en

Reese, T. S., & Karnovsky, M. J. (1967). Fine structural localization of a blood-brain barrier to exogenous peroxidase. *J Cell Biol*, *34*(1), 207-217. https://doi.org/10.1083/jcb.34.1.207

Reitner, A. (2018). *Der Einfluss von MeCP2 auf Barriereeigenschaften der Blut-Hirn Schranke* [Diplomarbeit, Universität Wien].

Remy, S., & Beck, H. (2006). Molecular and cellular mechanisms of pharmacoresistance in epilepsy. *Brain*, *129*(Pt 1), 18-35. https://doi.org/10.1093/brain/awh682

Rett, A. (1966). [On a unusual brain atrophy syndrome in hyperammonemia in childhood]. *Wien Med Wochenschr*, *116*(37), 723-726. (Uber ein eigenartiges hirnatrophisches Syndrom bei Hyperammonämie im Kindersalter.)

Rett, A. (1968). [Cerebral atrophic syndrome in hyperammonemia in children]. *Landarzt*, *44*(16), 797-801. (Ein zerebral-atrophisches Syndrom bei Hyperammonämie im Kindesalter.)

Rolando, S. (1985). Rett syndrome: report of eight cases. *Brain Dev*, *7*(3), 290-296. https://doi.org/10.1016/s0387-7604(85)80030-9

Rosenberg, G. A., & Yang, Y. (2007). Vasogenic edema due to tight junction disruption by matrix metalloproteinases in cerebral ischemia. *Neurosurg Focus*, *22*(5), E4. https://doi.org/10.3171/foc.2007.22.5.5

Saili, K. S., Zurlinden, T. J., Schwab, A. J., Silvin, A., Baker, N. C., Hunter, E. S., 3rd, Ginhoux, F., & Knudsen, T. B. (2017). Blood-brain barrier development: Systems modeling and predictive toxicology. *Birth Defects Res*, *109*(20), 1680-1710. https://doi.org/10.1002/bdr2.1180

Samaco, R. C., Nagarajan, R. P., Braunschweig, D., & LaSalle, J. M. (2004). Multiple pathways regulate MeCP2 expression in normal brain development and exhibit defects in autism-spectrum disorders. *Hum Mol Genet*, *13*(6), 629-639. https://doi.org/10.1093/hmg/ddh063

Saunders, N. R., Dreifuss, J. J., Dziegielewska, K. M., Johansson, P. A., Habgood, M. D., Møllgård, K., & Bauer, H. C. (2014). The rights and wrongs of blood-brain barrier

permeability studies: a walk through 100 years of history. *Front Neurosci*, *8*, 404. https://doi.org/10.3389/fnins.2014.00404

Schwarze, S. R., Ho, A., Vocero-Akbani, A., & Dowdy, S. F. (1999). In vivo protein transduction: delivery of a biologically active protein into the mouse. *Science*, *285*(5433), 1569-1572. https://doi.org/10.1126/science.285.5433.1569

Sekul, E. A., Moak, J. P., Schultz, R. J., Glaze, D. G., Dunn, J. K., & Percy, A. K. (1994). Electrocardiographic findings in Rett syndrome: an explanation for sudden death? *J Pediatr*, *125*(1), 80-82. https://doi.org/10.1016/s0022-3476(94)70128-8

Shahbazian, M. D., Antalffy, B., Armstrong, D. L., & Zoghbi, H. Y. (2002). Insight into Rett syndrome: MeCP2 levels display tissue- and cell-specific differences and correlate with neuronal maturation. *Hum Mol Genet*, *11*(2), 115-124. https://doi.org/10.1093/hmg/11.2.115

Shahbazian, M. D., & Zoghbi, H. Y. (2002). Rett syndrome and MeCP2: linking epigenetics and neuronal function. *Am J Hum Genet*, *71*(6), 1259-1272. https://doi.org/10.1086/345360

Singh, J., Saxena, A., Christodoulou, J., & Ravine, D. (2008). MECP2 genomic structure and function: insights from ENCODE. *Nucleic Acids Res*, *36*(19), 6035-6047. https://doi.org/10.1093/nar/gkn591

Sirianni, N., Naidu, S., Pereira, J., Pillotto, R. F., & Hoffman, E. P. (1998). Rett syndrome: confirmation of X-linked dominant inheritance, and localization of the gene to Xq28. *Am J Hum Genet*, *63*(5), 1552-1558. https://doi.org/10.1086/302105

Steinkellner, H., Kempaiah, P., Beribisky, A. V., Pferschy, S., Etzler, J., Huber, A., Sarne, V., Neuhaus, W., Kuttke, M., Bauer, J., Arunachalam, J. P., Christodoulou, J., Dressel, R., Mildner, A., Prinz, M., & Laccone, F. (2022). TAT-MeCP2 protein variants rescue disease phenotypes in human and mouse models of Rett syndrome. *Int J Biol Macromol*, *209*(Pt A), 972-983. https://doi.org/10.1016/j.ijbiomac.2022.04.080

Sweeney, M. D., Ayyadurai, S., & Zlokovic, B. V. (2016). Pericytes of the neurovascular unit: key functions and signaling pathways. *Nat Neurosci*, *19*(6), 771-783. https://doi.org/10.1038/nn.4288

Szulwach, K. E., Li, X., Smrt, R. D., Li, Y., Luo, Y., Lin, L., Santistevan, N. J., Li, W., Zhao, X., & Jin, P. (2010). Cross talk between microRNA and epigenetic regulation in adult neurogenesis. *J Cell Biol*, *189*(1), 127-141. https://doi.org/10.1083/jcb.200908151

Takano, K., Kakuki, T., Kaneko, Y., Kohno, T., Kikuchi, S., Himi, T., & Kojima, T. (2017). Histone deacetylase inhibition prevents cell death induced by loss of tricellular tight junction proteins in temperature-sensitive mouse cochlear cells. *PLoS One*, *12*(8), e0182291. https://doi.org/10.1371/journal.pone.0182291

Takeshita, Y., & Ransohoff, R. M. (2012). Inflammatory cell trafficking across the blood-brain barrier: chemokine regulation and in vitro models. *Immunol Rev*, *248*(1), 228-239. https://doi.org/10.1111/j.1600-065X.2012.01127.x

Tang, F., Hartz, A. M. S., & Bauer, B. (2017). Drug-Resistant Epilepsy: Multiple Hypotheses, Few Answers [Review]. *Frontiers in Neurology*, *8*. https://doi.org/10.3389/fneur.2017.00301

Tao, J., Van Esch, H., Hagedorn-Greiwe, M., Hoffmann, K., Moser, B., Raynaud, M., Sperner, J., Fryns, J. P., Schwinger, E., Gécz, J., Ropers, H. H., & Kalscheuer, V. M. (2004). Mutations in the X-linked cyclin-dependent kinase-like 5 (CDKL5/STK9) gene are associated with severe neurodevelopmental retardation. *Am J Hum Genet*, *75*(6), 1149-1154. https://doi.org/10.1086/426460

Tarquinio, D. C., Motil, K. J., Hou, W., Lee, H. S., Glaze, D. G., Skinner, S. A., Neul, J. L., Annese, F., McNair, L., Barrish, J. O., Geerts, S. P., Lane, J. B., & Percy, A. K. (2012). Growth failure and outcome in Rett syndrome: specific growth references. *Neurology*, *79*(16), 1653-1661. https://doi.org/10.1212/WNL.0b013e31826e9a70

Thermo-Fisher-Scientific. (2020). *Pierce™ BCA Protein Assay Kit-User Guide*. Retrieved 11.09.2023 from https://assets.thermofisher.com/TFS-Assets/LSG/manuals/MAN0011430_Pierce_BCA_Protein_Asy_UG.pdf

Trazzi, S., De Franceschi, M., Fuchs, C., Bastianini, S., Viggiano, R., Lupori, L., Mazziotti, R., Medici, G., Lo Martire, V., Ren, E., Rimondini, R., Zoccoli, G., Bartesaghi, R., Pizzorusso, T., & Ciani, E. (2018). CDKL5 protein substitution therapy rescues neurological phenotypes of a mouse model of CDKL5 disorder. *Hum Mol Genet*, *27*(9), 1572-1592. https://doi.org/10.1093/hmg/ddy064

Tropea, D., Giacometti, E., Wilson, N. R., Beard, C., McCurry, C., Fu, D. D., Flannery, R., Jaenisch, R., & Sur, M. (2009). Partial reversal of Rett Syndrome-like symptoms in MeCP2 mutant mice. *Proc Natl Acad Sci U S A*, *106*(6), 2029-2034. https://doi.org/10.1073/pnas.0812394106

Troutman, M. D., & Thakker, D. R. (2003). Efflux ratio cannot assess P-glycoprotein-mediated attenuation of absorptive transport: asymmetric effect of P-glycoprotein on absorptive and secretory transport across Caco-2 cell monolayers. *Pharm Res*, *20*(8), 1200-1209. https://doi.org/10.1023/a:1025049014674

van Assema, D. M., & van Berckel, B. N. (2016). Blood-Brain Barrier ABC-transporter P-glycoprotein in Alzheimer's Disease: Still a Suspect? *Curr Pharm Des*, *22*(38), 5808-5816. https://doi.org/10.2174/1381612822666160804094544

Van Esch, H., Bauters, M., Ignatius, J., Jansen, M., Raynaud, M., Hollanders, K., Lugtenberg, D., Bienvenu, T., Jensen, L. R., Gecz, J., Moraine, C., Marynen, P., Fryns, J. P., & Froyen, G. (2005). Duplication of the MECP2 region is a frequent cause of severe mental

retardation and progressive neurological symptoms in males. *Am J Hum Genet*, *77*(3), 442-453. https://doi.org/10.1086/444549

Vashi, N., & Justice, M. J. (2019). Treating Rett syndrome: from mouse models to human therapies. *Mamm Genome*, *30*(5-6), 90-110. https://doi.org/10.1007/s00335-019-09793-5

Vasiliou, V., Vasiliou, K., & Nebert, D. W. (2009). Human ATP-binding cassette (ABC) transporter family. *Hum Genomics*, *3*(3), 281-290. https://doi.org/10.1186/1479-7364-3-3-281

Viemari, J. C., Roux, J. C., Tryba, A. K., Saywell, V., Burnet, H., Peña, F., Zanella, S., Bévengut, M., Barthelemy-Requin, M., Herzing, L. B., Moncla, A., Mancini, J., Ramirez, J. M., Villard, L., & Hilaire, G. (2005). Mecp2 deficiency disrupts norepinephrine and respiratory systems in mice. *J Neurosci*, *25*(50), 11521-11530. https://doi.org/10.1523/jneurosci.4373-05.2005

Voituron, N., & Hilaire, G. (2011). The benzodiazepine Midazolam mitigates the breathing defects of Mecp2-deficient mice. *Respir Physiol Neurobiol*, *177*(1), 56-60. https://doi.org/10.1016/j.resp.2011.02.002

Wakefield, R. I., Smith, B. O., Nan, X., Free, A., Soteriou, A., Uhrin, D., Bird, A. P., & Barlow, P. N. (1999). The solution structure of the domain from MeCP2 that binds to methylated DNA. *J Mol Biol*, *291*(5), 1055-1065. https://doi.org/10.1006/jmbi.1999.3023

Watanabe, K., Yamamoto, M., Xin, B., Ooshio, T., Goto, M., Fujii, K., Liu, Y., Okada, Y., Furukawa, H., & Nishikawa, Y. (2019). Emergence of the Dedifferentiated Phenotype in Hepatocyte-Derived Tumors in Mice: Roles of Oncogene-Induced Epigenetic Alterations. *Hepatol Commun*, *3*(5), 697-715. https://doi.org/10.1002/hep4.1327

Wenk, G. L. (1995). Alterations in dopaminergic function in Rett syndrome. *Neuropediatrics*, *26*(2), 123-125. https://doi.org/10.1055/s-2007-979741

Winkler, E. A., Bell, R. D., & Zlokovic, B. V. (2011). Central nervous system pericytes in health and disease. *Nat Neurosci*, *14*(11), 1398-1405. https://doi.org/10.1038/nn.2946

Wolburg, H., & Lippoldt, A. (2002). Tight junctions of the blood-brain barrier: development, composition and regulation. *Vascul Pharmacol*, *38*(6), 323-337. https://doi.org/10.1016/s1537-1891(02)00200-8

Wu, X., Liu, S., Lyu, J., Zhou, S., Yang, Y., Wang, C., Gu, W., Zuo, Q., Li, B., & Fan, C. (2017). Endogenous controls of gene expression in N-methyl-N-nitrosourea-induced T-cell lymphoma in p53-deficient mice. *BMC Cancer*, *17*(1), 545. https://doi.org/10.1186/s12885-017-3536-6

Ye, J., Coulouris, G., Zaretskaya, I., Cutcutache, I., Rozen, S., & Madden, T. L. (2012). Primer-BLAST: a tool to design target-specific primers for polymerase chain reaction. *BMC Bioinformatics*, *13*, 134. https://doi.org/10.1186/1471-2105-13-134

Young, J. I., Hong, E. P., Castle, J. C., Crespo-Barreto, J., Bowman, A. B., Rose, M. F., Kang, D., Richman, R., Johnson, J. M., Berget, S., & Zoghbi, H. Y. (2005). Regulation of RNA splicing by the methylation-dependent transcriptional repressor methyl-CpG binding

protein 2. *Proc Natl Acad Sci U S A*, *102*(49), 17551-17558. https://doi.org/10.1073/pnas.0507856102

Yu, X., Ji, C., & Shao, A. (2020). Neurovascular Unit Dysfunction and Neurodegenerative Disorders. *Front Neurosci*, *14*, 334. https://doi.org/10.3389/fnins.2020.00334

Zachariah, R. M., Olson, C. O., Ezeonwuka, C., & Rastegar, M. (2012). Novel MeCP2 isoform-specific antibody reveals the endogenous MeCP2E1 expression in murine brain, primary neurons and astrocytes. *PLoS One*, *7*(11), e49763. https://doi.org/10.1371/journal.pone.0049763

Zachariah, R. M., & Rastegar, M. (2012). Linking epigenetics to human disease and Rett syndrome: the emerging novel and challenging concepts in MeCP2 research. *Neural Plast*, *2012*, 415825. https://doi.org/10.1155/2012/415825

Zanella, S., Mebarek, S., Lajard, A. M., Picard, N., Dutschmann, M., & Hilaire, G. (2008). Oral treatment with desipramine improves breathing and life span in Rett syndrome mouse model. *Respir Physiol Neurobiol*, *160*(1), 116-121. https://doi.org/10.1016/j.resp.2007.08.009

Zappella, M. (1992). The Rett girls with preserved speech. *Brain Dev*, *14*(2), 98-101. https://doi.org/10.1016/s0387-7604(12)80094-5

Zeev, B. B., Bebbington, A., Ho, G., Leonard, H., de Klerk, N., Gak, E., Vecsler, M., & Christodoulou, J. (2009). The common BDNF polymorphism may be a modifier of disease severity in Rett syndrome. *Neurology*, *72*(14), 1242-1247. https://doi.org/10.1212/01.wnl.0000345664.72220.6a

Zlokovic, B. V. (2008). The blood-brain barrier in health and chronic neurodegenerative disorders. *Neuron*, *57*(2), 178-201. https://doi.org/10.1016/j.neuron.2008.01.003

Zweier, M., Gregor, A., Zweier, C., Engels, H., Sticht, H., Wohlleber, E., Bijlsma, E. K., Holder, S. E., Zenker, M., Rossier, E., Grasshoff, U., Johnson, D. S., Robertson, L., Firth, H. V., Ekici, A. B., Reis, A., & Rauch, A. (2010). Mutations in MEF2C from the 5q14.3q15 microdeletion syndrome region are a frequent cause of severe mental retardation and diminish MECP2 and CDKL5 expression. *Hum Mutat*, *31*(6), 722-733. https://doi.org/10.1002/humu.21253

Appendix

Zusammenfassung

Das Rett-Syndrom (RTT) ist eine fortschreitende neurologische Entwicklungsstörung, die bei den betroffenen Patienten zu geistiger Retardierung führt. RTT betrifft fast ausschließlich Frauen mit einer Inzidenz von 1:10.000–15.000. Der Hauptgrund für RTT ist eine Mutation im Gen für das Methyl-CpG-Bindeprotein 2 (MeCP2). Die Blut-Hirn-Schranke (BHS) trennt das Zentralnervensystem (ZNS) vom Blutkreislauf, indem die Gehirnendothelzellen eine selektive Barriere zwischen dem Blutkreislauf in den Gehirnkapillaren und dem Nervengewebe bilden. Bei neurologischen Erkrankungen wie Epilepsie oder Alzheimer, sowie dem Rett-Syndrom sind die Eigenschaften der Blut-Hirn-Schranke funktionell verändert.

Ein Ziel dieser Arbeit war es, Quantifizierungsmethoden für neue mögliche MeCP2-abhängige Gene, sowie für bekannte Targets zu etablieren. Ein weiteres Ziel bestand darin, zu evaluieren, ob ein substituiertes TAT-MeCP2-Fusionsprotein eine abweichende Proteinexpression in immortalisierten MeCP2-Knock-out Maus-Gehirnepithelzellen (cerebENDs) umkehren kann.

Literaturrecherche und Primer-design wurden genutzt, um zuverlässige Primer zur Quantifizierung vorgegebener Targets zu erhalten. Experimente mit verschiedenen Konzentrationen von TAT-MeCP2 wurden mit drei cerebEND-Zelllinien (Wildtyp, HDR-Kontrolle und Knock-out) durchgeführt. Western Blot und qPCR wurden durchgeführt, um Unterschiede in der Protein- und mRNA-Expression vorgegebener Targets anzuzeigen.

Die Datenanalyse der qPCR ergab eine Regulation der BHS-Marker Bcrp und Pgp, sowie der DNA-Methyltransferase DNMT1 in MeCP2 KO cerebENDs. Darüber hinaus konnte die Zugabe von TAT-MeCP2 den pathologischen Anstieg der Pgp-Proteinexpression in cerebEND-Knock-out-Zellen umkehren. Diese Erkenntnis könnte zu einer möglichen Proteinersatztherapie für RTT-Patienten beitragen.